Design of Solar Dehydrator, Coupled with Energy Storage in Rock Bed Reservoir for Fish Drying Process

Sh. Khoshmanesh
"M.S of Mechanical Engineering, Sharif University of Science and Technology, Tehran, Iran, email: sharif_khoshmanesh@yahoo.com

Key word: Solar dehydrator, soar heater, energy storage

Abstract

In this research firstly, requirements of fish drying process such as minimum moisture Content, air temperature, air velocity, etc, has been investigated and formulated; secondly the solar dehydrator based on the dehydrating of 834kg fish(200 kg fish without water) in period of 48 hour, for weather condition of Boushehr province in Iran has been designed. Solar heater with 200m^2 collectors in natural mode and 100 m^2 collectors in forced mode produce the heated air at the average temperature of 50^{o}c and the air flow rate of 1kg/sec which are the requirements of drying process for this plant during 48 hour. For continuing the drying during the night 56cube meter rock bed will be charged with 300m^2 collectors to supply the hot air at the temperature of 50^{o}c during 14 hour. The theoretical and experimental result has been compared by a small unit at the scaling of 1/300 the main plant.

1-Introduction

Fish drying by solar heater with the energy storage in rock bed at the industrial scale is the purpose of this paper.
Hot air produced from solar heater is directed to fish reservoir during the day, during the day another solar heater will charge the rock bed reservoir that produces the hot air during the night for continuing the drying process.
Each phenomenon separately has been investigated before, but the coupling of them to do the fish drying, in this paper follows. Solar heater and performance of them was considered by Jazaeri [11]and other refrences, [12],[13],[14].Drying process has been investigated by G.M flat[1] and others [2],[3].rock bed energy storage has been studied by Bahadori [8]and [6],[7].
At this research we analyze the fish drying process, to obtain the drying time, drying curve and the requirements of drying and then the amount of collector area for doing the drying process is followed. For continuing the drying process during the night the amount of rock bed and solar collector for charging the rock bed has been calculated, finally the empirical result of pilot plant in 1/300 of main plant has been shown.

2-Fish drying calculation

Removing the moisture (water) content of fish called the fish drying. Moisture content on the basis of wet mass (in percent) defined as [1].

$$M= \{(m-m_d)/m\}*100 \quad (1)$$

The other parameter defined as

$$M_i= \{(m_i-m_d)/m_i\}*100 \quad (2)$$

$$m_w= m_i-m \quad (3)$$

$$m_{w=} m_i*(M_i-M)*100/(100-M) \quad (4)$$

$$M= (100m_w-m_iM_i)/(m_w-m_i) \quad (5)$$

The fish can be preserving in natural condition (room temperature) if the moisture content of it reaches to 19 percent (M_f =19) [1] .Initial moisture content (M_i) and the critical moisture content (M_c) for two kind fishes in this research are respectively 76 and 61 percent [1]. In terms of the rate at which moisture is lost, drying, as a process, has been separated into two distinct periods, the constant rate and the falling rate period.
In constant rate period the surface of fish is moist and remains wet during drying, so water is considered to evaporate as form a free water surface. Drying at this period is controlled by drying air condition such as, air temperature, air velocity, and humidity.
The rate of water removes the fish calculate as

$$dm/dt = h_c.A.(T_a-T_w)/h_{fg} \quad (6)$$

This rate of mass transfer continues up to critical moisture content (Mc), the mass of water removes from the surface of fish at constant rate calculated by

$$m_w=h*A(T_a-T_w)t/h_{fg} \quad (7)$$

From equation (5) with knowing the mass of evaporated water from the (7), moisture content in any time can be calculated.
The water has been removed from initial to critical time can be calculated by (4) with knowing that M at critical time reach to 61 percent.

$$m_{wc}= m_i(M_i-M_c)/(100-M_c) \quad (8)$$

With knowing the m_{wc} the critical time for finishing the constant rate can be calculated.

$$t_c=(h_{fg}*m_{wc})/(h*A*(T_a-T_w)) \quad (9)$$

For calculating the "h" we assume that fishes have been hanged in the separated row with distance of 4cm parallel together in the reservoir (with the reservoir area of 1*1 m^2 and the height of 4m).at the falling rate time the drying controlled by diffusion of water that traveling from interior to surface. At the constant rate this diffusion rate dominates the evaporation rate and the surface of fish remain wet and the drying controlled by rate of evaporation. This process continues, and at the critical time this two rate equals, as we exceed, the evaporation rate dominate the diffusion rate and the surface of fish remains dry at this time(falling rate). The main difficulty of diffusion process is to denote the diffusion coefficient. At this research diffusion coefficient denoted by

experimental data that has been take placed in Tehran, Sharif University of science and technology.

At falling rate period the mass transfer is calculated by bellow equations [1], [2].

$$dm/dt=-(D/(\pi/2d)^2)(m-m_e) \quad (10)$$

$$m= \{(8/\pi^2)*(m_c-m_e)*e^{-Dt/(\pi/2d)2}\}+m_e \quad (11)$$

The diffusion coefficient D at critical point can be calculated from equaling the (6) and (10) at critical time.

$$D_c=h_cA(T_a-T_w)(\pi/2d)^2/h_{fg}(m_c-m_e) \quad (12)$$

The diffusion coefficient depended on the time and with increasing the time, decrease the diffusion coefficient, so we obtain the average diffusion coefficient by the experimental data, as, $D_{av}=0.8D_c$.

This D_{av} can be used for drying calculation during falling rate, which match the experimental and theoretical data see section 6, fig15 and fig16.

The time of drying is depended on the air drying temperature and this dependency has been calculated and shown at the bellow fig1.

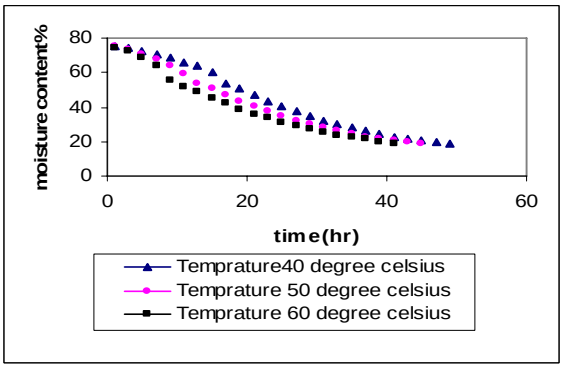

Fig1: moisture content versus time with different air temperature

The time of drying depended also on velocity of air and this dependency has been calculated and shown in the figure2.

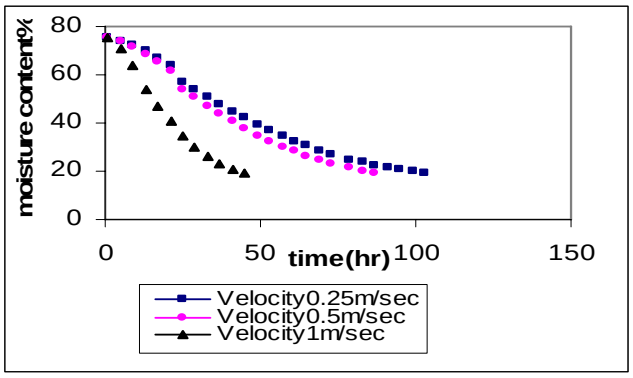

Fig2: moisture content versus time with different air velocity

As we see with increasing the air temperature and velocity the time of drying decreases. Increasing the air temperature and velocity, increase the solar collector area and increase the cost of plant, so we get the air temperature of 50 ^oc and velocity 1m/sec (air flow rate of nearly 1kg/sec for $1*1m^2$ reservoir area of fish) with humidity of 90 percent (humidity of Boushehr province in Iran) as the air condition properties for drying process.

3-Fish reservoir

The fish reservoir shall be capable to place the 834kg fish with attention to bellow constrains.

a) The area of fish reservoir is directly effect the incoming velocity, so increasing the area (Velocity=mass flow rate/area*density) decrease the velocity and increase the time of drying.

b) The height of fish reservoir changes with area to place the 834kg fish it means that increase the height decrease the area and increase the air velocity and finally decrease the time of drying.

Increase the height causes the two basic problem, first problem is increasing the heat loss with the increasing the height which causes to decreases the temperature for end sections (rows) of reservoir.

Second problem is, increasing the height causes the difficulty for worker to put and replacing the fishes in reservoir.

With attention to above problems and considering the sizes of fish, reservoir area=$1*1m^2$ with the height of 3.96m (4m) has been selected [10].

4-Solar heater

The warm air for drying is produced by solar heater that schematically shown in fig3.

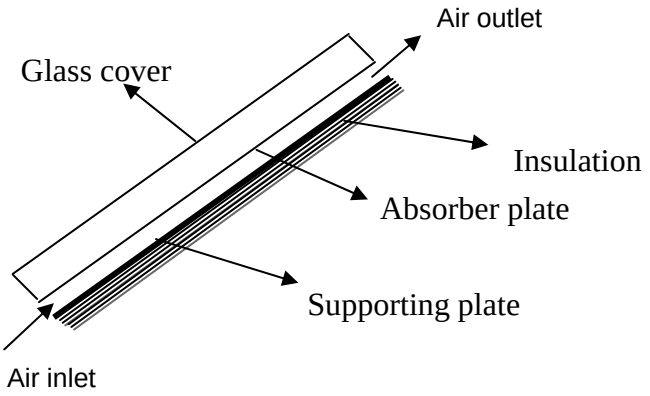

Fig3: schematic view of solar air heater

The air inlet can be produced naturally, that we call this case as natural mod, or can be produced by external device such as fan that we call this case as a forced mod.

The unsteady state equation for glass cover, air confined between glass cover and absorber plate, absorber plate, the air passing, between absorber plate and supporting plate, supporting plate and insulation have been come respectively here. Equation 13 trough 19 can be solved by finite difference method simultaneously.

For glass cover

$$\alpha_g S - h_{r,p-g}(T_g - T_P) - h_{r,g-s}(T_g - T_s) - h_{r,g-G}(T_g - T_G) - h_{c,g-ac}(T_g - T_{ac}) - h_{c,g-a}(T_g - T_a) = \frac{m_g c_g}{A_p}(dT_g / dt) \quad (13)$$

For confined air

$$\tau_g \alpha_p S - h_{c,p-ac}(T_p - T_{ac}) - h_{r,p-g}(T_p - T_g) - h_{r,p-b}(T_p - T_b) - h_{c,p-af}(T_p - T_{maf}) = \frac{m_p c_p}{A_p}(dT_p / dt) \quad (14)$$

For absorber plate

$$\tau_g \alpha_p S - h_{c,p-ac}(T_p - T_{ac}) - h_{r,p-g}(T_p - T_g) - h_{r,p-b}(T_p - T_b) - h_{c,p-af}(T_p - T_{maf}) = \frac{m_p c_p}{A_p}(dT_p / dt) \quad (15)$$

For passed air

$$h_{c,p-af}(T_p - T_{maf}) + h_{c,b-af}(T_b - T_{maf}) - \frac{2 \dot{m}_{af} C_{af}}{A_r}(T_{maf} - T_{afout}) = \frac{\rho_{af} C_{af} h_g A_{in}}{A_p}(dT_{af} / dt) \quad (16)$$

For supporting plate

$$h_{r,p-b}(T_p - T_b) - \frac{k_{ins}(T_b - T_{Ins,mid})}{d_{Ins,mid}} - h_{c,af-b}(T_b - T_{maf}) = \frac{m_b C_b}{A_p}(dT_b / dt) \quad (17)$$

For half of insulation

$$(T_b - T_{Ins,mid})\frac{k_{Ins}}{d_{Ins,mid}} - \frac{k_{Ins}}{d_{Insend}}(T_{Ins,mid} - T_{Ins,end}) = \frac{m_{Ins} c_{Ins}}{A_p}(dT_{Ins,mid} / dt) \quad (18)$$

For half end of insulation

$$(T_{Ins,end} - T_{Ins,mid})\frac{k_{Ins}}{d_{Ins,end}} = h_{c,Ins-a}(T_{Ins,end} - T_a) \quad (19)$$

Heat transfer coefficient for natural condition for confined space can be calculated from, [9].

$$Nu = 1 + 1.44\left[1 - \frac{1708}{RaCos\beta}\right]^{+}\left(\frac{(Sin(1.8\beta)^{1.6} \times 1708}{RaCos\beta}\right) + \left[\left(\frac{RaCos\beta}{5830}\right)^{\frac{1}{3}} - 1\right] \quad (20)$$

$$Nu = \frac{hd}{k} \quad (21)$$

$$Ra = \frac{g\beta' \Delta T s^3}{\upsilon \alpha} \quad (22)$$

The sign + in bracket means if the value of bracket gets into negative the bracket value shall be take to zero. The "d" is distance between two parallel surfaces.
For heat transfer coefficient in natural condition for free stream between absorber plate and supporting plate, [9]
For laminar flow

$$Nu = 4.99 + \frac{.0606\,(\mathrm{Re}\ P_r \quad D_H / L)^{\frac{1}{2}}}{1 + .0909\,(\mathrm{Re}\ p_r \frac{D_H}{L})^{0.7} P_r^{0.17}} \quad (23)$$

For turbulent flow

$$Nu = 0.0158\mathrm{Re}^{0.8} \quad (24)$$

$$D_H = 2d \quad (25)$$

Radiation heat transfer coefficient between two parallel surface "a" and "b" calculated by

$$h_r = \frac{\sigma (T_a + T_b)(T_a^2 + T_b^2)}{\frac{1}{\varepsilon_a} + \frac{1}{\varepsilon_b} - 1} \quad (26)$$

Mass flow rate of heated air can be calculated from, [9]

$$V = \left[\frac{2gh_g((T_m - T_{in})/T_m)}{C}\right]^{\frac{1}{2}} \quad (27)$$

$$C = C_1\left(\frac{A_{in}}{A_{out}}\right)^2 + C_2 \approx 8\left(\frac{A_{in}}{A_{out}}\right)^2 + 2 \quad (28)$$

A_{in} and A_{out} are respectively the inlet and outlet area of air.

As we describe in section 1 the appropriate temperature and mass flow rate for drying condition were 50 degree Celsius and 1kg/sec respectively.
The solar heater with the collector area of $1*2$ m^2 area is available in market, so we series and parallel the collectors to gain the 50 degree Celsius and 1kg/sec mass flow rate.
By solving the equation 13 trough 19 simultaneously with serialize the two collectors the defined temperature (50 degree) will obtain, see fig 4

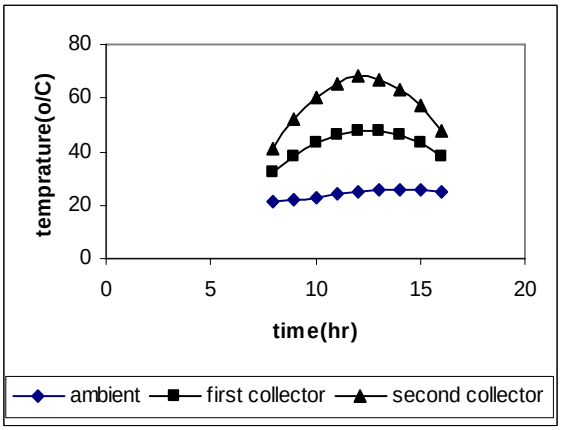

Fig4: temperature of one series collectors and ambient versus time

But as you see in fig6 the mass flow rate cannot be reached the 1kg/sec, therefore we shall parallel the collectors to reach this value.

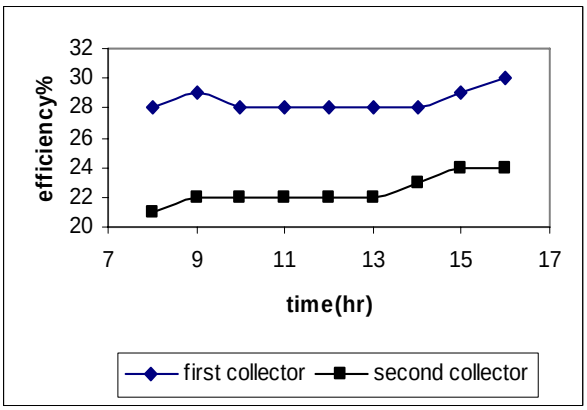

Fig5: efficiency of two series collectors versus time

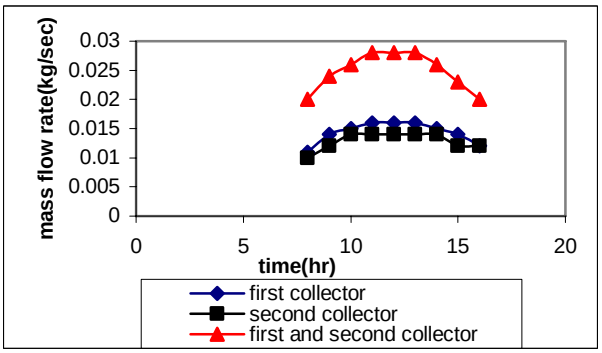

Fig6: mass flow rate of two series collectors versus time

With considering the fig6 we can see for reaching to mass flow rate 1kg/sec we need to parallelize nearly 50 number of collector, so the collector area is calculated as $50*4=200m^{2.}$
If we prepare the mass flow rate 1kg/sec by fan, the equation 13trough 18 can be solved in the same way, the only difference is the heat transfer coefficient between collector plate and supporting plate that applies for force convection mode [14]. The serialize the 5 number solar collectors with 0.1kg/sec mass flow rate give the proper temperature 50^{o}c, see fig7

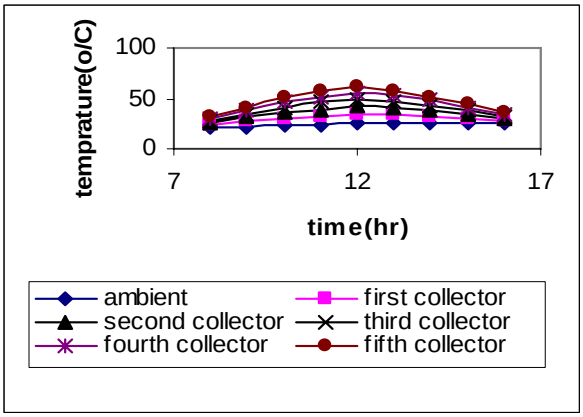

Fig7: temperature of five series collectors and ambient versus time

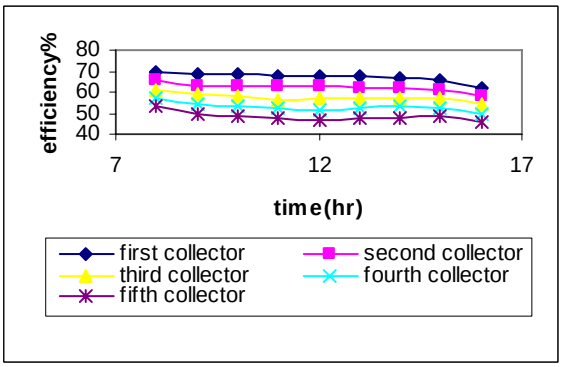

Fig8: efficiency of five series collectors versus time

To obtain 1kg/sec mass flow rate it is required to parallel 10 collectors, so the area required is $10*10=100m^2$ which is half in compare with natural mode

5-Storage energy

Time of drying is near the 48hour, so we use the rock bed reservoir for storage the energy and retrieving during the night. The rock bed reservoir that stored the energy during the day must be capable of producing the 50 degree Celsius air temperature during 14 hour by passing the 1kg/sec outdoor air on it by fan. The size of reservoir has been calculated by solving the related equation numerically.

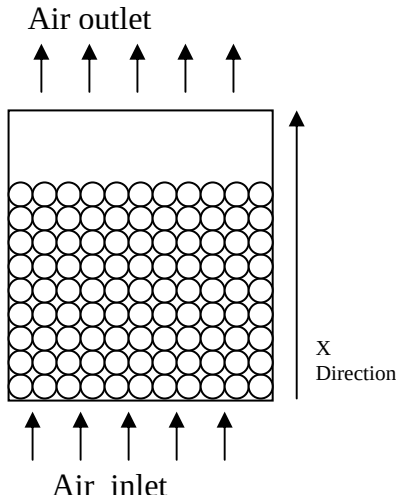

Fig9: schematic view of rock bed reservoir

Two bellow equations for analyzing the rock bed reservoir can be used, [5]

$$\frac{\partial T_a}{\partial t} + \frac{G}{\rho_a f}\frac{\partial T_a}{\partial x} = \frac{h_v}{\rho_a c_a f}(T_S - T_a) \quad (29)$$

$$\frac{k_s}{\rho_s(1-f)c_s}\frac{\partial^2 T_s}{\partial x^2} + \frac{h_v}{\rho_s(1-f)c_s}(T_a - T_s) = \frac{\partial T_S}{\partial t} \quad (30)$$

The x is the direction of rock bed parallel to the flow passing on it, we consider the change of variable as bellow

$$Y = \frac{h_v}{CG_a}x \quad (31)$$

$$Z = \frac{h_v}{\rho_S C_s(1-f)}t \quad (32)$$

The equation 29 and 30 simplified to

$$\frac{\partial T_a}{\partial y} + k_3\frac{\partial T_a}{\partial z} = T_s - T_a \quad (33)$$

$$\frac{\partial T_s}{\partial y} + k_3\frac{\partial T_s}{\partial z} = T_a - T_s + k_2\frac{\partial^2 T_s}{\partial y^2} \quad (34)$$

The K_3 and K_2 is related to heat transfer by conduction and air heat capacity and neglecting so,

$$\frac{\partial T_a}{\partial y} = T_s - T_a \quad (35)$$

$$\frac{\partial T_s}{\partial z} = T_a - T_s \quad (36)$$

h_v can be obtained by[6].

$$\frac{h_v D_e^2}{k} = 1.45\left(\frac{\rho V D_e}{\mu}\right)^{.7} \qquad 100 < \frac{\rho V D_e}{\mu} < 1000 \quad (37)$$

$$.38 \le f \le .46$$

$$\frac{h_v D_e^2}{k} = 2.72\left(\frac{\rho V D_e}{\mu}\right)^{.7} \qquad 500 < \frac{\rho V D_e}{\mu} < 50000 \quad (38)$$

$$.38 \le f \le .46$$

$$D_e = \left(\frac{6}{\pi} \times (rock's \quad volume \div rock's \quad number)\right)^{\frac{1}{3}} \quad (39)$$

By solving the equations (35), (36) numerically, the volume of rock bed to supply the 50^oc hot air for 14 hour during the night has been obtained. The result has been shown in bellow table

Table1: sizes of rock bed reservoir

Flow rate(kg/sec)	Reservoir Area	Reservoir height
1	0.5×1	112
1	1×1	56
1	1×2	28
1	4×2	7

As you see near the $56m^3$ volume rock need to achieve the proper condition of drying. For charging the $56m^3$ rock bed we can use $300m^2$ solar collector ($10*30$) with the total flow rate of 2kg/sec for charging the rock bed reservoir. See fig10

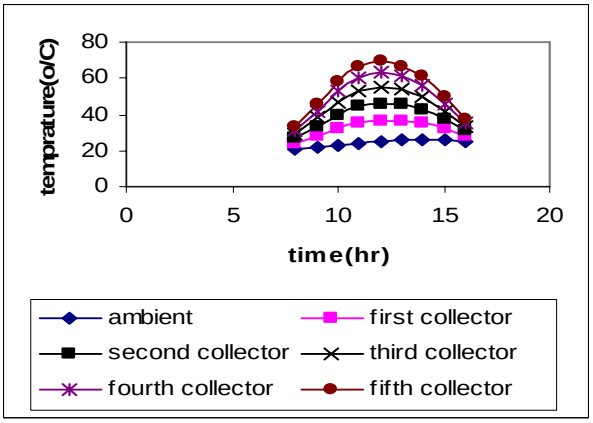

Fig10: temperature of 5 series collectors and ambient versus time for charging the rock bed reservoir

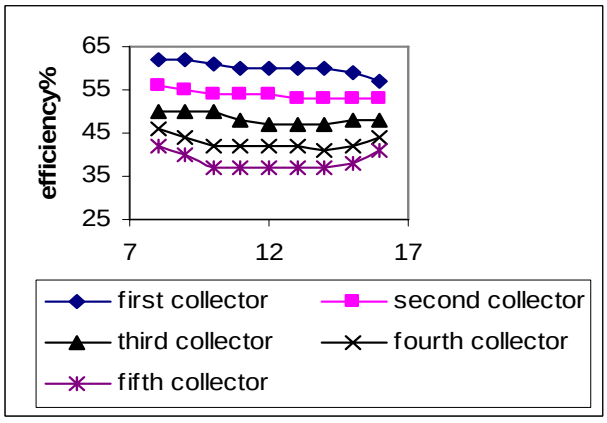

Fig11: efficiency of 5 series collectors versus time For charging the rock bed reservoir

The temperature of the rock reservoir with 1m height by outlet air temperature from fig10, at different sections has been shown on fig12.

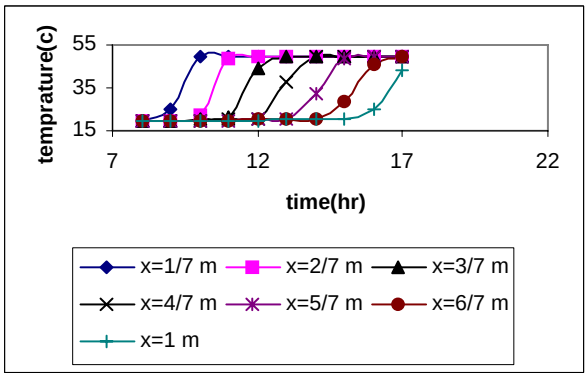

Fig12: temperature at different sections of rock reservoir versus time

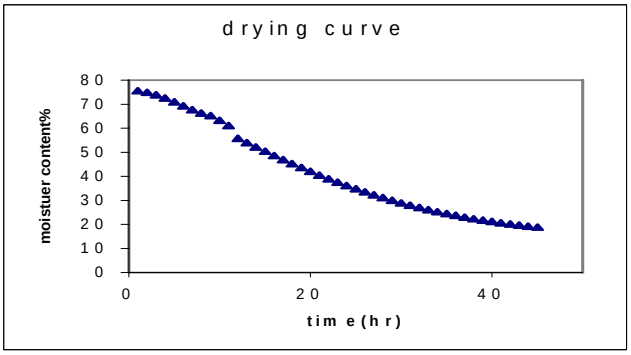

Fig13: moisture content versus time

If we dry the fish with temperature distribution that have been obtained during the above sequence, the drying curve in fig13 will obtain.

6-Pilot plant and experimental result

The pilot plant was constructed in 1/300 of the main plant; the size of different parts of plant and pilot plant have been given in table2

table2: different part's Sizes of main plant and pilot plant

	solar heater collector area for drying during day(m^2)	mass flow Rate(kg/s)	solar heater collector area for charging the rock bed (m^2)	mass flow rate of solar heater for charging and recharging the rock bed respectively(kg/sec)	volume of rock bed (m^3) L*W*H
main plant	100	1	300	2,1	56
pilot plant	0.33	0.003	1	0.006,0.003	0.5*0.46 *0.5

The $1m^2$ solar heater was available in laboratory of mechanical faculty, so we use this solar heater for drying the fish during the day and charging the rock bed during the another day. The only problem was the different between the pilot plant solar heater collector area ($0.33m^2$) and the available solar heater with $1m^2$ collector area. For solving this problem we increase the mass flow rate to three times (1/0.33 times) the mass flow rate of pilot plant.
We use the solar heater with the fan of mass flow rate of 0.01 for producing the hot air for drying the fish during the day and mass flow rate of 0.006 for charging the rock bed. The air outlet temperature for two cases have shown in fig14, 15

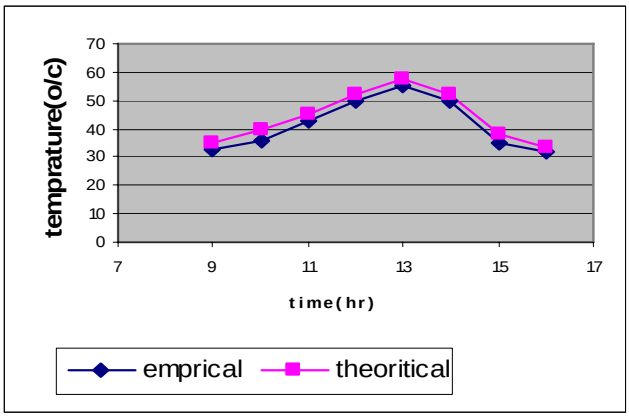

Fig14: air outlet temperature of solar heater for charging the rock bed versus time

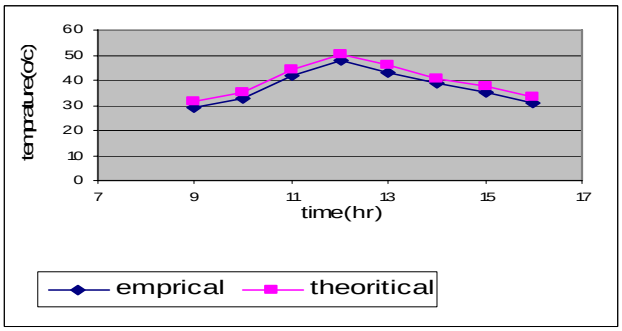

Fig15: air outlet temperature of solar heater for drying the fish bed

We charged the rock bed reservoir with outlet temperature of solar heater in fig14 that gives the 42°c temperature for all rock bed in reservoir during 10 hour charging. The recharging process for drying causes that the drying continues with 42°c in14 hour during night (from 17pm to 7am).We dry two kind of fishes with this temperature distribution, the bellow result will obtain.

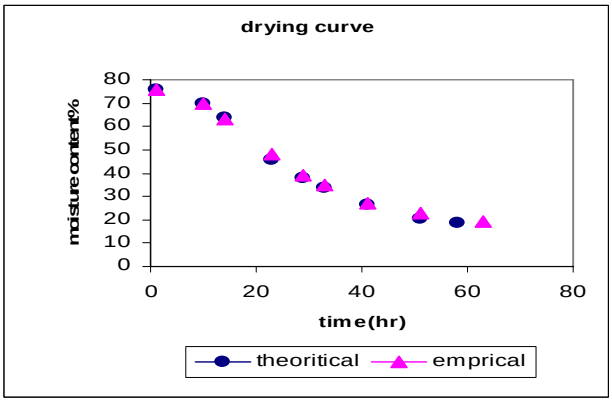

Fig16: moisture content versus the time for lion fish

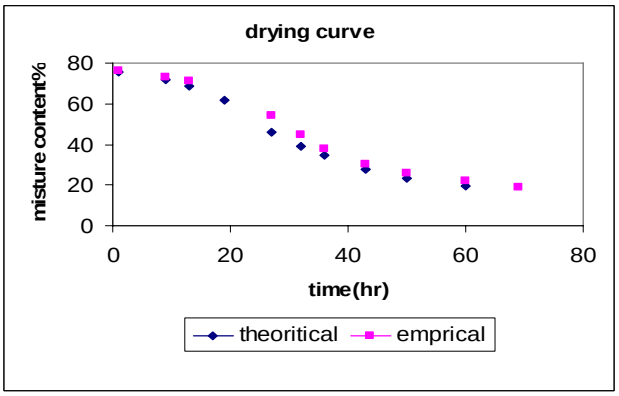

Fig17: moisture content versus the time for white fish

7-Conclusion

We can do the drying process in natural and forced mode. In natural mod we don't use any external device for producing the air flow but for forced mod we use the external device for producing the air flow. The absorber plate area for forced mode is half of the natural mode, so the forced mode drying is recommended because of lower cost value. We can also compare the cost value of plant with drying process by gas. If we consider the butane gas with L.H.V-45714kj/kg, the water mass that must be extract from the fish to reach the M_f=19 is nearly 586 kg of 834 kg mass of fish, so the energy required to extract is equal to 1445076kj (water mass $*$ h_{fg} =586$*$2466). The mass of gas required (the efficiency be 100) is equal to, (1445076) / (45714) =31.6kg. This amount of gas is enough for period of 48 hour drying.

Nomenclature

M	moisture content (%)
M_i	initial moisture content (%)
M_c	moisture content at critical time (%)
M_f	moisture content at final state (%)
M_e	moisture content at equilibrium state (%)
m	mass of fish(kg)
m_i	Initial mass of fish(kg)
m_d	mass of fish without water(kg)
m_c	mass of fish at critical time(kg)
m_f	final mass of fish(kg)
m_w	water evaporated(kg)
m_{wc}	water evaporated at critical time(kg)
m_e	mass of fish at equilibrium state(kg)
t	time(sec)
t_c	critical time(sec)
D	diffusion coefficient
d	thickness (meter)
h	convection heat transfer coefficient ($w/m^2.c^o$)
T	temperature(c^o)
T_a	air free stream temperature(c^o)
T_w	wet bulb temperature (c^o)
h_{fg}	latent heat of evaporation (kj/kg)
D_{av}	average diffusion coefficient
S	Sun intensity (w/m^2)
C	Specific heat($kj/kg.k^o$)
A_p	absorber area(m^2)
A_{out}	outlet area of air(m^2)
A_{in}	entrance area of air(m^2)
h_g	height of air channel (m)
ρ	density(kg/m3)
τ	transmissivity
α	absorptivity
Nu	Nusselt number
Ra	Rayleigh number
β	Inclined angle of solar collector
β'	Volume expansivity(1/k)
Pr	Prandtl number
D_H	hydrolic diameter (m)
L	Collector length (m)
h_v	Volumetric convection heat transfer coefficient($w/m^3.c^o$)
k	thermal conductivity($w/m.c^o$)
D_e	Effective Diameter of rock bed (m)
V	Velocity (m/s)
μ	dynamic Viscosity(kg/m.s)
f	void fraction
A	surface area (m^2)
ν	kinematics viscosity(m^2/s)
α	thermal diffusivity(m^2/s)
d	distance between two parallel surface(m)
L.H.V	low heat value (kj/kg)

Subscripts

a	air
s	rock bed
ac	confined air
p	absorber plate
af	air flow passing
maf	mean value of air flow passing
afout	outlet air flow
g	glass cover
b	supporting plate
Ins	insulation
mid	mid of insulation
end	end of insulation
c	convection
r	radiation
ins	insulation
p-g	between absorber plate and glass
g-s	between glass and sky
g-G	between glass and ground
g-ac	between glass and air confined
g-a	between glass and outdoor air
p-ac	between absorber plate and air confined
p-b	between absorber and back plate
p-af	between absorber plate and air flow passing
b-af	between back plate and air flow passing
ins-a	between insulation and outdoor air
in	input
out	output
m	mean value

References

[1]. G.M.flat "Fish processing technology", 1999

[2]. Mujum dar, A.S. "Handbook of Industrial Drying", Deker,987

[3]. Doulia, K.Tzia, V.edkas "Aknowledge base for the apparent mass diffusion coefficient of food"

[4]. Agenus, V.asiedu-Bondzie "Solar drying with convective self-flow and energy storage

[5]. Pascal and Faber "Two application of Numerical Approach of heat transfer Process within Rock beds", solar energy, Vol29, No 6, pp.451-462 , 1982.

[6]. Chandra "presure drop and heat transfer characteristics of Air-Rockbed thermal storage system, solar energy, vol27, No6. Pp.547-553, 1981.

[7]. Saze "Dynamic Response of a packed bed thermal storage system-Amodel for solar air heating "solar Energy Vol.29 No pp.201-206, 1982.

[8]. M.N, Bahaori "Thermal Energy storage" Iranian Journal of science and Technology Vol.5, pp.159-171, 1976.

[9]. Duffie and R.Beckman "Solar energy of thermal process", john wiley & Sons. Inc, N.Y.(1980)

[10].Sh.Khoshmanesh"design of fish solar dehydrator with energy storage in rock bed" M.S thesis Sharif university of science and technology, Tehran, Iran

[11].Jazaeri " performance's investigation of two kind of solar heater"M.S thesis Sharif university of science and technology, Tehran, Iran

[12]. L.F.Azevedo, E.M.Sparrow, "Natural convection in open-ended inclined channels", J.Of hefat transfer. Trans of ASME, Vol.107, pp893-901 (1985)

[13]. K.G.Holland. T.E.Unny, G.D.Raithby and L.konick, "Free convection heat transfer across incliened thin layers", ASME paper No. 75-HT-55, (1975).

[14]. F. P.Incropera, Fandementals of heat and Mass transfer,John Wiley & Sons, 1990

Performance evaluation of a solar photovoltaic energy system designed for supplying electricity and water for remote communities

A Zahedi, Solar Photovoltaic Energy Applications Research Group
Monash University, Department of Electrical and Computer Systems Engineering, Victoria, 3800, AUSTRALIA, Email: ahmad.zahedi@eng.monash.edu.au

Abstract
Electricity and fresh water are two essential needs for continuation of life by human beings. There are unfortunately a large number of people on the earth that do not have access to reliable electricity and fresh water.

The objective of this paper is to present the design aspects of a solar photovoltaic (PV) energy system including desalination unit, in which electricity and fresh water are produced as the main products.

A further objective of this work is to present the results of a computer simulation program developed to determine the optimum size of all components in this system. And finally, computer simulation results about prediction of the system's performance will also be presented.

Introduction

The system under investigation is a system that is specially designed for remote communities, where access to the national electricity grid is not available and also fresh water is not easily accessible. This system is most suitable for communities located at a distance of 2 or more kilometres away from electricity network but near the sea water.

The size of the system under investigation is determined for the household consisting of four family members. As the system is modular, so it can be expanded to any size if needed.

The average daily consumption of electricity per household of 4 people (2 adults and 2 children) is assumed to be approximately 15 kWh per day, which is equivalent to the typical daily average of electricity consumption by Australian households.

Obviously, usage in winter will exceed this average due to the use for heating which consumes a large amount of electricity, and in contrast summer will consume less electricity, provided no air-conditioning unit is used.

A battery bank is included into the system. As the battery bank is the weakest component in the system, so this component requires special care to make sure that it is always in healthy condition and never fails. In order to make sure that this component is always in a good operating condition, a generator set is included into the system for the purpose of supporting and backing up the battery bank.

The daily production of fresh, drinkable water from this plant is approximately 100 litres per day. Although the typical Australian daily water consumption per household (2 adults and 2 children) is about 500 litres per day, in our investigation we assumed that only 20% of that is used as drinking water.

System Configuration

The main component of this system is a solar photovoltaic (PV) array, which provides electricity:

i) To supply electricity needed by the electrical appliances in the household
ii) To supply enough electricity for the desalination unit and its related electrical devices

An inverter is used at the electrical part of the system to convert DC electricity into AC.

As the entire system is designed for electrification of a remote located community with no access to an electricity grid, a battery bank is considered to support the solar array. The battery bank is used for two purposes as follows:

i) To absorb and store the excess power generated during the day and also to make sure that enough electricity is available for consumption by electrical components during the night time and cloudy days.

ii) To supply electricity for 5 consecutive no-sun-days. (According to information received from the Australian Bureau of Meteorology, BOM, three consecutive no-sun-days is likely to happen in Australia. However, for the purpose of increasing the system's reliability, in our calculations we have assumed a 5 consecutive no sun days.

A generator is also considered for the purpose of battery back-up. Figure 1 shows the single line diagram of the proposed solar photovoltaic electrification system, which includes desalination plant, for an off-grid community. For the purpose of producing fresh water, a Reverse Osmosis desalination unit is included into the system to produce 100 litre of fresh drinkable water per day. Also an electric pump is required to pump the sea water into the desalination unit.

Water desalination unit, Reverse Osmosis vs. Distillation unit

There are two main options available for the purpose of water desalination. These two options are distillation and reverse osmosis. For this project we have chosen the reverse osmosis technology mainly because it requires less electricity and works mainly in an inherent process. The main electricity unit in this system is solar photovoltaic (PV) array and as we know, the PV electricity is expensive, so we need to minimize the consumption of PV electricity. In order to clarify this, the author wishes to give an idea on the amount of electricity needed for a distillation system. In ideal situations, approximately 260 MJ of energy is needed to convert 100 liters of sea water into fresh water desalination. This is equivalent to 72 kWh. In order to produce 72 kWh of electricity per day in a location with a climate similar to Melbourne, a solar PV array of 17.5 kW is needed.

In contrast, the amount of electricity needed for the reverse osmosis option is just that for producing the reverse osmosis pressure, which is in the range of a couple of kWh. The author needs to mention here that a certain amount of electricity is required to run a pump for pumping the sea water. But this is needed for both options.

Optimum Sizing of System's Components

Depending on the sun radiation available at the site, the daily electricity demand by electric loads and fresh water consumption, the optimum size of each component is determined.

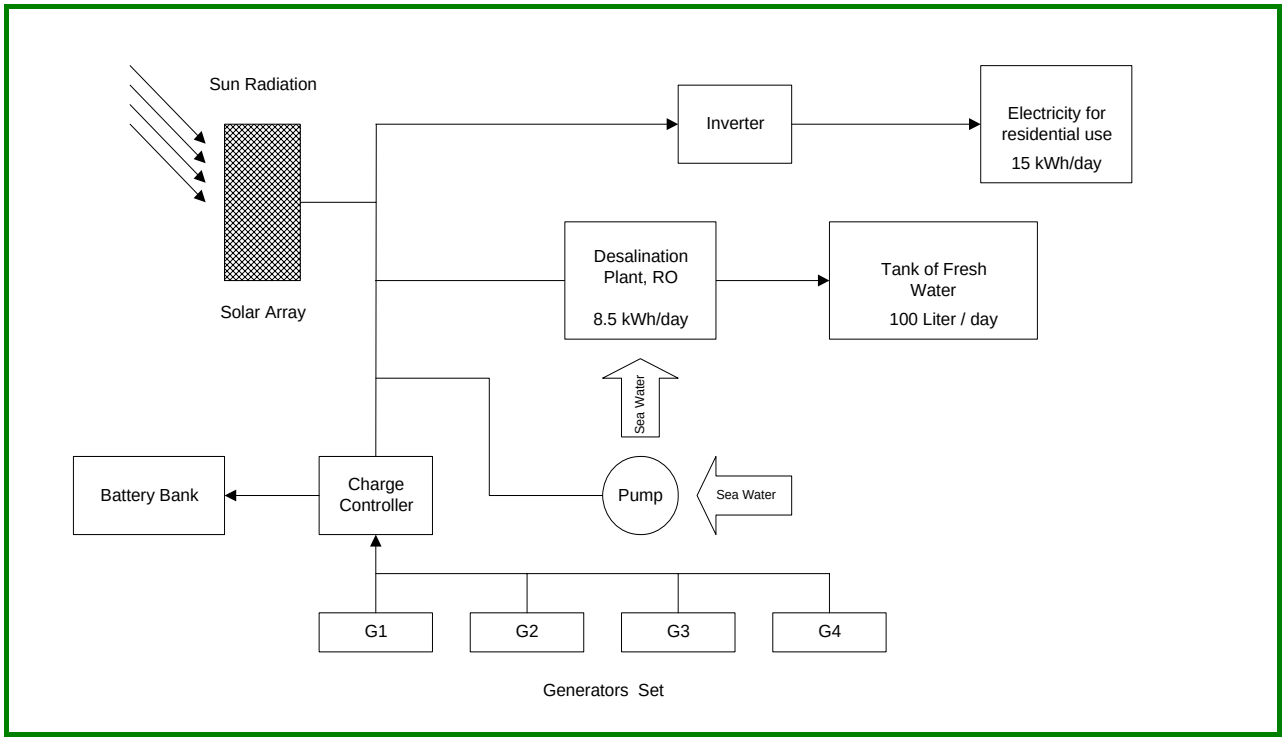

Figure 1 Single line diagram of proposed solar photovoltaic desalination plant suitable for remote located communities.

Optimum sizing of the components in the system is the most important part of the system's design. The optimum sizing is important not only for the purpose of reliability but also for the economics of the system. Obviously a solar PV hybrid power system is already an expensive system with a relatively high capital cost and unit price of electricity ($/kWh). Over-sizing makes the system more expensive, while under-sizing makes the system unreliable. So every effort needs to be made to optimize the components' sizes.

The daily operational time of the generator set for each month has been calculated. This is to ensure that the battery bank is maintained in a healthy condition and its capacity never falls below the permitted depth of discharge (DOD), which is set at 80%. Although 4 DG units are included in the system, but only one unit at the time will be enough to operate to charge the battery bank. Size of Battery bank is 192 kWh and size of Gen-set is 23 kW.

In our research group we have recently developed a computer program, which is able to determine the optimum sizing of all components in any solar PV systems for any applications. And also this program is able to determine the capital costs as well as electricity cost ($/kWh) and unit price ($/litre) of fresh water. In all economical aspects and cost calculations, the time value of money is taken into account. And finally, in order to make sure that the designed PV system is operating as expected and is able to meet the demand under all different climate conditions, the program is able to predict the system's performance.

Results

Following section presents results of Photovoltaic Size-Optimisation for five different cases: A, B, C, D, and E.

Case A: we have assumed that the amount of energy needed by the entire system in summer if fully covered by the PV array.
Case B: we have assumed that the amount of energy needed by the entire system in autumn if fully covered by the PV array.
Case C: we have assumed that the amount of energy needed by the entire system in winter if fully covered by the PV array.
Case D: we have assumed that the amount of energy needed by the entire system in spring if fully covered by the PV array.
And finally, Case E refers to the case that we used the annual average PSH to determine the size of PV array.

Table 1 compares the final results of these cases, while the Table 2 shows the operational time per day of the generator set. State of Charge of the battery bank for all 5 different cases has been shown in Figure 2-6.

	PSH	PV Size	% PV	% DG	Fuel (L)	Electricity $/kWh	Excess Electricity year	kWh/ day	Total kWh/year for water
Case A, Summer	6.39	6.40	61.5	38.5	1176	1.85	100	8	3020
Case B, Autumn	3.17	12.91	89.3	10.7	453	2.43	2996	8	5916
Case C, Winter	2.02	20.23	99.2	0.8	45	3.25	7248	8	10168
Case D, Spring	4.82	8.49	75.4	24.6	812	1.93	674	8	3594
Case E, Annual-Average	4.08	10.02	82.2	17.8	635	2.10	1343	8	4263

Table 1

	J	F	M	A	M	J	J	A	S	O	N	D
Case A, Summer	0	0	2	3	3	5	4	4	2	2	1	0
Case B, Autumn	0	0	0	0	2	3	2	2	1	0	0	0
Case C, Winter	0	0	0	0	0	1	1	0	0	0	0	0
Case D, Spring	0	0	0	2	3	4	3	3	3	0	0	0
Case E, Annual-Average	0	0	0	1	3	3	3	3	1	0	0	0

Table 2

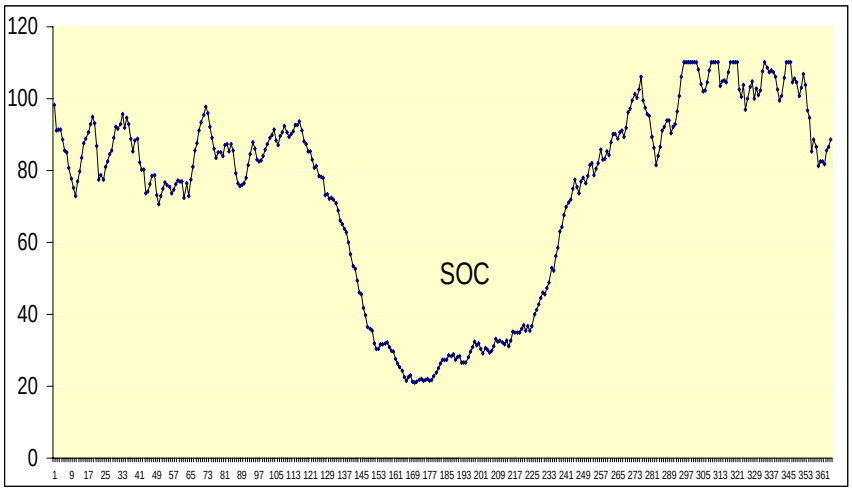

Figure 2 Case A: State of charge (SOC) of the battery bank

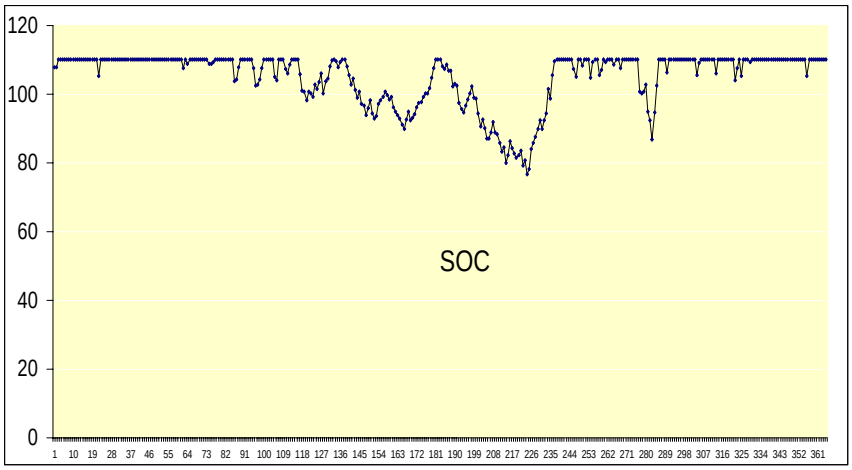

Figure 3 Case B: State of charge (SOC) of the battery bank

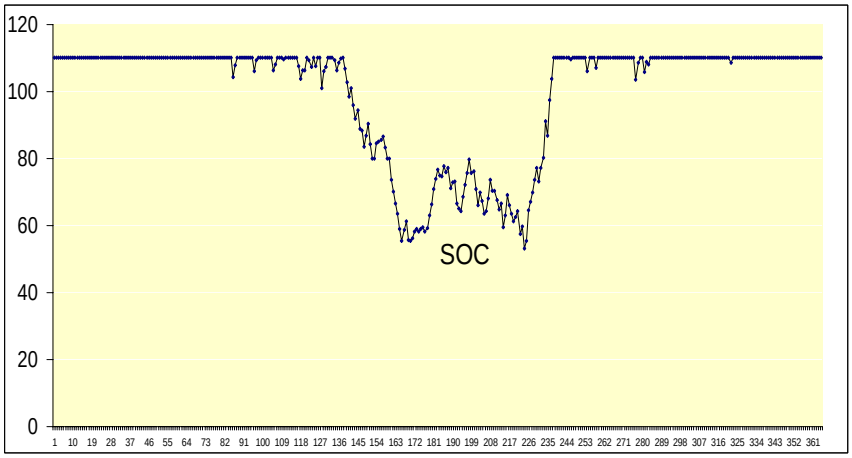

Figure 4 Case C: State of charge (SOC) of the battery bank

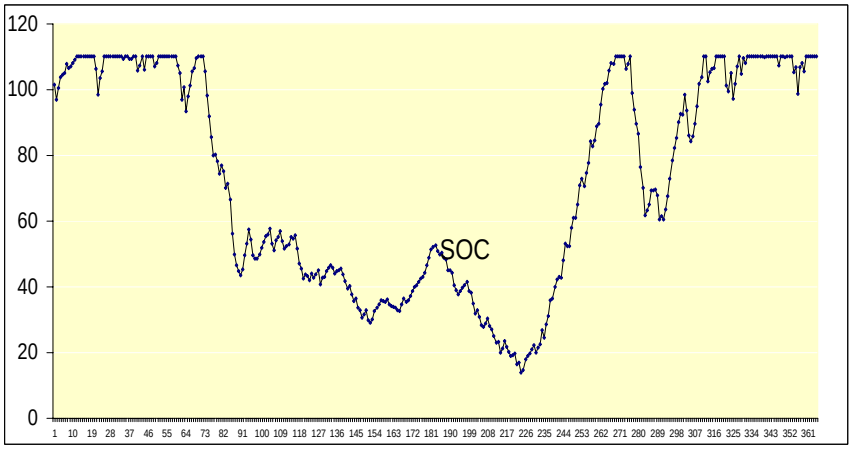

Figure 5 Case D: State of charge (SOC) of the battery bank

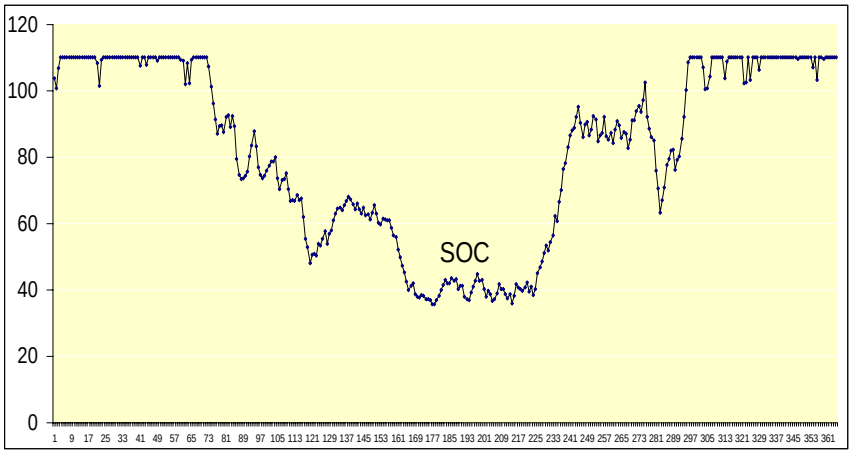

Figure 6 Case E: State of charge (SOC) of the battery bank

Conclusion and Remarks

An accurate sizing procedure of components of PV hybrid power system, which is designed to produce electricity and fresh water for remote located communities, has been presented.

This paper compares five different cases. In each case the size of PV array is determined according to PSHs of four seasons. While in case number 5 the size of PV array is determined according to annual average PSHs. Size of PV array has direct effect on the operational time of Gen Set and consequently the annual fuel consumption.

This arrangement offers all the benefits of PV systems with respect to low operation and maintenance costs, and also ensures that PV electricity is not wasted.

This paper has also presented an approach for evaluating the performance of PV hybrid power systems. The computer program that our research group has developed is in fact a useful tool for optimum sizing of the components in any PV hybrid power system for any application, as well as predicting the performance of the power system. As the battery is the weakest component in the system, the performance prediction of the system is mainly based on the SOC (state of charge) of the batteries.

This program is a useful tool as it makes possible for PV engineers to ensure that a designed PV system, before being installed, is able to perform as expected. The program can be used for any locations by any applications provided solar radiations data are available and daily electricity consumption are known.

Acknowledgement

Author is grateful of contribution made by his students Ms. Eunyeong Kim and Mr. William Lei Wang to carry out this project.

References

[1] Sun Utility Network, Sustainable Solution Provider website: http://www.sunutility.com/html_pg/residensial.html
[2] Website of the International Solar Energy Society: http://www.iea.org/

[3] Kellogg, W., M. H. Nahrir, G. Venkataramanan, and V. Gerez, “Generation unit sizing and cost analysis for stand-alone wind, PV, and hybrid wind/PV systems,” IEEE Trans. On Energy Conversion, vol. 13, no. 1, March 1988.
[4] Chedid R. and S. Rahman, “Unit sizing and control of hybrid wind-solar power systems, “IEEE Trans. On Energy Conversion, vol. 12, no. 1, March 1997.
[5] Salameh, ZM, M. A. Casacca, and W. A. Lynch, “A mathematical model for lead acid batteries, “IEEE Trans. on Energy Conversion, vol. 7, no. 1, March 1992.
[6] Zahedi, A. “Design aspects of PV-hybrid power systems”, Journal for Renewable Energy, vol., no. , 2000
[7] Zahedi, A. “Solar photovoltaic energy systems; design and use”, the new World Publishing, 1998, Australia.
[8] Zahedi, A. “Engineering and Economics of solar photovoltaic energy systems”, The new World Publishing, 2004, Australia
[9] US Department of Energy Website: http://www.eere.energy.gov/consumerinfo/heatcool.html
[10] Electricity Australia 2003, published by Electricity Supply Association of Australia Limited (ESAA), website: http://www.esaa.com.au/

Design Considerations and Tidal Power from Sonmiani Bay

Afzal Ahmed[*], Jameel Ahmed Khan[+], Gul Rehman[+]

*Professor, National University of Science and Technology, Pakistan Navy Engineering College, Karachi, E.mail: ahmed_462001@yahoo.com
[+] NED University of Engineering & Technology, Karachi

Keywords: Tidal , Energy, renewal energy, ocean energy

Abstract

Because of increasing population and urbanization, agricultural and industrial growth the energy demand in Pakistan is currently growing at the rate of 4 % per year. The country is spending $ 3 billion in the import of oil which has a dent in the economy. The situation warrants exploring all avenues of energy. The country is blessed with sea and tides can also be a source of energy. Hence Sonmiani Bay at the Arabian coast line has been investigated as a source of tidal power. The average tidal head obtained is 2.12meter and 50MW is the tidal power available and 20 MW of energy could be realized. Consideration in the design of Sluice Gate, and Turbine have been elaborated.

1. Introduction

Pakistan is a developing country and has a population of about 160 million. It is experiencing burgeoning urbanization. The changing life style of people and the industrial growth enhanced energy consumption. The country has limited conventional resources of energy such as oil, gas and coal. In early nineties oil production was about 42 million barrels annually [1]. The gas reserves are estimated as 662 billion cubic meter [1]. Coal reserves are estimated at 17 billion tons [1]. However, much of the coal has a low calorific value and a high ash and sulfur content, which limits its value and use. Because of limited traditional energy resources, Pakistan is giving emphasis on renewable energy. Hydroelectric power is already a major energy source generating 28% of the electricity of the country. At present Tarbela dam located on Indus river has the installed capacity of 2164 megawatt and Mangla dam situated at Jehlum river has the installed capacity of 125 megawatt[1]. Hydroelectric power potential is estimated as 1000 megawatt and more new sites for dams for hydroelectric power generation are being developed At present Pakistan has two nuclear power plant. One at Karachi producing 125 megawatt of electricity and other at Chashma producing 300megawatt energy[1]. Pakistan is now placing more emphasis on nuclear energy to meet future energy requirements. It is expensive and difficult to connect the rural remote areas to national grid, so the government is planning to harness solar power to provide electricity to rural remote areas. According to a recent media report a plan envisages the development of 3000 megawatt electricity by 2020, whereas it is also reported that Pakistan could face up to 5000 megawatts of power shortage by 2010 [2]. This is going to be a troubling situation , hence all avenues of tapping energies must be explored that is efforts must be directed towards renewable energy resources- wind, solar, micro hydro, tidal energy, wave energy, ocean thermal energy, fuel cell, biomass ,biogas. Pakistan is blessed with the Arabian sea shore and tides can also be a source of energy. This paper investigates the Sonmiani bay as a possible site for generation of tidal energy.

2. Origin of Tidal Wave

The tides are created due to the gravitational force of the moon and the rotation of the earth. Figure 1 shows how the gravitational forces affect the tide in ocean. The magnitude of attraction will depend on the mass of the object and how far the object is. The moon having much less mass than that of sun has greater attraction because it is much nearer to earth. The gravitational force of the moon forces the ocean water to bulge along an axis towards the moon. The rotation of earth causes the rise and fall of the tides. When the sun and the moon are in line ,their attraction combines and the tide is called spring tide. When they are at 90 degree to each other, their gravitational attraction pulls water in different direction and the resulting tide is called a neap tide. The rotation of moon is around four weeks, while the earth rotates once in 24 hours. This results in tidal cycle of around 12.5 hours.

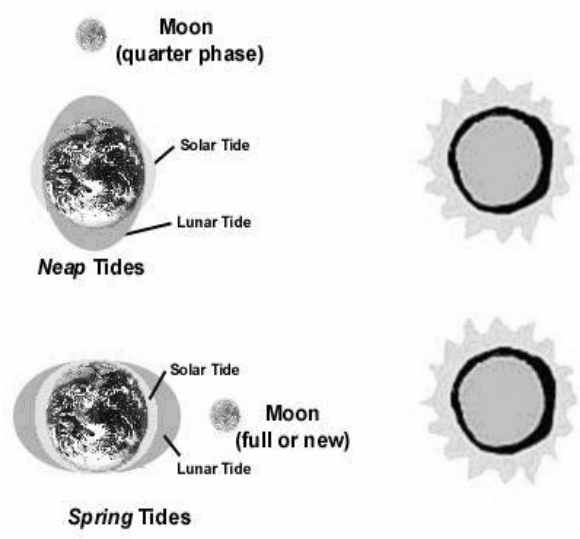

Figure 1: Gravitational effect of the Sun and the Moon on tidal range
Sourced: (ACRE) Australian CRC for Renewable Energy Ltd.

3.Current status of Tidal Energy

In contrast to solar, wind and wave energy, the advantage of the tidal power is highly predictable because of its regularity. The first and largest operational tidal power plant is the La Rance plant on the Brittany coast of northern France at the mouth of the La Rance estuary: the plant produces 240 MW of electricity[3]. Some other operational power plant exist at Kislaya in Russia, Jiangxia in China and Annapolis in Canada[4].Major potential sites are the bay of Fundy in Canada which has a mean tidal range of 11m is the highest tide in the world and Severn Estuary off Britain[4]. It is estimated that the United Kingdom could generate up to 50.2 TW h/yr with tidal power plants, while western Europe as a whole could generate up to 105.4 TW h/yr. Total world wide potential is estimated to be about 500-1000 TW h/yr, though a fraction of this energy is likely to be exploited due to economic constraints[4]. Table 1 shows the mean tidal range, the basin area and the installed capacity of various potential sites in different part of world for tidal energy projects[5].

4.Elements of Tidal Power System

As shown in Figure 2 a huge dam or barrage is built across an estuary that experiences an adequate tidal range. The barrage has sluice or gates built in it. The sluice is opened to allow the tide to flow into estuary. The water is trapped in the estuary and produces hydrostatic head. As the sea level drops the gates in the barrage that contains turbine are opened. The hydrostatic head causes the water to flow through these gates driving the turbine and generating power. Power can be generated in both directions through the barrage but at the cost of efficiency.

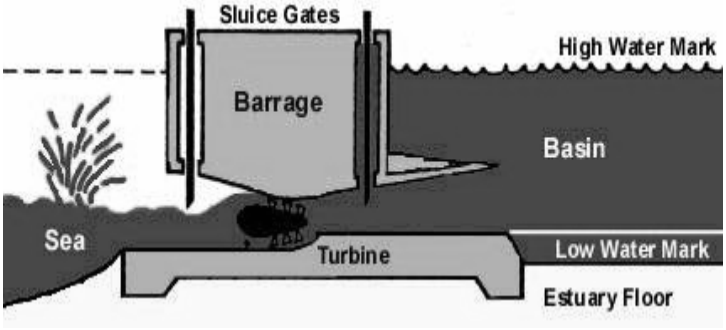

Figure 2: Elements of a tidal energy generating system.

(Adapted from Energy Authority of NSW Tidal Power Fact Sheet) Sourced: (ACRE) Australian CRC for Renewable Energy Ltd.

5.Tidal Energy from Sunami Bay

Baluchistan- a province of Pakistan has the coast line with Arabian sea and Sonmiani Bay is situated along this coast line. With the cooperation of National Institute of Oceanography and Naval Hydrographic Department tide data for 29 days was used to find the maximum height and the minimum height of the tide. The data is tabulated in Table2. The average tidal range is given by the relation:

$$H_{day} = \frac{H_{max} + H_{min}}{2} \qquad [1]$$

Where H_{day} = average tidal range in m
H_{max}= tidal range at maximum tide in m
H_{min}= tidal range at minimum tide in m

From the data of Table 2 the average tidal range is calculated as 2.12 m and is assumed to be the average for the whole year. Area of the Sonmiani basin for high water level is 150 km^2. Since the sea water is not maintaining the high level for whole year hence the area for low water is used which is about one third of high water level [6]. Hence an area of 50 km^2 is taken for the basin.
The famous experts in tidal power such as Gilrat in 1906, Bernshtein in 1939 and Mosonyi in 1963 have calculated the potential energy of tidal power by the following empirical relation [7]:

$$E_p = K \times 10^6 \times AR^2 \qquad [2]$$

Where K= constant

Table1: |Prospective sites for tidal energy projects

Country	**Country**	**Mean tidal range (m)**	**Basin area (km^2)**	**Installed capacity (MW)**
Argentina	San José	5.8	778	5 040
	Golfo Nuevo	3.7	2 376	6 570
	Rio Deseado	3.6	73	180
	Santa Cruz	7.5	222	2 420
	Rio Gallegos	7.5	177	1 900
Australia	Secure Bay	7.0	140	1 480
	Walcott Inlet	7.0	260	2 800
Canada	Cobequid	12.4	240	5 338
	Cumberland	10.9	90	1 400
	Shepody	10.0	115	1 800
India	Gulf of Kutch	5.0	170	900
	Gulf of Khambat	7.0	1 970	7 000
Korea (Rep.)	Garolim	4.7	100	400
	Cheonsu	4.5		
Mexico	Rio Colorado	6-7		
UK	Severn	7.0	520	8 640
	Mersey	6.5	61	700
	Duddon	5.6	20	100
	Wyre	6.0	5.8	64
	Conwy	5.2	5.5	33
USA	Pasamaquoddy	5.5		
	Knik Arm	7.5		2 900
	Turnagain Arm	7.5		6 500
Russian Fed.	Mezen	6.7	2 640	15 000
	Tugur *	6.8	1 080	7 800
	Penzhinsk	11.4	20 530	87 400

Table 2: Minimum and maximum level of tides and average tidal range from 25th October to 22nd November,1987.

Date	H_{min} (m)	H_{max}(m)	H_{day}(m)
25 Oct.	0.55	2.84	1.69
26	0.60	2.90	1.75
27	0.70	2.60	1.65
28	0.8	2.90	1.85
29	1.10	2.70	1.90
30	1.70	2.80	2.25
31	1.70	2.80	2.25
1stNov.	1.30	2.95	2.13
2	1.00	3.10	2.05
3	0.80	3.10	1.45
4	0.55	3.25	2.40
5	0.6	3.20	1.90
6	0.64	3.22	1.93
7	1.55	3.22	2.39
8	0.64	3.38	2.02
9	1.16	3.54	2.85
10	1.22	3.05	2.13
11	1.52	2.96	2.24
12	1.65	3.05	2.35
13	1.65	2.87	2.26
14	1.92	2.93	2.45
15	1.52	2.99	2.25
16	1.5	3.12	2.32
17	1.4	3.00	2.20
18	1.2	3.20	2.20
19	1.00	3.30	2.15
20	0.91	3.35	2.13
21	0.73	3.35	2.13
22	0.85	3.44	2.15

A= area of basin in km^2
R= average tidal range in meter
E_p= potential energy of tidal power in kW h/yr

The value of K given by Bernstein and Gibrat is 1.97 and by Mosonyi 1.92. In the present analysis the value of K is taken as 1.97[7]. On substitution of the values in the equation 2, The value of E_p is 442.6984×10^6 kWh/yr. Hence the available tidal energy is 50536 kW. Using the utilization factor of 0.4 for ebb generation of power the power which can be extracted is 0.4×50536 kW [6]. That is 20.21 MW.

6. Some Design Considerations

For an economic development of a tidal power plant It is necessary to consider the following points:

1. Design should be functional with maximum economy in construction and minimum operating and maintenance costs.
2. Power plant should based on one-way ebb generation or two way generation depending on the constraints.
3. Water passages should be efficient.
4. Provisions should be made for inspection, maintenance and replacement of equipment.
5. Suitability and requirement be considered of single effect and double effect generating units.
6. Adaptability to construction in the dry or in wet should be taken into account.

6.1 Sluiceways

Tidal power plants operate on the continuously varying difference in level between the water in the basin and the water in the sea. The basin must be filled from the sea or emptied to the sea as required by the operating regime of the power plant so that the production can be coordinated with the load curve of the power network with which it is interconnected.
This requires suitable sluiceways equipped with gates which can be operated quickly and reliably. These gates must be as free from maintenance as feasible. And should be protected from the impact of storm produced waves, masses of ice carried by the flow , freezing of the operating mechanism and the coating thereof with ice as well as damage due to the corrosive nature of the marine environment.

6.2 Selection of turbine

For heads above 2meters, the tube turbine and the bulb turbine can be used in tidal power plants. However, for an output range of 20kW to 4000kW tube turbines are recommended whereas for an output range of 1000kW to 100,000 kW bulb turbines are favored for tidal power plants. A bulb turbine has generator bulb on the upstream side of the Kaplan runner with guide vanes. In contrast tube turbine has external generator and the bulb is of smaller dimensions and serves as housing of the bearing of the shaft.

7.Conclusion

For Pakistan facing energy crisis in the wake of dwindling conventional energy resources and ever rising imported fuel cost extracting energy from the renewable energy sources is imperative and tidal energy offers as one of the prospects. Somniami bay though having a low tidal range of about 2.12 meter has the basin area which has the potential of 50.5 MW energy and 20 MW energy could be realized by hydroelectric generation.

Reference

[1] Pakistan :Environmental issues, August 2003
[2] Pakistan's alternative energy development plan, Islamabad, December 29,2005,IRNA.
[3] Claude H. Lebarbier, Powerfrom tides-The Rance tidal power station, *Naval Engineers Journal,* pp 57-71, April,1975.
[4] T.J. Hammons , Tidal Power. *Proceedings of the IEEE*, 89, 3 pp. 419–433 ,1993
[5] World Energy Council, Survey of engineering resources,http://www.worldenergy.org.wec-geis/edc
[6] D.Prandle, Simple theory of designing tidal power schemes,Adv.Water Resources,Vol. 7,pp 21-27,March1984.
[7] G. Rehman, A.Mehmood ,K.N.Masood,J.A.Samad, *Assessment of tidal power at Sonmiani and design for power generation*, Project Report, Department of Mechanical Engineering, NED University of Engineering and Technology, Karachi,Pakistan

Pyrolysis Characteristics and Kinetics of Palm Shell Waste Mixtures with Mukah Balingian Coal

A. Hussain, F.N Ani, A.N. Darus

Faculty of Mechanical Engineering, Universiti Teknologi Malaysia, 81310, Skudai, Johor.
Corresponding author email**:** ahmadutm@gmail.com

Keywords: Co-combustion, kinetic parameters, poor coals, solid bio fuels, thermogravimetric analysis

Abstract

The coal-biomass co-combustion is one of the most promising short-term options for the use of renewable fuels. This process allows the consumption of fossil fuels to be reduced. Further, the existing coal-fuelled power plants may be generally used with very little modifications. The high volatile matter yield of biomass fuels is an important aspect for the co-gasification. The coal used had an organic fraction too low to support an auto-thermal gasification: the synergistic effects of mixing biomass waste to coals make the co-gasification an attractive and economical utilization of poor coals. The paper presents the results of kinetic parameters and main devolatilisation characteristics of palm shell waste and its blends with sub-bituminous Mukah Balingian coal from Sarawak. The pyrolysis was done in a thermogravimetric analyser, under dynamic conditions. The effect of material particle size and heating rate was investigated both on the pyrolysis behavior and reaction kinetics, over the temperature range of 25-950 ˚C. However, no significant influence of the particle size was detected, both on the devolatilisation characteristics and kinetics. The effect of the heating rate on the pyrolysis behavior was more pronounced for palm shell waste rather than for Mukah coal. Their decomposition kinetics was successfully modeled by first-order reaction, describing the devolatisation of solid fuel. A comparison between slow and fast heating rate tests reveals a small displacement of the DTG profiles to higher temperatures. It was concluded that such `solid bio fuels' could support the combustion of poor coals, because of the faster and in much higher quantity release of volatile compounds

1 Introduction

Malaysia has a coal mining history dating as far back as 1851 when the first coal mine was opened at Labuan. In fact the known coal resources in the country were swiftly dealt with by describing it as of "low quality and of little potential". The present coal resource figure stands at 1,025 million tonnes; 725 million tonnes are found in Sarawak, 282 million tonnes in

Sabah and 17 million tonnes in Peninsular Malaysia. The coal fields are identified as Merit Pila, Bintulu and Mukah Balingian in Sarawak and Malibau coal areas in Sabah. The coal areas of the country are shown in Figure 1. Coal quality ranges from the lignite rank to anthracite; sub-bituminous coal, however, predominates. As a result of the oil crises of 1973 and 1979, it was thought inevitable for energy diversification from oil

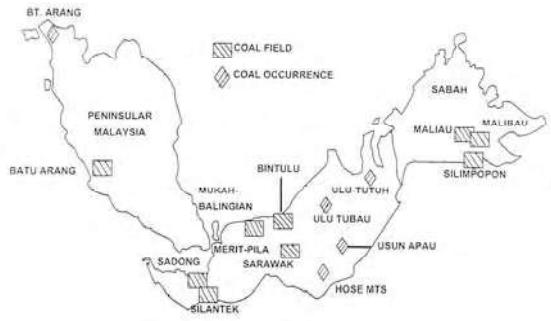

Figure 1: Locations of Coal reserves in Malaysia [1]

In 1980, oil and petroleum products contributed 87.8% of the commercial energy supply, and in 1984 the Malaysia's four-fuel strategy based on oil, gas, hydropower and coal was promulgated. This basically set the scene for greater coal use. The first 600 Mw coal-fired Sultan Salahuddin Abdul Aziz (SSAA) power station in Kapar, Peninsular Malaysia was commissioned in 1985. Since then one additional 100 MW station started operation in 1997 in Sejingkat, Sarawak.

The projected coal demand in Asia to the year 2010 have been a buoyant one, with most countries like Korea, Hong Kong, Philippines, Malaysia, India and Thailand reporting increasing use of coal. Even major coal producing countries like Indonesia and China are projected to face shortage and their capacity for export is expected to be largely curtailed, with production barely matching local demand. Australia has been looked on to meet the increase in coal demand by

stepping up production and export. The power generation mix in Malaysia is shown below.

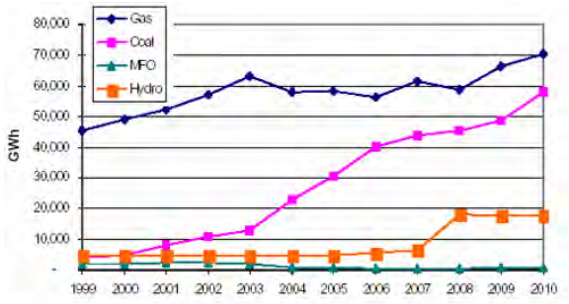

Figure 2: Power Generation Mix in GW [2]

In the background of this regional development, Malaysia was projected for steep increase in coal use in the next decade with the construction of at least 2 more cement plants and several large coal fired power stations. Within Malaysia, there is a large market for coal, and the demand is projected to rise steeply to a total of about 14 million tonnes, to the year 2010. Although it may not be possible to meet this entire demand by indigenous sources, estimate shows that it may be possible to produce 6.2 million tonnes, or 40% of the demand. The focus of this projection is that the attractive coal deposits like Mukah coal in Sarawak which have not been utilized much. This study is focused on identifying the pyrolysis behaviour of Mukah coal and its blends with oil palm shell waste.

2 Thermogravimetric analysis (TGA) of Mukah coal and its blends

In this paper, pyrolysis of Mukah coal and its blends, were carried out using thermogravimetric analysis (TGA). The effects pyrolytic temperature and heating rate on the pyrolytic properties (for example, the shape of thermograms) were investigated to determine the main factor affecting the pyrolytic process.

The samples were dried to remove free moisture absorbed. The pre-dried samples were crushed and sieved to several size fractions. The pyrolysis was carried out using a thermogravimetric analyzer (Perkin Elmer Pyris TGA). Approximately, 20 mg sample was placed in a platinum pan, which was suspended by a platinum wire. The furnace was heated from ambient temperature to a programmed temperature of 1000 °C at a constant heating rates (25 & 80 °C/min). Purified nitrogen (99.9995% purity) at a constant flow rate was used as the purge gas to provide an inert atmosphere for pyrolysis and to remove any gaseous and condensable products evolved, thus minimizing any secondary vapor-phase interactions. The sample was heated by both radiation from the furnace wall and convection of the purge-gas rushing through the furnace chamber. The sample weight was measured continuously by a microbalance as a function of time or temperature.

3 Determination of kinetic parameters

Thermogravimetric data is used in characterizing the fuel as well as in investigating the thermodynamics and kinetics of the reaction and transitions that results from the pyrolysis of samples. TGA is useful in providing kinetic data as a function of various reaction parameters such as temperature and heating rate [3]. Currently several methods were available in the literature that can be used to calculate kinetic parameters [4]. The rate of reaction is given by:

$$\frac{d\alpha}{dt} = A e^{-E/RT} (1-\alpha)^n \qquad (1)$$

where A (min^{-1}) is the frequency or pre-exponential factor of the pyrolytic process, E (J/mol) is the activation energy of the pyrolytic process, R (J/mol K) is the universal gas constant, T (K) is the absolute temperature, n is the order of reaction, t is the time, and α is the fraction of reactant decomposed at time t (min).

The fractional reaction α is defined in terms of change in the mass of the sample

$$\alpha = \frac{w_o - w}{w_o - w_f} \qquad (2)$$

Where w_o, w, w_f are the initial, actual and final weights (mg) of the sample, respectively.

In order to determine the values of kinetic parameters, the integral method is used to solve Equation (1).

For constant heating rate β :

$$\beta = \frac{dT}{dt} \qquad (3)$$

Equation (1) can be expressed by the following equation:

$$\frac{d\alpha}{dT} = \frac{A}{\beta} e^{-E/RT} (1-\alpha)^n \qquad (4)$$

Rearranging and integrating Equation (4),
the following expressions can be obtained:

$$\frac{1-(1-\alpha)^{1-n}}{1-n} = \frac{A}{\beta} \int_0^T e^{-E/RT}\, dT \qquad (5)$$

Since $\int e^{-E/RT}\, dT$ has no exact integral, $e^{-E/RT}$ can be expressed as an asymptotic series and integrated, with the higher order terms ignored.

$$\frac{1-(1-\alpha)^{1-n}}{1-n}=\frac{ART^2}{\beta E}\left[1-\frac{2RT}{E}\right]e^{-E/RT} \qquad (6)$$

Expressing Equation (6) in logarithmic form

$$\ln\left[\frac{1-(1-\alpha)^{1-n}}{T^2(1-n)}\right]=\ln\left[\frac{AR}{\beta E}\left[1-\frac{2RT}{E}\right]\right]-\frac{E}{RT}\ (for\ n\neq 1) \qquad (7)$$

If 2RT/E << 1 is assumed, Equation (7) becomes

$$\ln\left[\frac{1-(1-\alpha)^{1-n}}{T^2(1-n)}\right]=\ln\left[\frac{AR}{\beta E}\right]-\frac{E}{RT}\ (for\ n\neq 1) \qquad (8)$$

If n=1, the following equation can be used

$$\ln\left[-\frac{\ln(1-\alpha)}{T^2}\right]=\ln\left[\frac{AR}{\beta E}\right]-\frac{E}{RT}\ (for\ n=1) \qquad (9)$$

Thus, a plot of

$$\ln\left[\frac{1-(1-\alpha)^{1-n}}{T^2(1-n)}\right]\ versus\ \frac{1}{T}\ (for\ n\neq 1) \qquad (10)$$

or

$$\ln\left[-\frac{\ln(1-\alpha)}{T^2}\right]\ versus\ \frac{1}{T}\ (for\ n=1) \qquad (11)$$

should result in a straight line of slope –E/R for the proper value of n. The criterion used for the acceptable values of E and A is that the final value of n should yield the values of E whose linear correlation coefficient are the best.

4 Results and discussions

Figure 3 shows the residual weight fractions of Mukah coal undergoing pyrolysis for heating rates of 25 and 80 °C/min. Figure 3 also shows the thermal events observed during pyrolysis. It should be noted that each thermal event is defined as the region where the slope of TGA curve is constant. A major shift in the slope of the TGA curve was thus treated as the end of a thermal event and commencement of a new thermal event. The thermograms shows that as the heat wave propagates into the solid then inherent moisture evaporates and this ends at about 130 °C. This is represented by 'Thermal Event 1' in Figure 3. As the temperature is further increased, the breakdown of more stable polymers begins. The thermograms showed that pyrolysis commences after about 260 °C. Subsequently, it showed a significant weight loss, indicating the occurrence of main decomposition. These are represented by 'Thermal Event 2' and 'Thermal Event 3'. Similar trends for the Mukah coal blends with oil palm shell wastes having 10% 0r 20% coal are shown in Figures 4-5.

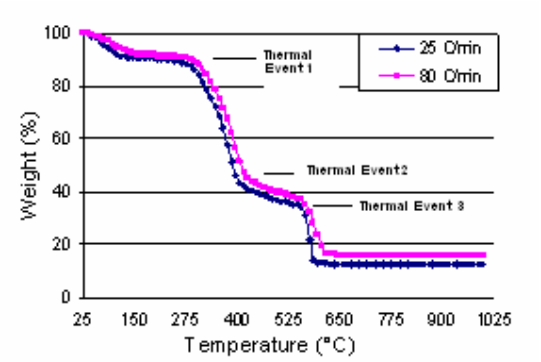

Figure 3: Variation of weight percent with time for pyrolysis of different Malaysian coals at a heating rate of 25 °C/min

.

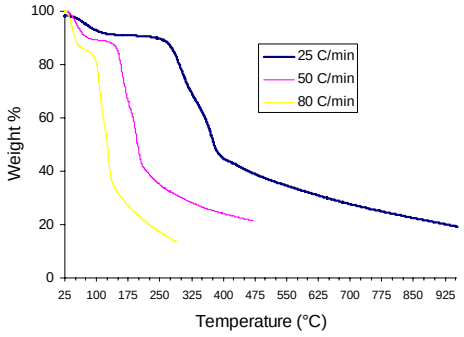

Figure 4: Variation of weight percent for pyrolysis of 10% coal blend at different heating rate

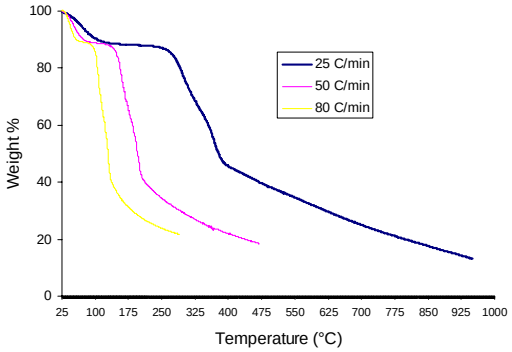

Figure 5: Variation of weight percent with temperature for pyrolysis of 20% coal blend at different heating rate

At the beginning, CO_2 and CO were released as the main gaseous products and at the main decomposition period, a large amount of gaseous products such as CO_2, CO, H_2 and hydrocarbons (i.e. CH_4; C_2H_4; C_2H_6) were released, resulting in a significant weight loss

The heating rates influence the shape of the TGA curve. When a sample decomposes then the vapour pressure of the gaseous products exceeds the ambient partial pressure. At lower heating rates the sample temperature is more uniform and diffusion of the product gases can occur through the sample but when the heating rate is increased then such free diffusion is inhibited and decomposition temperature is increased. Also it was found that at lower heating rates the decomposition atmosphere is more uniform and the decomposition reaction is completed within a narrower temperature interval.

Figure 4-5 shows the residual weight fractions for pyrolysis of coal blends at various heating rates. It could be seen that there is an obvious lateral shift in the thermograms for different heating rates. In addition, there is an effect of heating rate on the total weight loss. As the heating rate was increased, a faster pyrolytic reaction occurred, resulting in higher pyrolytic conversion to volatile species.

In Figure 6, the main decomposition for Mukah coal was essentially completed by an elapsed duration of 9 min and 15 min for heating rates of 80 and 25 °C/min respectively.

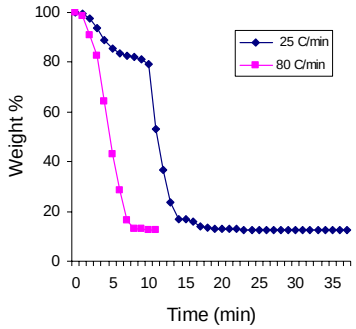

Figure 6: Variation of weight percent with time for pyrolysis of Mukah coals at different heating rates

Figures 7 show the derivative thermograms (dm/dt) for the pyrolysis of Mukah coal at various heating rates. The height of the peak at any temperature gives the rate of mass change at that temperature.

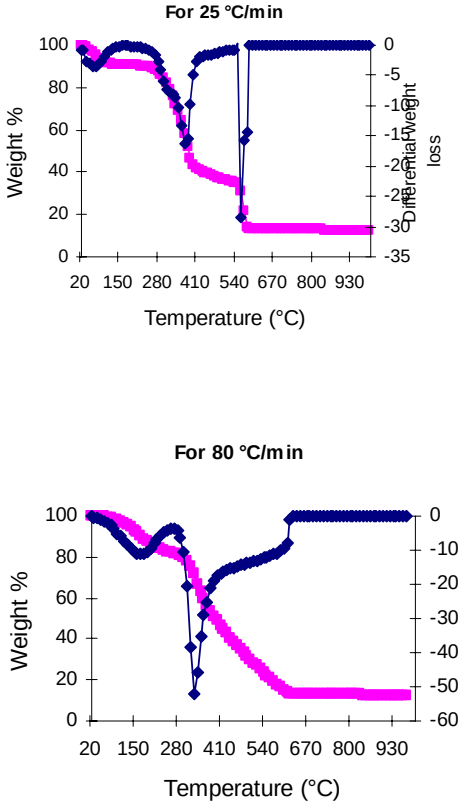

Figure 7: Differential thermogram (DTG) for pyrolysis of different Mukah coal at a heating rates of 25 and 80 °C/min

Figures 7, suggest that for the heating rates 25 and 80 °C/min the maximum decomposition rates are 30 and 50 mg/°C. The decomposition rates are identical for different particle sizes as the particle sizes below 2 mm are primarily considered as fine particles and their pyrolysis is pure reaction kinetics controlled. It could be seen clearly that there existed separate steps of reactions that took place in distinct temperature regimes with obvious maximas for different heating rates. The heating rate had influenced not only the maximum rate of pyrolysis and its temperature, but also the starting and ending temperatures for the pyrolytic process. This phenomena is also confirmed by the fact that there was a lateral shift to higher temperatures during pyrolysis as the heating rate was increased.

Using data from the pyrolysis thermograms (Figures 3-5, the kinetic parameters, the activation energy (E) and the frequency factor (A), were estimated using Figure 8 with high correlation coefficients (above 0.94) and all results are listed in Table 1.

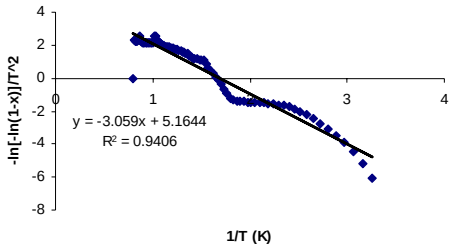

Figure 8: Determination of kinetic parameters using curve fitting

Table 1: Kinetic Parameters for the pyrolysis of Mukah coal and its blends

Fuel Type	**Heating rate °C/min**	**Activation Energy 'E' kJ/mole**	**Frequency factor 'A' 1/sec**
Mukah Coal	25	110.6	1.05×10^4
	80	123.6	9.4×10^3
10% Blend	25	100.8	4.9×10^3
20% Blend	25	93.3	4.2×10^3

For all the heating rates, the orders of reaction were first-order reaction mechanism for all fuels. As the heating rate was increased, the activation energy changed a bit but the frequency factor was dependent on heating rate, increasing progressively from 9.4×10^3 to 1.04×10^4 sec^{-1} for Mukah coal. This suggests that the higher the heating rate, the easier and faster would be the pyrolytic reaction. These parameters can be used to predict the time-conversion profiles for the pyrolytic process of different heating rates. A similar pyrolytic behaviour can be seen for 10% and 20% coal blends with oil palm shell wastes.

5 Conclusions

Based on the thermogravimetric analysis, pyrolytic temperature and heating rate were found to have significant influences on the pyrolysis of Mukah coal and its blends. The two-stage reaction characteristic was confirmed by obvious maximas in the derivative thermogram (DTG) for pyrolysis under different heating rates. DTG curves suggest that heating rates affect the decomposition rates. However, as the particle were primarily fine particles so the pyrolysis was not affected by particle size rather it was found to be pure reaction kinetics controlled. It could be seen clearly that there existed separate steps of reactions that took place in distinct temperature regimes with obvious maximas for different heating rates. Kinetic parameters (activation energy and frequency factor) were obtained by curve fitting the experimental data.

Acknowledgement

The author (AH) would like to thank Malaysian Government Commonwealth Secretariat, Public Service Department Malaysia (JPA), Putrajaya for funding the PhD program. Thanks are due to SIRIM Environment and Bioprocess Technology Centre for granting permission to use their experimental facilities

References

[1] Pei, C. K. (2000). The status of Malaysian coal industry. *Proceedings of the Asia Pacific Mining and Quarrying (APMQ) 2000*, Kuala Lumpur, Malaysia , 123-139.

[2] Cox, R., Chen, S.P., Hon, V., Unya, A. and Batoi, R. (2000) . Economic geology and mineral potential of west Sarawak, Malaysia. *Proceedings of the Asia Pacific Mining and Quarrying (APMQ) 2000*, Kuala Lumpur, Malaysia , 155-174.

[3] Ismail , A. F., Shamsuddin, A. H. and Mahdi F. M. A. (1999). Reactivity studies of rice husk combustion using TGA. *Proceedings of the World Renewable Energy Congress, Malaysia*, 44-50.

[4] Guo, J. and Lua, A. C. (2001). Kinetic study on pyrolytic process of oil palm solid waste using two step consecutive reaction model. *Biomass & Bioenergy* 20: 223-233.

The Study and Evaluation of Maximum Power Point Tracking Systems

Balakrishna S, Thansoe, Nabil A, Rajamohan G, Kenneth A.S., Ling C. J.

School of Engineering & Science,
Curtin University of Technology,
Sarawak Campus, Malaysia
Tel: +60 –85 – 443825
Fax: +60 –85 - 443939
E-mail: balakrishna@curtin.edu.my

Keywords: Maximum Power Point Tracking, Perturb and Observe, Incremental Conductance, Open Circuit, Short Circuit, Renewable Energy

Abstract

The Maximum Power Point Tracking (MPPT) is a technique used in power electronic circuits to extract maximum energy from the Photovoltaic (PV) Systems. In the recent days, PV power generation has gained more importance due its numerous advantages such as fuel free, requires very little maintenance and environmental benefits. However, high initial cost and low energy conversion efficiency are the two major obstacles for the use of PV systems. To improve the energy efficiency, it is important to operate PV system always at its maximum power point. So far, lot of research is carried out and many papers were published and proposed various methods for obtaining maximum power point. But, among the available techniques sufficient comparative study particularly with variable environmental conditions is not done. This paper is an attempt to study and evaluate four main types of MPPT techniques namely Perturb and Observe, Incremental conductance, Open-circuit voltage and Short-circuit current. The detailed comparison of each technique is reported. The SIMULINK simulation results of P and O and IncCond methods with changing radiation and temperature are presented.

1 Introduction

To meet the ever-increasing energy demand, the world is focussing on and very keen to search for the alternative energy resources. Among the available Renewable Energy (RE) sources, energy from the PV is gaining more importance and is used in wide variety of applications. The current conversion efficiencies of renewable energy systems are quite low particularly for the PV systems; the efficiencies are in the order of 12 to 15%. The maximum power point tracker is used with PV modules to extract maximum energy from the Sun [1]. Typical characteristics of the PV module shown in Fig.1 clearly indicate that the operating point of the module (intersection point of load line and IV characteristic) is not same as the maximum power point of the module. To remove this mismatch or to operate the module at MPP, a dc-to-dc power electronic converter is accompanied with the PV system as shown in Fig.2 [2]. The electrical characteristics of PV module depend on the intensity of solar radiation and operating temperature. Increased radiation with reduced temperature results in higher module output [12]. The aim of the tracker is to derive maximum power always against the variations in sunlight, atmosphere, local surface reflectivity, and temperature.

Finding the location of MPP of PV module requires a special search algorithm. Based on the algorithm, the converter is fed with the corresponding PWM signal derived from the calculation performed by the microcontroller [1].

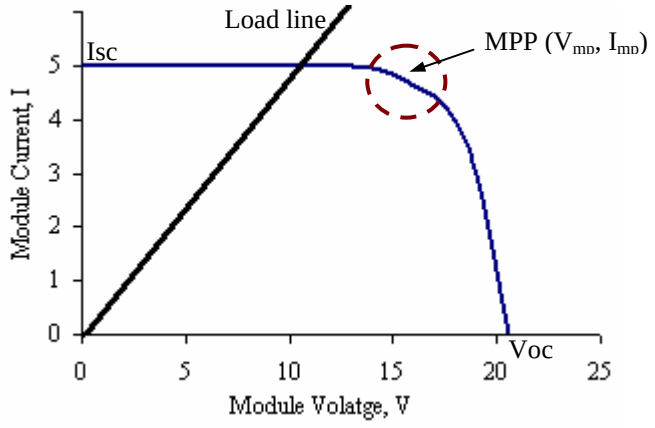

Figure 1: PV Module Characteristics

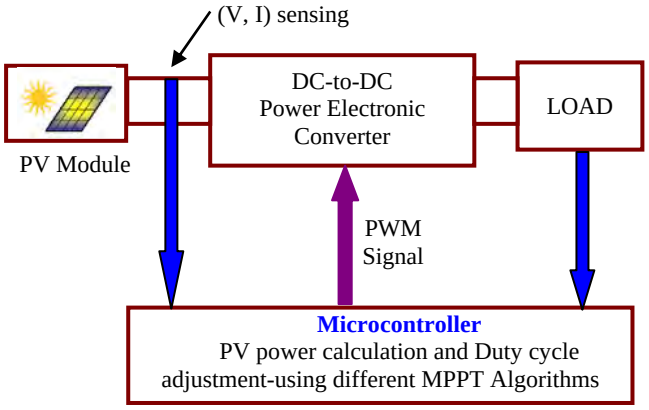

Figure 2: Microcontroller based MPPT System

2 MPPT Methods

The tracking algorithm works based on the fact that the derivative of the output power P with respect to the panel voltage V is equal to zero at the maximum power point as in Fig.3. The module P-V characteristics are shown in Fig.2 show further that the derivative is greater than zero to the left of the peak point and is less than zero to the right.

$$\partial P/\partial V = 0 \text{ for } V = V_{mp} \quad (1)$$

$$\partial P/\partial V > 0 \text{ for } V < V_{mp} \quad (2)$$

$$\partial P/\partial V < 0 \text{ for } V > V_{mp} \quad (3)$$

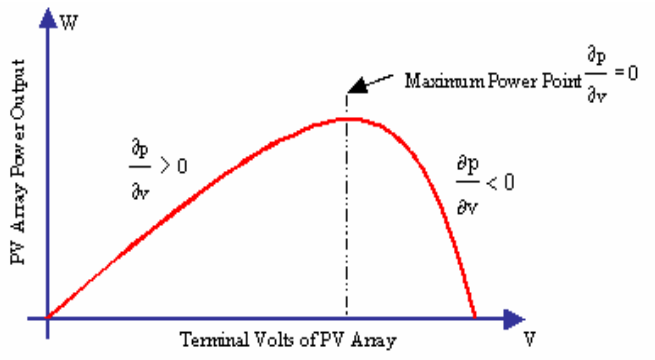

Figure 3: P-V Characteristics of a module

In the literature, various MPP algorithms are available in order to improve the performance of PV system by effectively tracking the MPP. However, most widely used MPPT algorithms are considered here, they are

a) Perturb and Observe (P&O)
b) Incremental conductance (InCond)
c) Open Circuit Voltage
d) Short Circuit Current

2.1Perturb and Observe

The most commonly used MPPT algorithm is P&O method and is also known as hill-climbing algorithm. This technique employs simple feedback arrangement and few measured parameters. In this approach, the array voltage is periodically given a perturbation and the corresponding output power is compared with that at the previous perturbing cycle. However, the operating point oscillates around the MPP as the system is continuously perturbed. This method can be implemented easily [4].

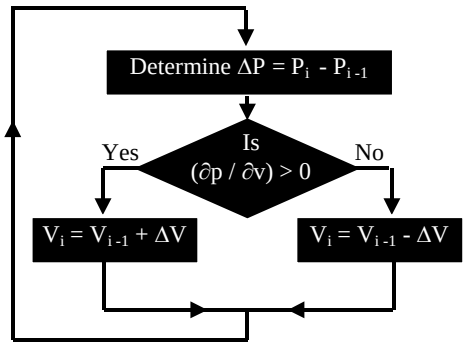

Figure 4: P and O

In this simple algorithm, the operating voltage is perturbed with a small change $\pm\Delta V$ and the power output is observed. Depending on the sign of observed power, further perturbation will be given to voltage as described in Fig.4.

2.2 Incremental Conductance

In this method, incremental conductance is compared with instantaneous conductance. We have,

$$P = V\,I \quad (4)$$

Applying the chain rule for the derivative of products yields to

$$\partial P/\partial V = [\partial(VI)]/\partial V = I[\partial V/\partial V] + V[\partial I/\partial V] = I + V[\partial I/\partial V] \quad (5)$$

At MPP, as $\partial P/\partial V=0$, the equation (5) could be written in terms of array voltage V and array current I as

$$\partial I/\partial V = -I/V \quad (6)$$

Here $\partial I/\partial V$ is an incremental conductance where as I/V is an instantaneous conductance. The microcontroller shown in Fig.2 regulates the PWM control signal of the dc – to - dc converter until the condition: $(\partial I/\partial V) + (I/V) = 0$ is satisfied.

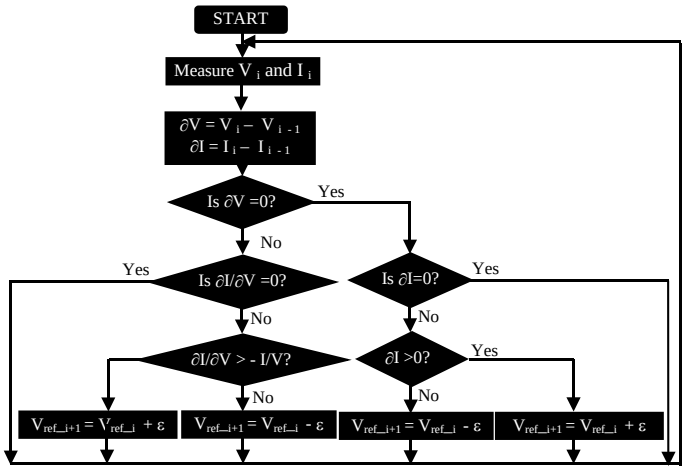

Figure 5: Incremental Conductance

Detailed flowchart of the IncCond algorithm is depicted in Fig.5. The aim is to find and adjust the module operating voltage by maintaining MPP condition through simple incremental conductance and instantaneous conductance measurement [5]. The microcontroller regulates the duty cycle of the converter.

2.3 Open-Circuit Voltage

This technique is also known as constant voltage method. It uses fraction of open circuit voltage to determine the module's voltage at the maximum power point [6].

$$V_{mp} = k_1 * V_{oc} \quad (7)$$

Here the factor k_1 is always <1. Fig.6 shows the flow chart of this method. It looks very simple but determining best value of k_1 is very difficult and k_1 varies from 0.73 to 0.8. The

common value used is 0.76; hence this algorithm is also called as 76% algorithm [6].

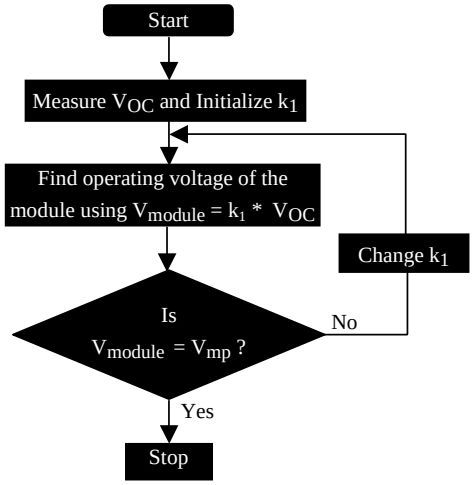

Figure 6: Open Circuit voltage

2.3 Short -Circuit Current

This technique is similar to the open circuit method and is also known as constant current method. It uses fraction of short circuit current to determine the module's current at the maximum power point [8].

$$I_{mp} = k_2 * I_{SC} \qquad (8)$$

The factor k_2 is a constant and is much closer to 1 but always <1. The flow chart is shown in Fig.7.

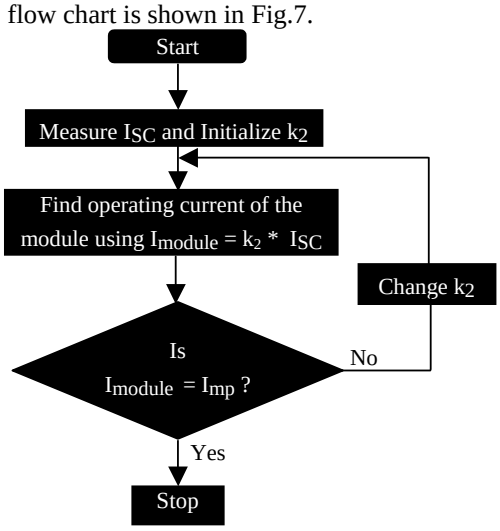

Figure 7: Short Circuit current

When the PV array output current is approximately 90% of the short circuit current, solar module operates at its MPP [8]. In other words, the common value of k_2 is 0.9.

3 Discussion

The inclusion of tracker with PV system increases the energy output approximately 20 to 40% when compared with the system without tracker depending on how we design MPPT [9 – 12]. Microcontroller controls the dc-to-dc converter and performs all control functions required for MPP Tracking process. Low-cost and low powered microcontroller is preferred and microcontroller is complimentary due to its flexibility, compatibility, and quickness. Detailed design aspects of microcontroller based MPPT system are covered in [1,11]. As discussed before, the MPP of a module varies with radiation and temperature as illustrated in Fig.8 and Fig.9. The variation of MPP position under changing conditions demands optimized algorithm, which in turn control the dc-to-dc converter operation (see Fig.2) to increase the PV efficiency.

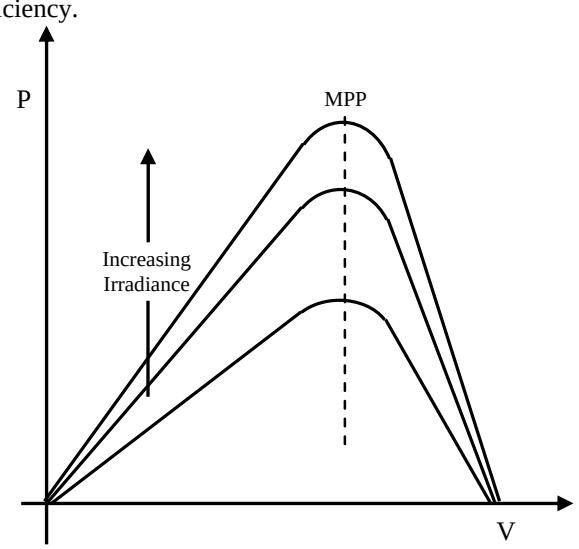

Figure 8: Variation of MPP with changing irradiance but temperature constant

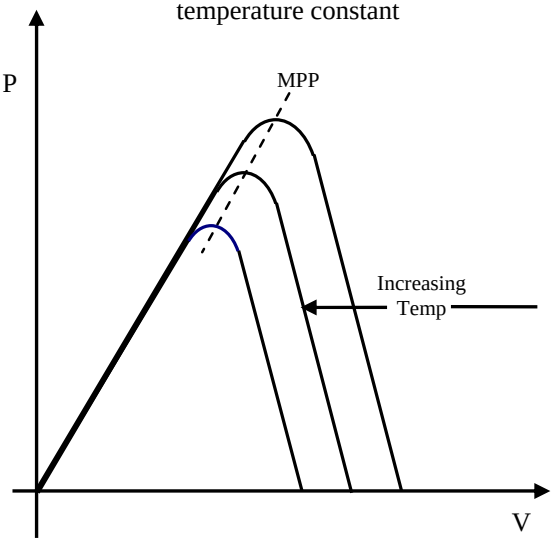

Figure 9: Variation of MPP with changing temperature but irradiance constant

Table.1 shows the detailed comparisons of the above four methods [1, 2, 4, 6 – 12]. Each MPPT algorithm has its own merits and barriers in view of changing environmental conditions.

The Open circuit voltage and short circuit current methods are simple and easy for implementation. However, it is very tedious to find the optimal value of k factor for the changing temperature and irradiance. These methods also suffer from low efficiencies, as it is very tedious to identify the exact MPP. Also, these methods fail to find MPP when partially

shaded PV module or damaged cells are present [9]. The advantage of these methods is, response is quick as I_{SC} or V_{OC} are linearly proportional to the I_{mp} or V_{mp} respectively. Hence, they also give faster response for changing conditions.

Specification	***Perturb and Observe***	***Inc Cond***	***Open Circuit Voltage***	***Short Circuit Current***
Efficiency	Medium About 95% depending on how method is optimized	High About 98% depending on how method is optimized	Low About 90%	Low About 90%
Complexity	Easy but complex when site conditions vary	Difficult	Very simple but very difficult to get optimal k_1	Very simple but very difficult to choose optimal k_2
Realization	Easy to implement as few measured parameters.	More complex, hence microcontroller / DSP is needed.	Easy to implement with Analog hardware	Easy to implement with Analog hardware
Cost	Relatively Lower	Involves higher costs	Relatively Lower	Relatively Lower
Reliability	Not very accurate and difficult to identify whether operating at MPP or not	Accurate and operates at MPP but response time dependent	Not accurate and may not operate exactly at MPP (below to it)	Not accurate and may not operate exactly at MPP (below to it)
Rapidly changing atmospheric conditions. (Varying Radiation & Temp)	Unpredictable performance with oscillations around MPP. Slower response.	Good and automatically adjusts module operating voltage with no oscillations	Faster response as V_{mp} is proportional to the V_{OC} but may not locate correct MPP	Faster response as I_{mp} is proportional to the I_{SC} but may not locate correct MPP
k factor	N/A	N/A	$0.73 < k_1 < 0.8$ $k_1 \approx 0.76$ Varies with Temp and Irradiance	$0.85 < k_2 < 0.9$ $k_2 \approx 0.9$ Varies with Temp and Irradiance
Other Limitations	Difficult to locate the MPP.	Voltage and Current sensors are needed and are usually expensive	Fail to track MPP when partially shaded or cells are damaged	Fail to track MPP when partially shaded or cells are damaged
Power Electronic Converters	Generally Buck converter is used. However, depending on the load requirement, either Buck or Boost or combination such as Buck-Boost or Cuk converters is recommended.			

Table 1: Comparison of MPPT methods

The P & O method is easy to implement as few parameters are to be measured and gives moderate efficiencies about 95%. However, the algorithm becomes complex when rapidly changing site conditions are present and the efficiency depends on how the method is optimised at design stage. The implementation cost of this method is relatively lower. The problems with this method are it gives arbitrary performance with oscillations around MPP particularly with rapidly changing conditions and provides slow response. Sometimes, this method is not reliable as it is difficult to judge whether the algorithm has located the MPP or not.

The incremental conductance method offers high efficiencies about 98%. Even though, this method is complex and difficult to implement, it has several advantages such as more accurate, highly efficient and operates at maximum power point. This method operates very soundly with rapidly changing atmospheric conditions as it automatically adjusts the module's operating voltage to track exact MPP with almost no oscillations. The drawbacks of this method are algorithm is complex, comparatively costlier as it requires microcontroller, and requires V and I sensors with associated peripherals.

3 Simulation results:

The P and O and IncCond methods are implemented in using SIMULINK. Figures 10 and 11 show simulation block diagrams of the P and O and IncCond methods and are realized using the algorithms given in Fig.4 and Fig.5 respectively. The Simulink PV Module model shown has characteristics similar to BP Solar BP280 module [3]. The module manufacturer specifications at STC considered are

Parameter	**Value**
Voltage at MPP, V_{mpp}	17.3 V
Current at MPP, I_{mpp}	4.6 A
Short-circuit current, I_{sc}	5 A
Open circuit voltage, V_{oc}	21.9 V
Maximum Power Rating, P_{mpp}	80 W
Minimum Power Rating, P_{min}	75 W
Coefficient of voltage, α_{SCT}	1.57 mA/^{o}C
Coefficient of current, β_{OCT}	78.2 mV/^{o}C

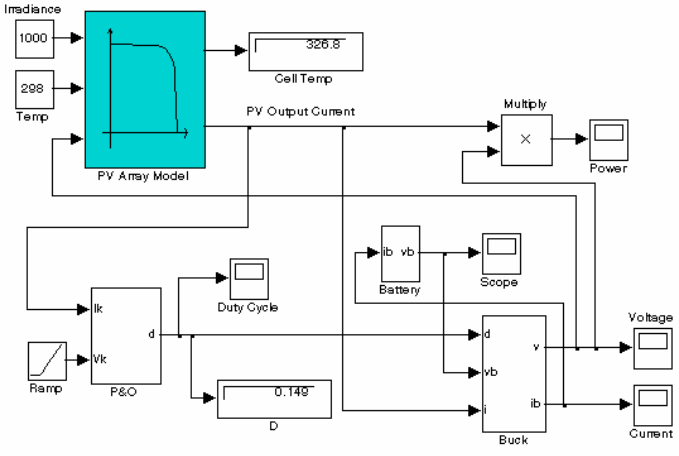

Figure 10: Simulink block diagram of P and O

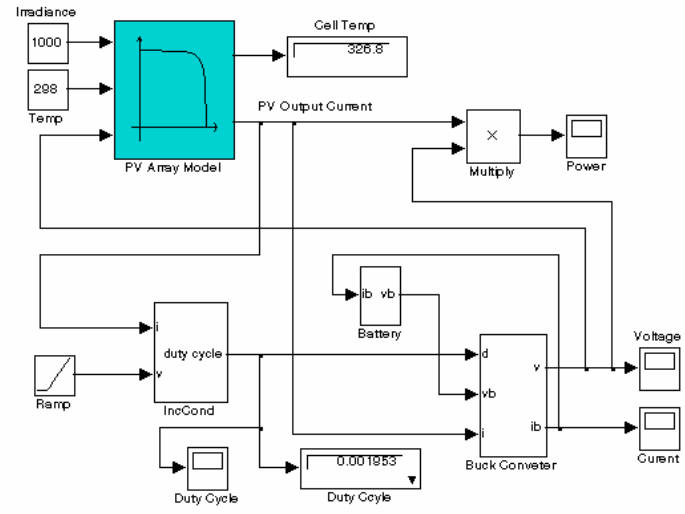

Figure 12: IncCond Simulink block diagram

The Efficiency of maximum power point tracker is defined as

$$\eta_{MPPT} = \frac{\int_0^1 P_{actual}(t)dt}{\int_0^1 P_{max}(t)\,dt} \qquad (9)$$

Where P_{actual} refer to the actual power produced by the module with MPPT included where as P_{max} refer to the theoretical maximum power of the module.

Fig.13 and Fig.14 show the simulation results of the P and O method with changing radiation as 1000w/m^2, 800w/m^2 and 600 w/m^2 and with changing temperature as 298 ^{o}K, 308 ^{o}K and 318 ^{o}K. Where as Fig.14 and Fig.15 show the simulation results of the IncCond method. The results clearly indicate that, the IncCond method is comparatively good in terms of tracking the peak power point (at that particular situation) when irradiation and temperature is changing.

At STC conditions (1000 w/m^2, 298 ^{0}K), the efficiency of P and O method is calculated using Eqn.(9) as 94.32% and for IncCond as 98.45%. These values are relatively high and obviously validate the algorithm of the two methods.

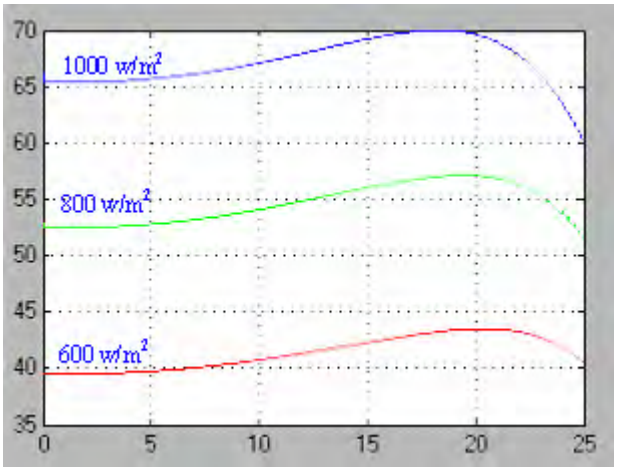

Figure 13: P and O with varying Irradiance and constant Temperature (298 ^{0}K)

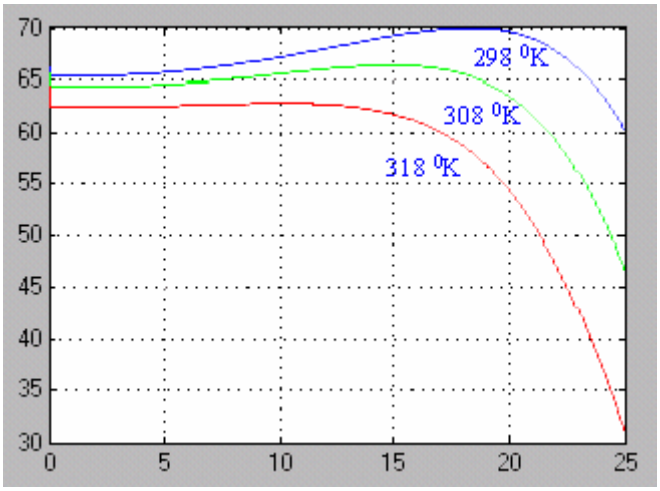

Figure 14: P and O with varying Temperature and constant Irradiance (1000 w/m^2)

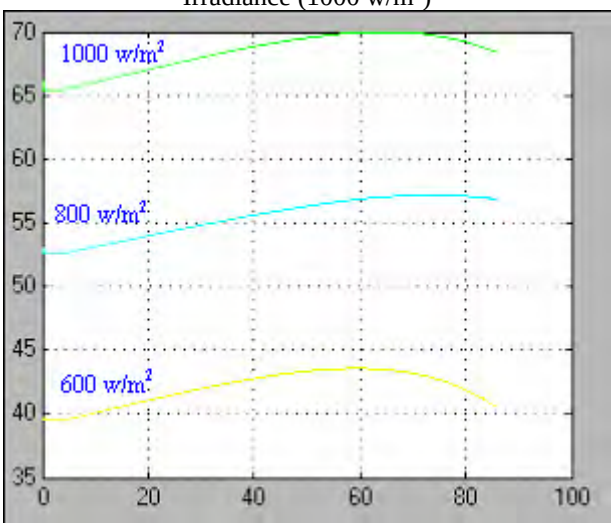

Figure 15: IncCond with varying Irradiance and constant Temperature (298 ^{0}K)

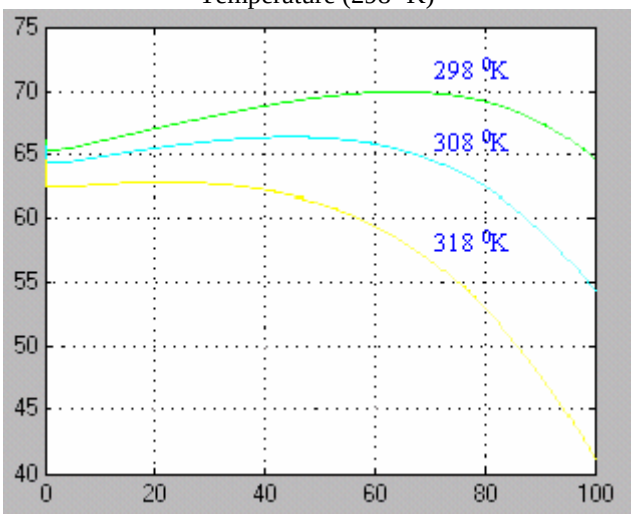

Figure 16: IncCond with varying Temperature and constant Irradiance (1000 w/m^2)

4 Conclusions

The maximum power point tracking is a technique used with PV system to improve its conversion efficiency. To eliminate

mismatch between the load line and I–V characteristic, an MPPT control algorithm is necessary. The derivative of the output power P with respect to the panel voltage V is equal to zero at the maximum power point ($\partial P/\partial V = 0$). Employing microcontroller improves flexibility and fast response. Methodology of four major algorithms P and O, incremental conductance, open circuit voltage and short circuit current are discussed. The conversion efficiency of these methods depends on how it is optimized. Constant current and constant voltage methods are relatively simple and could be realized easily with analog software. The efficiency of these methods is quite low because the algorithm is not very accurate and do not operate exactly at peak power point. The P and O is easy to implement and offers relatively moderate efficiencies but results in unpredictable performance against rapidly changing conditions. The incremental conductance method is complex and expensive when compared to other methods. However, the IncCond method gives very high efficiencies about 98% and performs well with changing radiation and temperature. It can be concluded that, if economical aspect is not a constraint and rapidly changing site conditions are obligatory, the IncCond method is the best choice among the four methods discussed. A comprehensive evaluation of these four methods with the simulation results is also stated. Irrespective of the drawbacks, the incremental conductance is said to be the best method among the four methods discussed in view of tracking the maximum power point.

5 Current Status and Future Prospects

Currently we are developing the PIC Microcontroller based MPPT system using IncCond algorithm. In future, we will build all four MPPT algorithms on a single microcontroller chip along with an artificial neural network / fuzzy logic techniques (to optimise the chosen method to deliver maximum power with varying available resources and site conditions) to experimentally validate this paper.

Acknowledgements

The authors are grateful to A/Prof Chua Han Bing, Director, School of Engineering & Sc, A/Prof Nader Barsoum, Head, Dept of Electrical and Computer Engineering, A/Prof Kaniraj, R & D Director, Curtin University of Technology, Malaysia for their help and encouragement to carry out this work. The author is also obliged to the Management of Curtin University of Technology, Malaysia for their continuous support and for providing computational facilities.

References

[1] S. Balakrishna, V. Gajendra, M. Mohan, M. Suresh, "Design Aspects Of Microcontroller Based Maximum Power Point Tracking Controller For PV System", *Proceedings of 2nd International Conference on Mechatronics 2005*, Vol.1, pp 263 – 269, Malaysia, 2005

[2] Balakrishna S, Keyna Chung, Chua Han Bing, Veeramani S, Rajamohan G, "Design and Simulation of Microcontroller Based MPPT using Incremental Conductance Algorithm", *Proceedings of 2nd International Conference on Electrical and Computer Engineering 2005*, pp 144 -148, Ethiopia, 2005

[3] Wichert B, *Control of PV Diesel Hybrid Energy Systems*, PhD Thesis, Curtin University of Technology, Western Australia, 2000.

[4] D. P. Hohm and M. E. Ropp, "Comparative Study of Maximum Power Point Tracking Algorithms Using an Experimental, Programmable, Maximum Power Point Tracking Test Bed", *IEEE Proc. of photovoltaic specialists conference*, pp1699-1702, 2000.

[5] Keyna Chung, *Design and Simulation of MPPT Using Incremental Conductance Technique*, B. Eng. Thesis, Curtin University of Technology, Sarawak, Malaysia, 2005.

[6] D.P. Hohm, D.P, M.E. Ropp, "Comparative Study of Maximum Power Point Tracking Algorithms, *Journal of Progress in Photovoltaics: Research and Applications*, Wiley Interscience, vol. 11, no. 1, pp. 47-62, 2003.

[7] W. Swiegers, J. Enslin, "An lntearated Maximum Power Point Tracker For Photovoltaic Panels", *Proceedings of IEEE International Symposium on Industrial Electronics*, Vol. 1, p 40-44, 1998.

[8] T. Noguchi, S. Togashi, and R. Nakamoto, "Short-current pulse-based Maximum Power Point Tracking Method for Multiple Photovoltaic-and-Converter Module System", IEEE Trans on Ind. Elec., Vol. 49, 2002.

[9] E. Solodovnik, S. Liu and R. Dougal, "Power Controller Design for Maximum Power Tracking in Solar Installations", *IEEE Transactions on Power Electronics*, Vol. 19, No. 5, pp.1295-1304, 2004.

[10] Hussein, K.H., Murta,I., Hoshino,T., Osakada,M., "Maximum photovoltaic power tracking: an algorithm for rapidly changing atmospheric conditions", *IEEE Proceedings of Generation, Transmission and Distribution*, vol. 142, No.1, 1995.

[11] E. Koutroulis, K. Kalaitzakis and N.C. Voulgaris, "Development of a microcontroller-based, photovoltaic maximum power point tracking control system", *IEEE Trans. on Power Electronics*, vol. 16, pp. 46–54, 2001.

[12] W. Swiegers, J. Enslin, "An lntearated Maximum Power Point Tracker For Photovoltaic Panels", *IEEE Proceedings of the International Symposium on Industrial Electronics*, Vol. 1, p 40-44, 1998.

Investigation of a Small-Scale Segmented Oscillating Water Column Utilizing a Savonius Rotor Turbine

D. G. Dorrell and W. Fillet

Dept of Electronics and Electrical Engineering
University of Glasgow
Glasgow, G12 8LT
UK
Contact: d.dorrell@elec.gla.ac.uk

Keywords: Oscillating water column, Savonius turbine.

Abstract

The paper develops a simple algorithm for predicting the performance of an oscillating water column type of generating device that utilizes a Savonius rotor as the bi-directional turbine. A small scale model is constructed and tested in a wave tank and good agreement is found with the predicted performance. A design is put forward for a 1 kW device. Additional required work is detailed which recommends that the algorithm is developed further since it predicts the performance at low speed and conservative outputs, leading to a low conversion factor performance calculation.

1 Introduction

This paper reports on an initial study into the operation of a small segmented-chamber oscillating water column using a Savonius rotor turbine. This device could be used along a harbour wall or in a location where the waves are of poor quality. It consists of a line of chambers. Each chamber has a Savonius rotor and these rotors are all connected along the same axis so that they only require one generator at the end of the drive axle. This is illustrated in Fig.1. The advantage of this device is that this does not require the wave fronts to hit the device parallel to the front edge. The paper will first briefly review some of the basics of the oscillating water columns that have been constructed then develop the theory and design of the Savonius rotor oscillating water column. A small scale model has been constructed and the simulation results will be compared to the experimental results and conclusions drawn. A full scale design will then be outlined in terms of its dimensions and predicted output performance. This is not a high conversion device (the Savonius rotor only has a conversion factor up to about 25 % at an absolute maximum) but it is expected that this would represent a simple and robust device for use in remote and developing locations for low-power applications.

2 Wave Energy, Devices and Behaviour

There are various books that discuss behaviour of waves in terms of energy resource and behaviour [1]-[3]. These often go on to discuss the various wave energy devices that are in development. There has now been a rapid growth in the number of different devices that are being assessed for their viability. These are briefly described in [4]. Here we will simple review shoreline devices which are essentially the oscillating water column type of device.

The wave generation industry is still debating about the best design and in a recent count there were over 1000 patented ideas for wave energy conversion. They can be broken down into five basic technology groups [5]:

- Oscillating Water Column (OWC)
- Overtopping device
- Point Absorbers (floating or mounted on the sea bed)
- Surging devices
- Mechanical Extraction

The best design will depend upon the situation in which it is to be utilised.

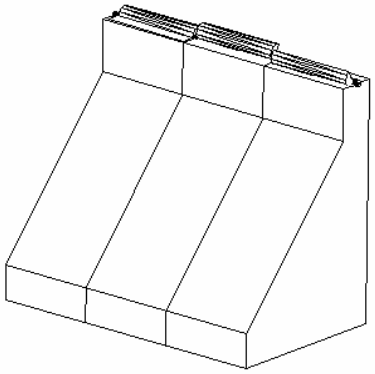

Figure 1: OWC with Savonius rotor turbine

2.1 Shoreline Wave Energy Generator Devices

Because these devices are located at the shoreline, they have the advantage of relatively easy installation and maintenance. They do not require deep-water moorings or long lengths of underwater electrical cable. Nevertheless, the deployment of such devices can be limited by requirements for shoreline geology, tidal range and preservation of coastal scenery.

The first generation of devices to be developed were usually of the oscillating water column (OWC) type. Another type example (of an overtopping device) is the TAPCHAN (Tapered Channel Wave Power Device), a prototype of which

was built on the Norwegian coast in 1985 and operated for several years.

The OWC device consists of a party submerged concrete and/or steel structure, open below the water surface. Inside which air is trapped above the water surface. The heave motion of the sea surface alternately pressurises and depressurises the air inside the chamber generating a reciprocating flow through a Wells turbine which is located at the top of chamber. The axial-flow Wells turbine, invented in the 1970s, has the advantage of not requiring rectifying valves. It has been used in almost all OWC prototypes. However it is not necessary to use a Wells turbine, and indeed, below a certain size, the Wells turbine does become poor in terms of its conversion performance [6].

Two OWCs that have been developed in Europe are the LIMPET (UK) and the European Pilot Plant (Pico Island, Portugal). The LIMPET is a 500 kW plant located in Islay, Scotland. It has two chambers and two contra-rotating Wells turbines each coupled to a 250 kW induction generator. It is in operation and connected to the electrical grid. The PICO plant is rated 400 kW. It has a single chamber and one Wells turbine coupled to a synchronous generator. The machine room is prepared for the installation of a second (variable-pitch) turbine and generator. It is also connected to the electrical grid.

A near-shore OWC, with a parabolic-shaped reflector to concentrate the wave resource onto the OWC (of about 40 m width), is planned in Port Kembla, Australia.

The basic OWC arrangement is shown in Fig. 2. This is illustrated with a Wells turbine. However here we are looking at developing an OWC using a Savonius rotor. The advantage of this is that it is a vertical-axis turbine, so that the chamber can be sectioned and the several turbines connected in series, as illustrated in Fig. 1. This is represents a low-speed, economical and robust arrangement although the disadvantage is that the turbine does not have a high conversion rate.

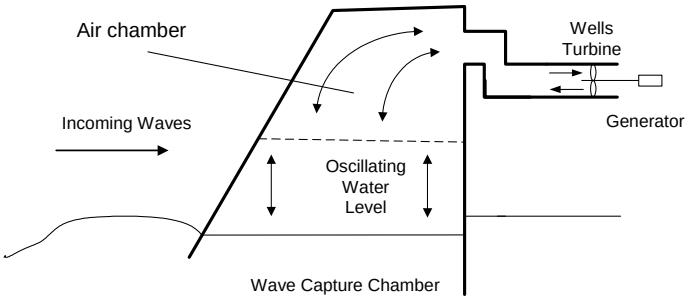

Figure 2: OWC with Wells Turbine

2.2 Wave Behaviour

Addressing the wave in Fig. 3, for a height to wavelength ratio H/λ of 1/50 or less, linear theory can be used to predict the kinematic properties of a wave. The mathematical expressions for the free-surface displacement and the wave period are [3]:

$$\eta = \frac{H}{2}\cos\left(\frac{2\pi x}{\lambda} - \frac{2\pi t}{T}\right) \tag{1}$$

$$T = 2\pi\left[\frac{2\pi g}{\lambda}\tanh\left(\frac{2\pi h}{\lambda}\right)\right]^{-1/2} \tag{2}$$

where the period $T = 1/f = 2\pi/\omega$ (with wave frequency f), g is the gravitational constant (9.81 m/s^2) and h is the water depth. The period T is normally considered to be invariant with both time t and depth h; however, this is not true over long distances and time [7]. The equation above can be rearranged to obtain the expression for the wavelength:

$$\lambda = \frac{gT^2}{2\pi}\tanh\left(\frac{2\pi h}{\lambda}\right) \tag{3}$$

In this equation λ is on both sides of the equality sign and cannot be isolated. The equation must, therefore, be solved by using either graphic or numerical techniques.

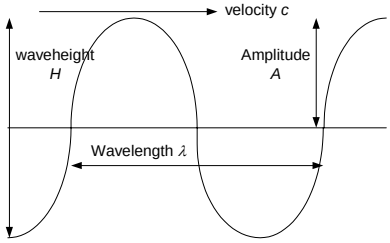

Figure 3: Wave parameter definitions

Deep Water

Deep water is assumed when the depth is greater than half the wavelength ($h > \lambda/2$). Individual waves travel at a phase velocity c where

$$c = \frac{\lambda}{T} = \frac{gT}{2\pi}\tanh(kh) \tag{4}$$

where k is the wave number defined by $k = 2\pi/\lambda$. The wave height H does not appear in these equations. Hence, the velocity and wavelength properties of a linear sea wave are functions of period and depth only. Wave energy conversion appears to be feasible in deep water where $h/\lambda \geq 1/2$, or $kh \geq \pi$. In this case we can approximate the wavelength and the velocity to:

$$\lambda = \frac{gT^2}{2\pi} \tag{5}$$

and

$$c = \frac{gT}{2\pi} \tag{6}$$

Shallow Water

The shallow water approximations of the wavelength and phase velocity are:

$$\lambda = \sqrt{gh}T \tag{7}$$

and

$$c = \sqrt{gh} \tag{8}$$

These equations are used when values of h/λ is 1/20 or less. The wavelength λ and the phase velocity c both decrease significantly as the wave approaches the shoreline. Theoretically λ and c approach zero values as h approaches

zero. Energy conversion is also possible in shallow water although the wave energy quality is lower.

Wave Particle Movement

The water particles move with horizontal and vertical velocity components where

$$u - \frac{\pi H}{T}\frac{\cosh[k(z+h)]}{\sinh(kh)}\cos(kx - wt) \quad (9)$$

$$w = \frac{\pi H}{T}\frac{\sinh[k(z+h)]}{\sinh(kh)}\sin(kx - wt) \quad (10)$$

The deep water approximations of these equation are

$$u = \frac{\pi H}{T}e^{KZ}\cos(kx - wt) \quad (11)$$

and $$w = \frac{\pi H}{T}e^{KZ}\sin(kx - wt) \quad (12)$$

In shallow water, where h/λ < 1/20, the approximate expressions are

$$u = \frac{H}{2}\sqrt{\frac{g}{h}}\cos(kx - \omega t) \quad (13)$$

and $$w = \frac{\pi H}{T}\frac{(z+h)}{h}\sin(kx - \omega t) \quad (14)$$

In deep water the particles travel with circular paths with a diameter that decreases exponentially with depth *z*. In shallow water the particles travel with elliptic paths with a constant horizontal axis and vertical axis that decreases with *z*.

2.3 Wave Power, Energy and Group Velocity

As derived by McCormick [3], and others, the total energy in a wave is obtained from

$$E = E_p + E_k = \frac{\rho g H^2 \lambda b}{8} \quad (15)$$

where b is the width of the crest, ρ is the mass density of water (1000 kg/m^3 for fresh water or 1030 kg/m^3 for saltwater). The total energy in deep water of a wave can be described by linear theory and is equally composed of potential energy E_p and kinetic energy E_k where

$$E_p = E_k = \frac{\rho g H^2 \lambda b}{16} \quad (16)$$

The potential energy is a progressive wave of height H, whereas the kinetic energy is dependent on the motion of the particles.

For a variable sea state, the transfer of wave energy from point to point in the direction of wave travel is characterised by the energy flux or, more commonly, wave power:

$$P = \frac{\rho g H^2 C_g b}{8} \quad (17)$$

where C_g is called the group velocity and is represented by:

$$C_{g=}\frac{C}{2}\left\{1 + \frac{2kh}{\sinh(2kh)}\right\} = nC \quad (18)$$

When a wave-train is observed travelling in deep water, that is, where $h \geq \lambda/2$, waves appear at the end of the train that travel to the front of the train, and then disappear. In the case of a deep water wave-train or group, the relationship between the phase velocity and the group velocity is $C_g = C/2$ (deep water).

In shallow water ($h \leq \lambda/20$), however, the waves remain stationary with respect to the group boundaries; thus $C_g = C$. A wave group is illustrated in Fig. 4.

This section, and the previous section, illustrates that the power will pulse both in terms of a wave period and in terms of a group period. The quality of the waves also deteriorates as the depth becomes shallower. Hence shore-line devices do represent a compromise device, however they have advantages in terms of maintenance and are suitable for smaller-scale and trial devices.

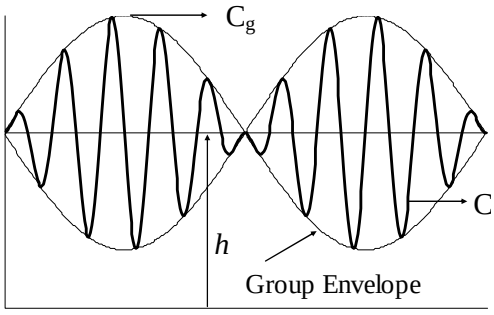

Figure 4: Group wave representation

3 Wave Tank Performance

The aim of this work is to develop a small OWC test device. The device has to be designed to fit within the available wave tank which is formed from a flume with paddle at the inlet and an overtopping beach at the outlet. Fig. 5 shows the flume and it was described in [8]; although the paddle has now been relocated to behind the flume inlet to give better wave quality.

Figure 5: Flume wave tank from inlet end

The tank has dimensions of 6230 mm length, 900 mm width and an overall height from 460 mm. The water level without any waves is about 300 mm. It is possible to adjust the wave frequency and amplitude though control of the paddle drive

(which is a 2-pole inverter-fed induction motor with a 25:1 step-down gearbox).

If it is assumed that the frequency is 0.5 Hz with an amplitude H = 200 mm then

$$P/b = \frac{\rho g H^2 C g}{8} = \frac{\rho g H^2 C}{16} \text{ with } C = \frac{gT}{2\pi}$$

so that $P/b = \frac{\rho g^2 H^2}{32\pi f}$ (W/m)

For the wave tank, b = 0.9 m, H = 0.2 m, f = 0.5 Hz and ρ = 1000 kg/m^3 so that

$$P = \frac{\rho g^2 H^2 b}{32\pi f} = 76 \text{ Watts}$$

However, if f = 2 Hz then P = 17 Watts. Hence the energy resource is small but measurable. These are the typical frequency boundaries for the flume.

4. OWC with Savonius Rotor

The device to be designed and tested is quite small and the conversion factor is expected to be low (as expected with most devices on this scale). This section will first look at the column device and design calculations, it will then proceed to address the Savonius rotor and operation and conclude by a design calculation for the wave tank model.

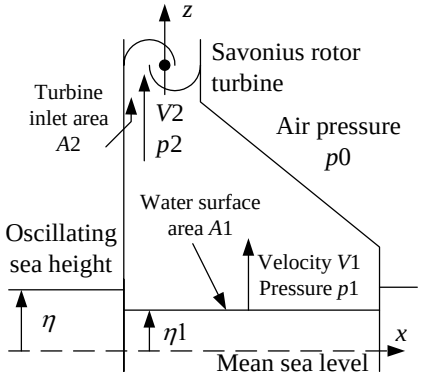

Figure 6: OWC parameters

4.1 Water Column

The general method of analysis is outlined here while using the results of the theoretical turbine analysis of Hiramoto [9]. Referring to the Fig. 6, the internal free-surface displacement from the equilibrium position is

$$\eta 1 = \frac{\overline{H_1}}{2}\cos(\omega t) \tag{19}$$

where $\overline{H_1}$ is the spatially averaged internal wave height. The velocity of the air adjacent to the internal free-surface is then

$$V1 = \frac{d\eta_1}{dt} = -\frac{\omega \overline{H_1}}{2}\sin(\omega t) \tag{20}$$

and assuming incompressible flow (since the system is low pressure), the axial velocity in the turbine passage is

$$V2 = \frac{A1}{A2}V1 = -\frac{A1}{A2}\frac{\omega \overline{H_1}}{2}\sin(\omega t) \tag{21}$$

where $A1$ and $A2$ are the flow areas of the chamber and the turbine passage, respectively. The power P available to the turbine depends on the pressure gradient and volume rate of airflow Q across the turbine:

$$P_t = (p2\text{-}p0)Q \tag{22}$$

where, from the equation of continuity

$$Q = V1 \times A1 = V2 \times A2 \tag{23}$$

The exhaust pressure $p0$ is assumed to be ambient and, for simplicity, constant in the neighbourhood of the turbine. Finally, the upstream pressure $p2$ is related to the pressure within the air chamber by the Bernoulli energy:

$$p2 = p1 + \frac{1}{2}\rho\left((V1)^2 - (V2)^2\right) + \rho\frac{\partial}{\partial t}(\varphi_1 - \varphi_2) \tag{24}$$

where the velocity potentials φ_1 and φ_2 are approximated by

$$\varphi_1 \approx V1\eta_1 = -\frac{\omega H_1^2}{4}\sin(\omega t)\cos(\omega t) \tag{25}$$

and

$$\varphi_2 \approx \frac{A1}{A2}\varphi_1 \tag{26}$$

Finally, the pressure difference in (22) is obtained from the linear momentum equation:

$$p2 - p0 \approx \rho\frac{A_1}{A_2}\frac{\partial \varphi_1}{\partial t} + \rho\frac{Q}{A_2}(V2 - V1) \tag{27}$$

Since the motion of the internal free surface is assumed to be known, the pressures $p1$ and $p2$ can now be determined:

$$P_t = \left[\rho\frac{A_1}{A_2}\frac{\partial \varphi_1}{\partial t} + \rho\frac{Q}{A_2}(V2 - V1)\right]Q \tag{28}$$

but

$$\frac{\partial \varphi_1}{\partial t} = -\frac{\bar{H}_1^{\,2}}{4}\omega^2\left(2\cos(\omega t)^2 - 1\right) \tag{29}$$

$$P_t = \left\{\begin{array}{l} -\rho\frac{A1}{A2}\frac{(\bar{H}_1\omega)^2}{4}\left(2\cos(\omega t)^2 - 1\right) \\ +\rho\frac{Q}{A2}(V2 - V1) \end{array}\right\}Q \tag{30}$$

4.2 Wave Height and Water Oscillation

Using the theory developed in [12] we can obtain expressions for the wave height and water oscillation. Applying Newton's Law:

$$\begin{aligned} &\sum F = ma \\ &\{\rho_s g(\eta - \eta 1) - \Delta p\}A1 \\ &= \frac{\mathrm{d}}{\mathrm{d}t}\left(\rho_s \eta 1 A1 \frac{d\eta 1}{dt}\right) = \frac{\partial^2 \eta 1}{\partial t^2}\left(\rho_s \eta 1 A1\right) \end{aligned} \tag{31}$$

where ρ_s is the density of seawater, g is the acceleration due to gravity and Δp is the total pressure drop across the rotor. Therefore, in a similar manner to (19):

$$\eta = \frac{H}{2}\sin(2\pi ft) \tag{31}$$

where f is the wave frequency.

$$V2 = \frac{1}{M}\frac{\mathrm{d}\eta 1}{\mathrm{d}t} \tag{32}$$

where $V2$ is the mean axial velocity of the turbine and $M = A2/A1$. Δp is a function of $\mathrm{d}\eta 1/\mathrm{d}t$ if the rotational speed Ur (the blade speed at mean radius) is given. Also ρ_a is the density of air so that

$$\frac{\Delta p}{\rho_a} = f\left(\frac{\mathrm{d}\eta 1}{\mathrm{d}t}\right) \tag{33}$$

$$\rho_s A1\left\{\left(\frac{\mathrm{d}\eta 1}{\mathrm{d}t}\right)^2 + \eta 1\frac{\partial^2 \eta 1}{\partial t^2}\right\} = A1\left\{\rho_s g(\eta - \eta 1) - \Delta p\right\} \tag{34}$$

Then $$\eta 1\frac{\partial^2 \eta 1}{\partial t^2} + \left(\frac{\mathrm{d}\eta 1}{\mathrm{d}t}\right)^2 + f\left(\frac{\mathrm{d}\eta 1}{\mathrm{d}t}\right) - g(\eta - \eta 1) = 0 \tag{35}$$

But we assume in this study that Δp has a negligible affect on the internal wave height $\eta 1$ so that

$$\eta 1\frac{\partial^2 \eta 1}{\partial t^2} + \left(\frac{\mathrm{d}\eta 1}{\mathrm{d}t}\right)^2 - g(\eta - \eta 1) = 0 \tag{36}$$

The Runge-Kutta method may be used to solve this differential equation and obtain the wave height within the air chamber.

4.3 Savonius Rotor Dynamics

The Savonius rotor is a low-cost rotor structure although the conversion factor is also low [10]. The relationship between the power coefficient (Cp) and the wind speed is fundamental to the basic theory of the Savonius rotor. The power that the rotor can extract from the wind P_w is less than the actual power available from the wind power P_a. Therefore $Cp = P_w/P_a$.

When the turbine is placed in a wind tunnel with an inlet (1) and an outlet (2) the power that can be extracted from the airflow is found by the following procedure. Find the average of wind speed through the rotor area where

$$V_{ave} = \frac{(V_t 1 + V_t 2)}{2} \tag{37}$$

Where V_t1 and V_t2 are the inlet/outlet wind speeds in m/s Define the mass m of the airflows passing through the S-rotor area:

$$m = \frac{\rho A(V1 + V2)}{2} \tag{38}$$

where $A = h$ x $(2d - S) = h$ x D [m^2] with $D = (2d - S)$. The dimensions d and S are defined in Fig. 7 and h is the turbine axial length.

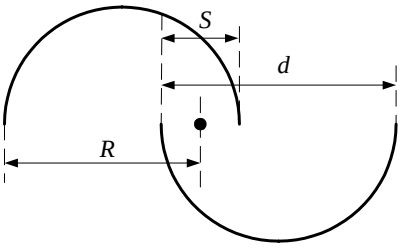

Figure 7: Savonius rotor dimensions

The kinetic energy, $K_E = mV^2/2$. Therefore the power extracted is

$$P_w = \frac{1}{2}m\left((V_t 1)^2 - (V_t 2)^2\right) \tag{40}$$

Substituting the mass of air into this formula, the power that the rotor can extract from the wind is:

$$P_w = \frac{\rho}{4}\left((V_t 1)^2 - (V_t 2)^2\right)(V_t 1 + V_t 2)A \tag{41}$$

Similarly, if the S-rotor generates the electrical power, the power that the rotor can extract from the wind is: $P_w = E \times I$ if a simple D.C. machine is fitted. The available power P_a from the wind is:

$$P_a = \frac{1}{2}m(V2)^2 = \frac{1}{2}\rho A2(V2)^3 \tag{42}$$

where $m = \rho A2 \times V2$. The power coefficient $Cp = P_w/P_a$ so that

$$P_w = Cp \times P_a = Cp\frac{1}{2}\rho A2(V2)^3 \tag{43}$$

which is the standard wind equation, $V2$ is the mean air velocity through the turbine.. We can also define the tip speed ratio:

$$X = \lambda = \frac{R\omega}{V2} \tag{44}$$

which is the blade tip speed divided by the airflow velocity.

The air flow kinetic energy term (43) is common to wind turbine analysis but the air pressure term $(p2 - p0)Q$ is unique to this application so that the power becomes, from (43) and (30):

$$P_{\text{total}} = Cp(P_t + P_w)$$

$$= Cp\left\{\left(\rho\frac{A1}{A2}\left[-\frac{(\bar{H}\omega)^2}{4}\left(2\cos(\omega t)^2 - 1\right)\right] + \rho\frac{Q}{A2}(V2 - V1)\right) + \frac{1}{2}\rho(V2)^2\right\}Q \tag{45}$$

4.4 Savonius Rotor Performance

Reference [10] details a study into the correct dimensions for a Savonius rotor. The general characteristic takes the form of that shown in Fig. 8. The performance at very low tip speed ratio, and also close to X_0, is often omitted from the performance studies and is therefore not clear. In [10] the maximum conversion factor was found to be 0.245 at a tip speed ratio of 0.95. This was for a S/d ratio of 0.2 – this ratio was also studied and 0.2 was found to give the best performance. However, in most other literature the most common maximum conversion factor is found to be about 0.2 at a tip speed ratio of 0.79. It must be noted that every study will use different wind speeds, turbine speed and turbine dimensions.

It is possible to use different arrangements for the turbine blades and it is not necessary to use two semi-circle shapes. The alternatives are reviewed in [11].

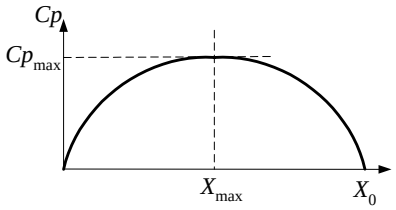

Figure 8: Conversion factor against tip speed ratio for a Savonius rotor

5. Design of Model Device

The theory in Section 4 was programmed in MATLAB to develop a simulation. However, the dimensions of the column were initially chosen to fit into the wave tank and the design and performance of the turbine assessed using the column design and the typical waves available in the tank.

5.1 OWC and Turbine Dimensions

The column was drawn up in Autocad and constructed. The dimensions are given in Figs. 9 and 10. This chamber fitted into the flume. Three chambers were fabricated so that three series-connected turbines were required. The turbine dimensions are shown in Fig. 11. Each turbine was 260 mm long.

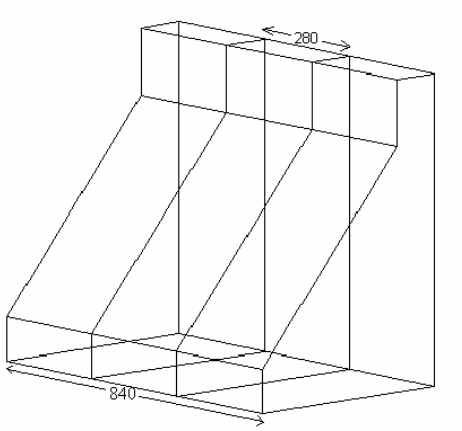

Figure 9: Chamber cross section

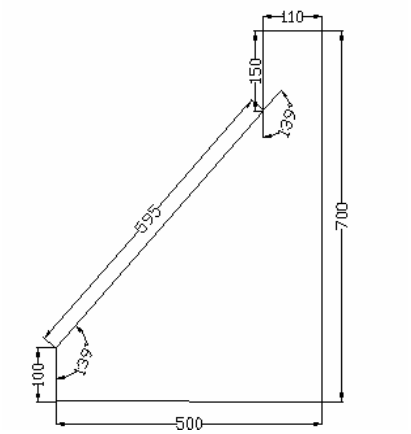

Figure 10: 3D section of chamber

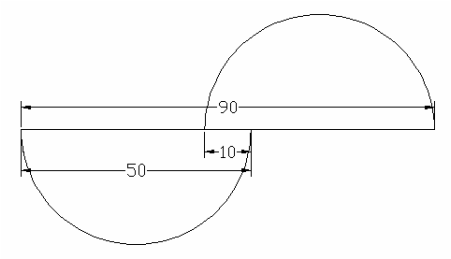

Figure 11: Savonius rotor dimensions

The manufactured OWC is shown in Fig. 12. Note that the front face of the turbine acts as a beach and it was therefore covered in a material that would absorb wave energy and reduce wave reflection. The waves move from right to left in this Figure.

To keep the system simple then a D.C. machine was fitted to the turbine and the speed measured by a simple hand-held tachometer. This system is a simple small-scale system and the conversion factor is low; in addition the per-unit friction and windage losses of such a small system dominate. Therefore, the machine was run as motor and the difference in input power at constant speed measured. The arrangement is shown in Fig. 13.

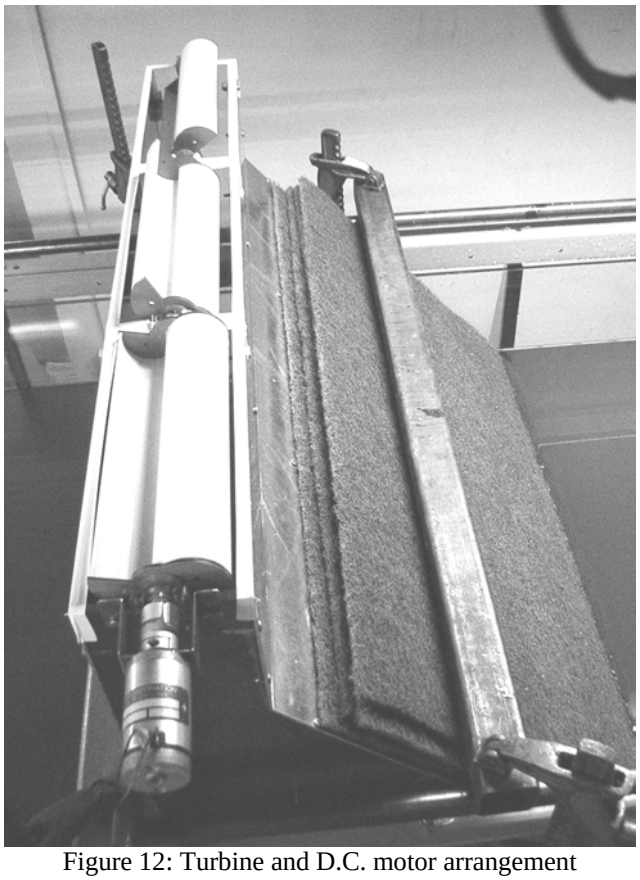

Figure 12: Turbine and D.C. motor arrangement

5.2 MATLAB Simulation

The design was simulated in the MATLAB environment. The program required the input of the following parameters:

- width of the OWC

- width of the duct
- length of the OWC
- incident wave frequency
- incident wave amplitude
- internal wave amplitude
- wave front length
- power coefficient Cp of the Savonius turbine

From these parameters, the program calculates:

- maximum wind speed above the surface
- maximum wind speed in the duct
- average wind speed above the surface
- average wind speed above the duct
- turbine speed in rpm (assuming that $\lambda = 1$)
- power in watts of waves
- average power extracted trough the turbine
- efficiency

The program calculates the phase velocity and the wave length in shallow or deep water conditions.

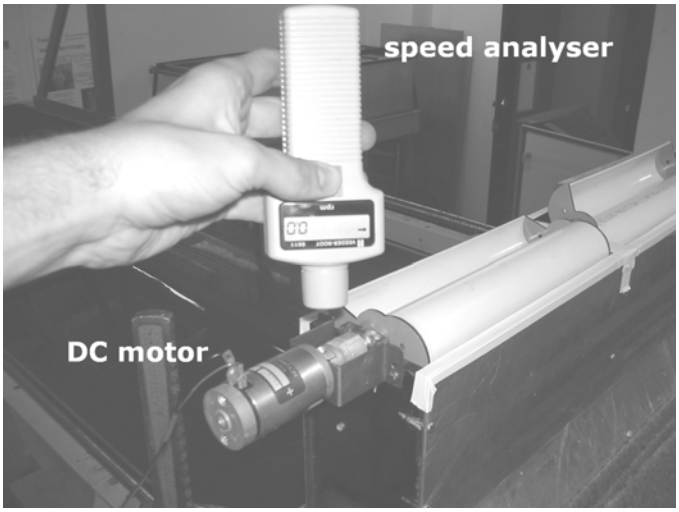

Figure 13: Speed measurement

6 Experimental and Simulation Results

6.1 Measurement method

The system was tested in the wave tank at different wave frequencies. The amount of power generated by this system is inevitably small and measuring the power can be difficult, especially without a torque transducer. Therefore it is worth firstly describing the method of calculation of the output torque. The equivalent circuit of the D.C. motor is shown in Fig. 14. There is a constant voltage drop across the brushes and a variable voltage drop across the armature (including any high resistance connections on the machine side of the power analyser). The voltage and current as well as the power could be measured. The voltage equation is therefore

$$V_t = I_a R_a + E_a + V_{brush} \tag{46}$$

If we multiply through by I_a then we get a power equation:

$$\begin{aligned} V_t I_a &= I_a^2 R_a + E_a I_a + V_{brush} I_a \\ P_{dc} &= I_a^2 R_a + E_a I_a + V_{brush} I_a \\ P_{dc} &= P_{cu} + \left(P_{f+w} - P_{turbine} \right) + P_{brush} \end{aligned} \tag{47}$$

where P_{f+w} is the windage and friction loss so that the absorbed mechanical power is P_{f+w} - $P_{turbine}$.

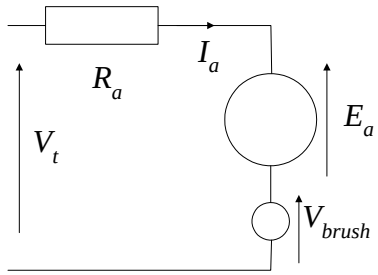

Figure 14: D.C. motor circuit

Since we are attempting to measure the power difference at a particular speed then we can take a measurement at one speed when the waves are flowing and when they are not so that

$$\begin{aligned} \Delta P_{turbine} &= \Delta P_{dc} - \Delta P_{cu} - \Delta P_{brush} \\ \Delta P_{turbine} &= V_{t1} I_{a1} - V_{t2} I_{a2} \\ &\quad -(I_{a1}^2 - I_{a2}^2) R_a + V_{brush} \left(I_{a2} - I_{a1} \right) \end{aligned} \tag{48}$$

Note that the friction and windage cancels out. However, it may not be possible to obtain test measurements at the same speed. However, it is possible to obtain curves for the voltage and currents and from these obtain curve fits for the characteristics and use the equations to obtain a performance curve. This is illustrated below.

6.2 Simulation settings

The system was tested at 0.55 Hz, 0.8 Hz and 1 Hz with the wave height nominally identical, although it does vary with frequency. The voltage and current results are shown below with the characteristic equation given for each curve. The voltages are linear while the currents are quadratic. Fig. 15 shows the operation of the column.

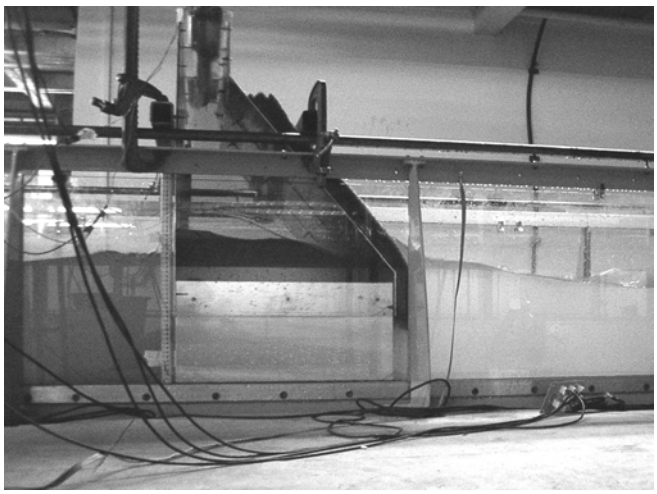

Figure 15: Column under operation

0.55 Hz Test Results

The paddle was set to operate at 0.55 Hz and the voltage and current results are shown in Figs. 16 and 17. The wave height is 150 mm while the internal column height was estimated as 120 mm. An internal probe could be used in this application however it can be seen in Fig. 15 that the level in the column is not constant and erroneous results may occur if this method was used.

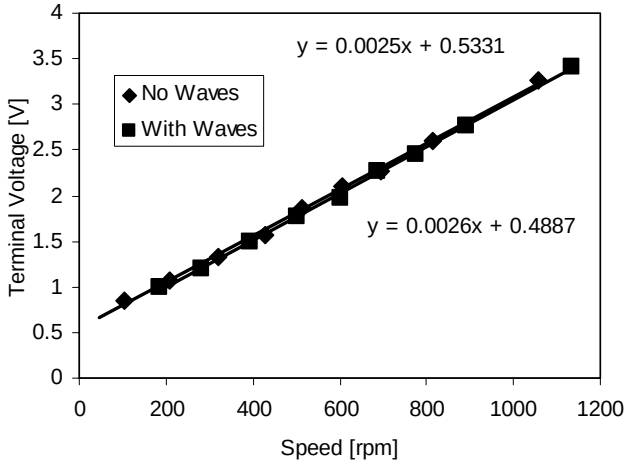

Figure 16: Terminal voltage with and without applied waves at a wave frequency of 0.55 Hz

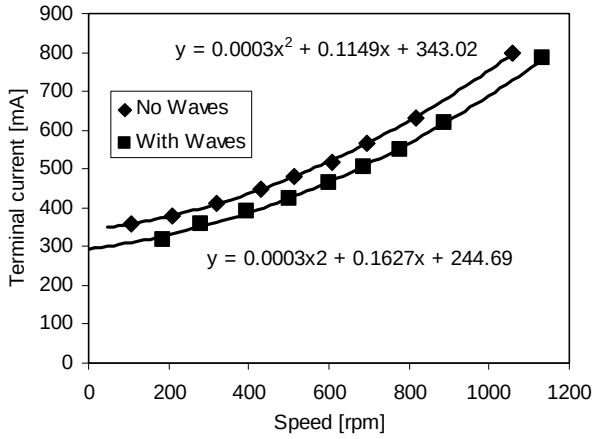

Figure 17: Terminal current with and without applied waves

0.8 Hz Test Results

The results from the 0.8 Hz test are shown in Figs. 18 and 19. The wave height was 150 mm while the internal height in water column was estimated to be 100 mm. The Microsoft Excel line fits is shown in all the curves in Figs. 16 to 21. It can be seen in Fig. 18 that there is a divergence between the voltage characteristics – this is probably due to a high resistance joint and this is accounted for in the analysis.

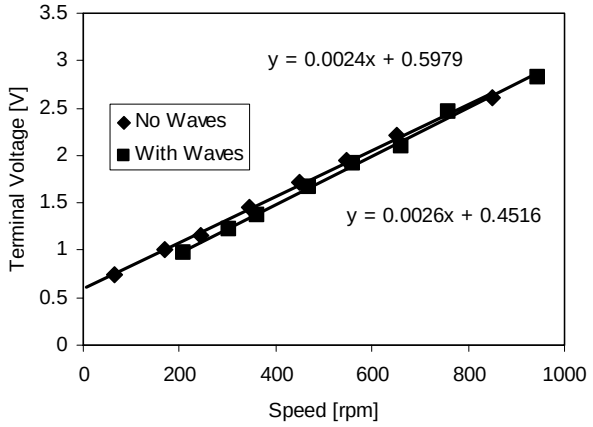

Figure 18: Terminal voltage with and without applied waves at 0.8 Hz wave frequency

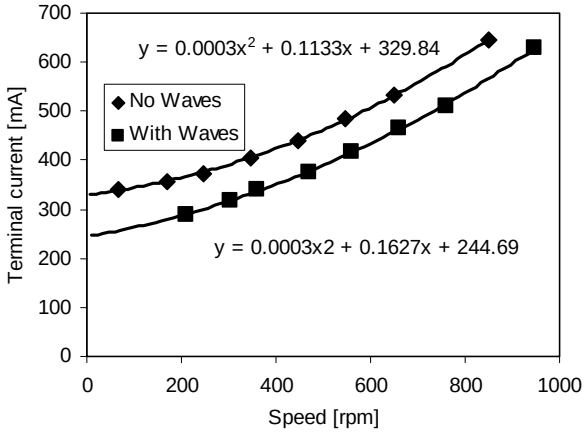

Figure 19: Terminal current with and without applied waves at 0.8 Hz wave frequency

1 Hz Test Results

The 1 Hz results are shown in Figs. 20 and 21. The wave height here is a little less at 130 mm and the internal wave height is estimated to be 70 mm, which seems a large decrease in the height.

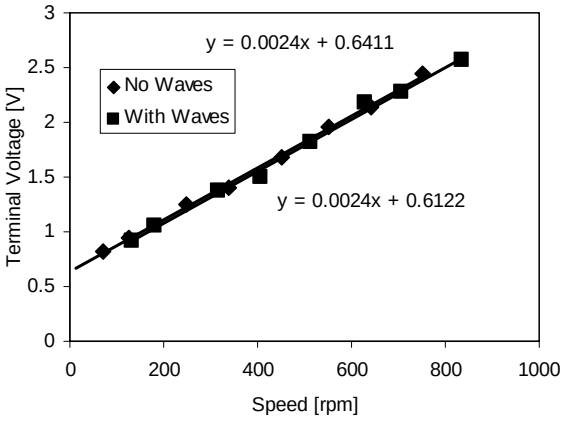

Figure 20: Terminal voltage with and without applied waves at 1 Hz wave frequency

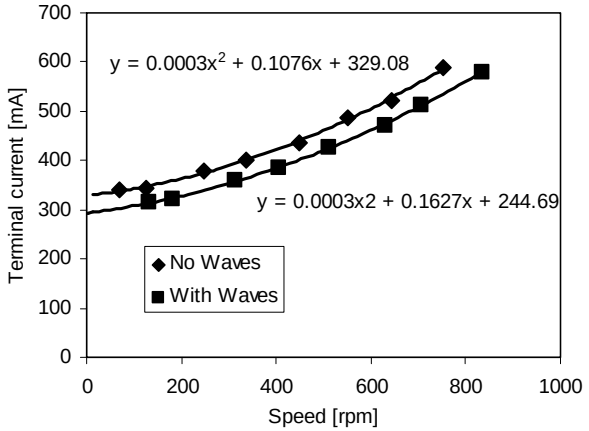

Figure 21: Terminal current with and without applied waves at 0.8 Hz wave frequency

6.3 Experimental Results and Simulation comparison

After processing the resulting using equation (48), the characteristics in Fig. 22 are obtained. In addition, the initial results from the simulation are illustrated for comparison. Good correlation is found. While the power generated is indeed very small it is predictable and further work on the design of the column could realise further improvement in performance

The simulation program is still in development and further work will realise a prediction across the whole speed range. A torque transducer that can measure the torque directly would also be advantageous however, this needs to be a high precision device to give accurate results.

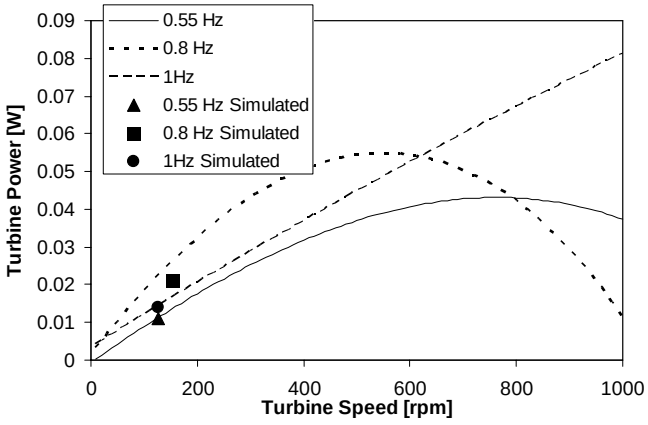

Figure 22: Processed results from measurements showing turbine power against turbine speed

6.4 Column Positioned Orthogonal to Waves

The results in this section are for when the column (which is divided into three sections) is placed orthogonal to the oncoming waves to test the concept of the sectional method. Fig. 23 shows this in the wave tank. Since the device is designed to act as a beach at the end of the flume, an additional section had to be inserted against the side oncoming-wave side of the column to so that the waves do no reflect back to the paddle.

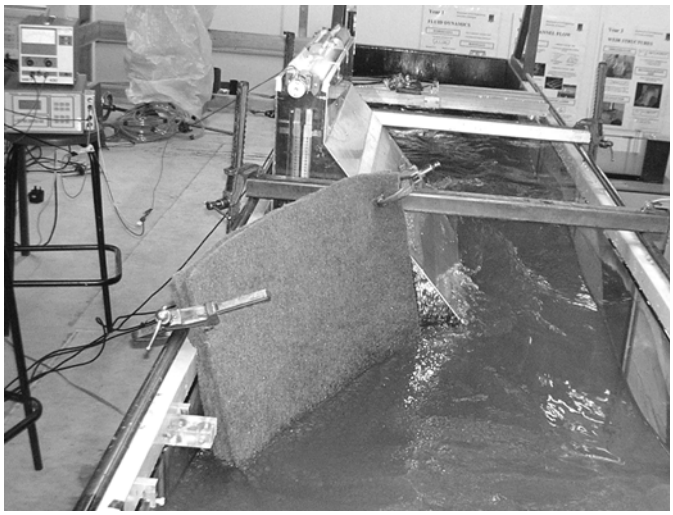

Figure 23: Water column placed orthogonal to oncoming waves

This was tested at a frequency of 0.7 Hz. The wave height was 110 mm. In the front chamber the water height was 20 mm, in the second chamber is was 60 mm and in the third chamber it was 100 mm.

The results are shown in Fig. 24 for this arrangement. Because of the variation of internal water heights and possibly because the OWC is not the termination of the wave tank, then it appears to give quite good results with a more liner characteristic than the 0.55 Hz and 0.8 Hz in Fig. 22. Further work is needed here to construct a more suitable column shape down one side of the flume.

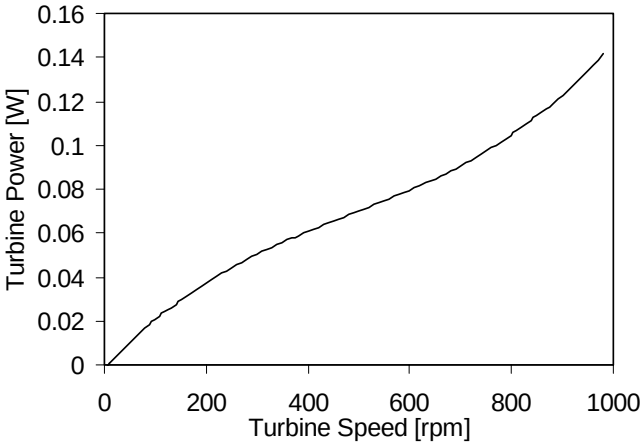

Figure 24: Power against turbine speed for orthogonal positioning

7 Larger System Simulation

The results in Section 6.3 show that the simulation program gives performance predictions that are with the range of operation. This section implements the program to predict the performance of 1 kW design. The following size was selected as well as a sea state that could well represent a shoreline location:

Width of the OWC 3 m

Width of the duct	0.1 m
Length of the OWC	5 m
Wave frequency	0.2 Hz
Height of the incident waves	2 m
Average water height in the OWC	1.5 m
Wave front length	5 m

The turbine is predicted to generate 1.59 kW at a speed of 3700 rpm. The power in the wave-front is 97 kW so that the conversion factor is still low at 1.6 %. However, there is still much work to do to refine the design program (this is obvious from Fig. 22) since it tends to generate a conservative power rating at a low speed.

In addition, the design is quite simple and could be implemented as part of a pier design where output conversion is not a prime priority.

8 Conclusions

This paper reports on an initial study into the performance of an oscillating water column with a Savonius rotor turbine. The constructed model is quite small however power was produced from it that was predictable using a simple design algorithm. Several tests were carried out of the OWC to examine its performance.

A scaling exercise was also carried out to assess the requirements of a 1.5 kW design. Since it was found that the performance prediction algorithm tended to give low values this design is essentially a worst-case scenario.

Further work is required in many areas. First of all a prediction program is required that can assess the performance over a full speed range and secondly, the full transient simulation is needed to predict the correct internal water height. This would allow the system to be tuned properly and also the correct size of turbine to be selected for the column size and predicted sea state so that an optimum-performance system can be designed.

Acknowledgements

Mr Fillet carried out this work while he was a visiting scholar from the Ecole Polytechnique Universitaire de Marseille (January-July 2006). He is grateful to them for their cooperation during this period

References

[1] M.J. Tucker and E.G. Pitt, *Waves in Ocean Engineering*, Elsevier Publishers, Ocean Engineering Series, 2001.

[2] R. Shaw, *Wave Energy: A design challenge*, Ellis Horwood Publishers, 1982.

[3] M. E. McCormick, *Ocean Energy conversion*, John Wiley & Sons Publishers, New York, 1981.

[4] J. R. Halliday and D. G. Dorrell, "Review of Wave Energy Resource and Wave generator Developments in the UK and the Rest of the World", *IASTED EuroPES conference*, Rhodes, Greece, 28-30 June 2004 (on CD).

[5] A. Clement, P. McCullen, A. Falcao, A. Fiorentino, F. Gardner, K. Hammarlund, G. Lemonis, T. Lewis, K. Nielsen, S. Petroncini, M.-T. Pontes, P. Schild, B.-O. Sjostrom, H.C. Sorensenaan and T. Thorpe., "*Wave Energy in Europe: current status and perspectives*", *Renewable and Sustainable Energy Reviews* Vol. 6, Elsevier Science Publishers, pp 405-431, 2002.

[6] D. G. Dorrell and M. Findlater, "Computational Fluid Dynamic modelling of a Wells Turbine", *IASTED EuroPES conference*, Rhodes, Greece, 28-30 June 2004 (on CD).

[7] J. R. Halliday, D. G. Dorrell and A. Wood, "Fourier Approach to Short Term Deterministic Wave Prediction", ISOPE-2006, *Sixteenth (2006) International Offshore and Polar Engineering Conference*, San Francisco, California, USA, May 28–June 2, 2006.

[8] D. G. Dorrell, R. Halliday, S. MacLean, P. Miller and F. Santamaria Mosquera, "Development of Small-Scale Facilities for Initiating Studies into Sea Wave Energy generation", *International Conference on Renewable Energy and power Quality*, Zaragoza, Spain, March 2005.

[9] A. Hiramoto, "The Theoretical analysis of an air turbine generation system", Proc Wave and Tidal Energy International Symposium, Canterbury, England, Sept. 27-29, 1978, Vol 1. pp 73-84.

[10] M. C. Percival, P. S. Leung and P. K. Datta, "The development of a vertical turbine for domestic electricity generation", *European Wind Energy Conference*, 22-25 Nov., London, 2004 (available on line).

[11] M. O. L. Hansen. *Aerodynamics of wind turbines*, Earthscan Publishers, January 2001.

[12] T.Setoguchi ,S. Santhakumar, M.Takao, T.H. Kim, K. Kaneko , "Effect of guide vane shape on the performance of a Wells turbine", *Renewable energy*, July 2000.

COMPARSION OF TWO NEURAL NETWORK MODELS FOR HOURLY WIND POWER PREDICTION

S.M.Tafreshi D.Panahi[1]
* Electrical Department, K.N.Toosi University of Technology, Tehran, Iran

Keywords: wind power, prediction, wind speed, neural networks

Abstract

The main objective of this paper is to introduce two intelligent methods for prediction of wind power in wind turbines. In first case a model has been introduced witch was based on Kohonen self organized neural networks; the other model has been based on Perceptron neural networks. The hourly prediction results of two networks in different horizons have been compared and the errors for each case have been calculated. At the end, the performance of two systems was compared.

1. Introduction

After critical conditions of oil market in 1973 and increasing of air pollution, there has been a growing trend towards the sustainable energy and green power sources. Wind energy is one of the economic sources of renewable energy sources and as a result, new problems in the field of energy management and operation have appeared on the electricity market. One of the important problems in wide uses of wind power is non-predictable power that generate by wind farms and difficulties of accurate wind power forecasts. Wind power forecasts are beneficial for wind plant operators, utility operators, and utility customers. An accurate forecast allows grid operators to schedule economically efficient generation to meet the demand of electrical customers.

One of the most important facts of wind energy production is related to the rapid changes in wind speed and direction, so the output put power of wind turbines vary with these changes. This paper describes two forecasting models that focus on short-term forecasts that can be useful in hour ahead markets[1],[2],[3].

2. The construction of intelligent wind power prediction system

The theoretical calculation shows that the output power of wind turbines varies with the cubic power of wind speed, wind direction, and air density. Therefore, these variables must be predicted before prediction of wind power at first. In the other step, the predicted variables uses in power curve modelling system. In this paper there has been introduced an intelligent system that consist of two subsystems. The schematic of system is shown in fig.1.

The system consists of two subsystems based on neural networks. Sub1 is a wind speed and direction neural network prediction system, Sub2 is another neural network used for turbines power curve modelling. In the other word by

[1] - Corresponding author. Tel.: +989144421252;
E-mail addresses:panahi_delshad@yahoo.com, 821312103@ee.kntu.ac.ir

cascading of these two intelligent systems, it was obtained a powerful tool for prediction of hourly power, generated by wind turbines. The method used in this paper based on prediction of wind speed and direction. Therefore in the next section the prediction of these parameters will be done by two different neural networks.

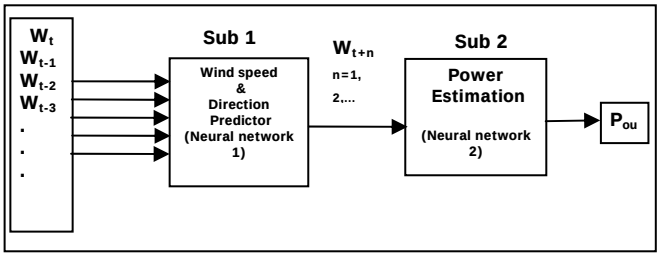

Fig. 1 artificial prediction system

3. Wind speed and direction prediction Models

As mentioned in previous section the wind characteristics are random variables, there for prediction of these parameters are so difficult but if it is done with an acceptable accuracy, it can be so useful for wind farm owner and consumers. On the other hand, if the prediction method is not expensive and easy to use, it can be carried out much more benefits.

The prediction function is like equation below:

$$W(T+1T_0) = F\{W(T), W(T-1T_0),...,W(T-nT_0)\}$$

Where,

$W(T-nT_0),\ldots,W(T-1T0),W(T),W(T+1T_0)$ are hourly time series of wind speed. W(T+1T0) is one hour ahead wind speed, that must be predicted. $W(T-nT_0)$,…,W(T-1T0),W(T) are past samples of wind speed, used as neural network inputs. n is numbers of neural network inputs used for prediction of one hour ahead. Evaluation of n depends on the ratio of correspondence between future sample and past samples of wind speed. A correlation analyze was done for evaluation of n. At first, a threshold level for correlation coefficient e.g. 0.5 was selected then correlation between W(T) and another past data samples of wind speed was calculated. The data with correlation>0.5 was selected as neural networks inputs. The correlation analyze was shown that only 8 past samples of wind speed had acceptable correlation with future sample of wind speed. There for value of n and the number of network inputs was evaluated.

The most important aim of this section is to develop two intelligent systems for wind characteristics prediction based on two different neural networks.

The first prediction model is based on Perceptron neural networks with back propagation training method. The other method is based on Kohonen neural networks, witch is a self-organized neural network. The software development of two networks was done and the results will be shown below for comparison.

The Perceptron neural networks generated great interest due to its ability to generalize from its training vectors and learn from initially randomly distributed connections. The Perceptron used in this paper, consist of three layer, input layer, hidden layer and output layer are three different layers of neural network. The construction of Perceptron neural network is shown in fig.2.

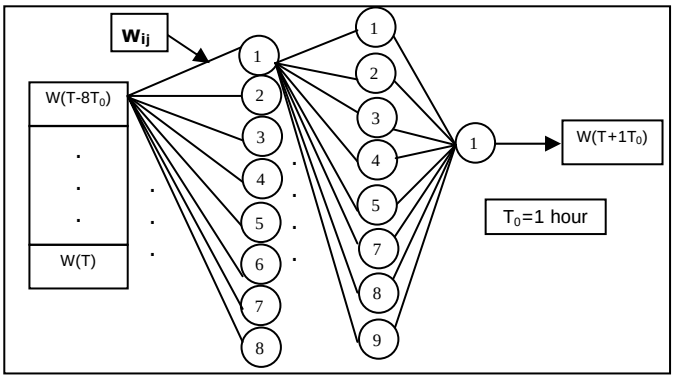

fig.2. The structure of Perceptron neural network for hourly prediction of wind speed and direction.

As mentioned above the other network witch was used in this paper, is a self-organized neural network. Kohonen neural network has a simple construction witch was consist of two layers, inputs and outputs are first layer and the competitive layer is second one. Kohonen can learn to detect regularities and correlations in their input and adapt the future responses to that input accordingly. The neurons of competitive layer learn to recognize groups of similar input vectors. The Kohonen rule allows the weights of a neuron to learn an input vector, and because of this it is useful in recognition applications thus, the neuron whose weight vector was closest

to the input vector is updated to be even closer. The result is that the winning neuron is more likely to win the competition the next time a similar vector is presented, and less likely to win when a very different input vector is presented. As more and more inputs are presented, each neuron in the layer closest to a group of input vectors soon adjusts its weight vector toward those input vectors [4],[5].The structure of Kohonen neural network is displayed in fig.3

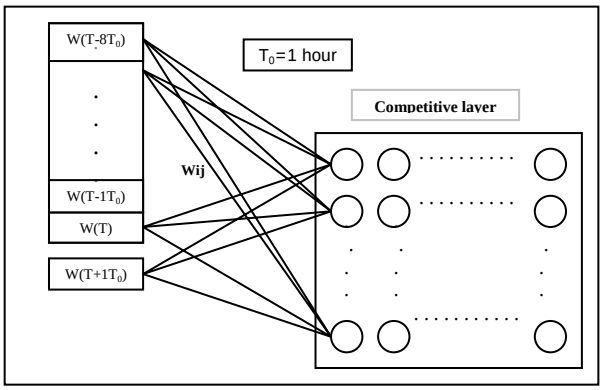

fig.3. the structure of Kohonen network for hourly prediction of wind speed and direction

4. Wind farm specification

The farm selected as a case study is a wind farm with 42 turbines and two measurement mast for measurement of wind speed and direction in different heights. A set of data in a period of one year used for development of prediction models. The database consist of wind speed and direction of two masts and wind speed and out power of each turbines in farm. Typical time series of hourly wind speed and direction from mast#1 are shown in fig.4,5. These data sets obtained by averaging of 10 min data samples that have been collected from wind farm[7].

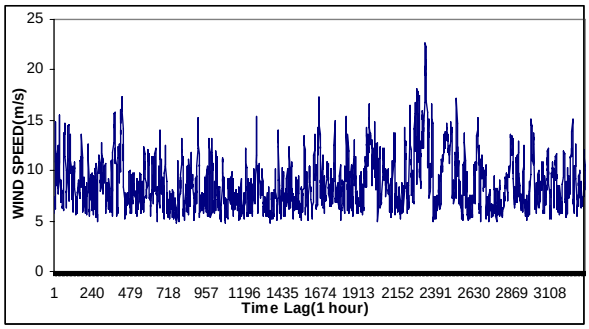

Fig. 4. Time series of hourly wind direction data

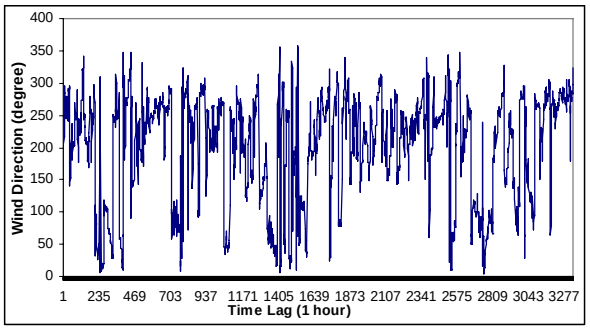

Fig.5. Time series of hourly wind speed data

5. Estimation of wind power with neural networks

According to fig. 2 after prediction of independent variables like wind speed and direction, a power estimation model will be needed. In the other word, using the data collected from masts and data collected from turbine hub height, an estimation model like sub2 was built. The input variables of model are hour ahead predicted values of wind speed and direction and the output is wind power of each turbine. According to good performance of neural networks in parameter identification and curve modeling an other neural network used for estimation of power and turbine curve modelling. Sub2 is a power curve modelling system based on Perceptron neural networks. The construction of model and inputs were shown in fig.6. Wind speed and direction from mast1 and mast2 and wind speed from hub height are 5 inputs of network and power of turbine is output of network. In the other word, we used wind speed and direction from all mast of the farm for estimation of wind power. In this way, the effects of all wind streams in farm were considered in power curve modelling, so an accurate model of power curve has been obtained[7].

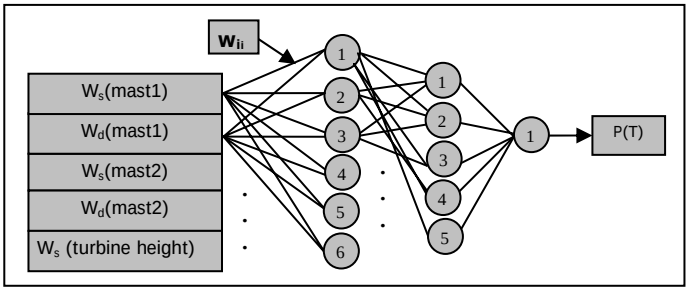

Fig.6. the structure of power curve modeling neural network

The input values of this network were predicted by sub1 in 1-hour ahead horizon. In the other word by cascading of sub1 and sub2, we could obtain a wind power predictor system.

6. Experimental results

In section 3 two different models for prediction of wind, speed and direction based on two different neural networks were introduced. In order to compare performances of Perceptron and Kohonen models, several tests in different time intervals were done. Three different errors were calculated for comparison of results. Mean absolute error (MAE), mean absolute deviation error (MAD), and mean square error (MSE) were calculated in each test [8]. Typical results are shown in fig.4 and fig.5. The errors for each case was shown in table.1

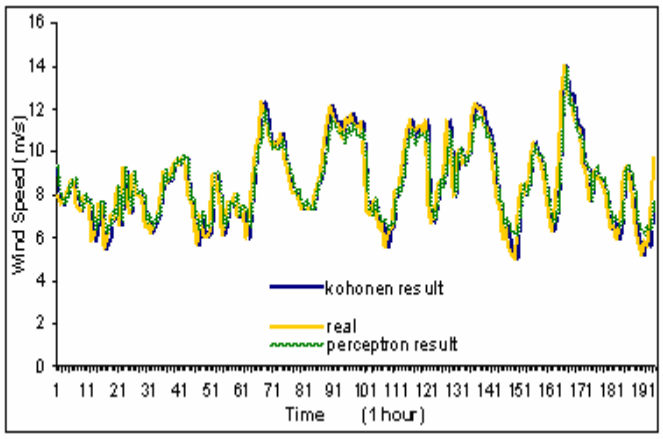

Fig.7. Comparison between Kohonen and Perceptron hourly wind speed prediction

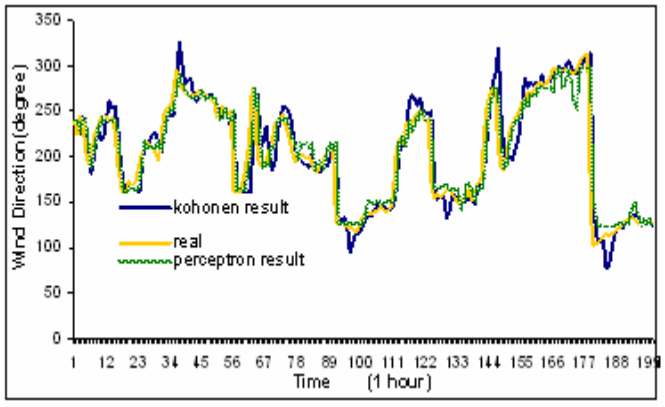

Fig.8. Comparison between Kohonen and Perceptron hourly wind direction prediction

Table.1 Error calculation for each network results

TEST No	Perceptron			Kohonen		
	MAD (%)	MSE	MAE	MAD (%)	MSE	MAE
1	6.47	0.51	0.54	7.47	0.66	0.61
2	6.4	0.53	0.53	7.85	0.76	0.65
3	7.48	0.63	0.56	9.36	1.03	0.7
4	7.65	2.1	0.96	5.84	0.81	0.64
5	6.99	0.59	0.5	9.08	0.98	0.65
6	4.69	0.31	0.43	5.56	0.43	0.5
7	4.95	0.28	0.41	5.88	0.41	0.48
8	7.34	0.38	0.48	8.40	0.53	0.55

By comparison, of errors in table.1, we can say that Perceptron neural network has greater prediction errors than Perceptron network. Therefore Perceptron was given better results than Kohonen, but Kohonen has a very simple structure and training algorithm of Kohonen is rather easy than Perceptron. The time interval for training and testing of Kohonen is very shorter than Perceptron; therefore, in real time conditions it is better to use Kohonen because of fast and simple prediction method.

Hardware requirements for Kohonen network are simpler than Perceptron.

Typical results of this prediction system are shown in figure.7 and figure.8. Total errors for each test were shown in table.2. These errors are summation of wind speed and direction prediction error and power estimation error, in the other word total error of sub1 and sub2 was calculated. Total error of Perceptron system is lower than Kohonen prediction system but as mentioned before, the Kohonen has some benefits rather than Perceptron.

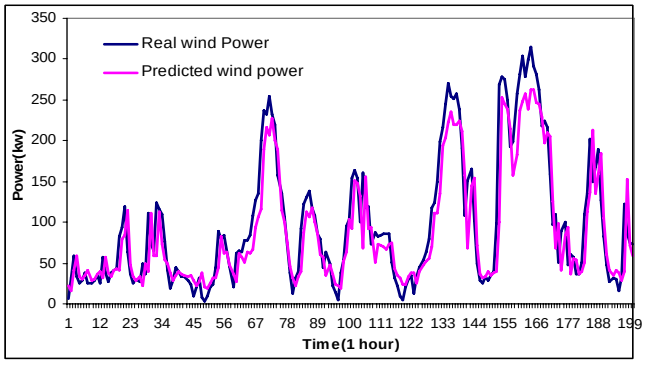

Figure.7 one hour wind power prediction

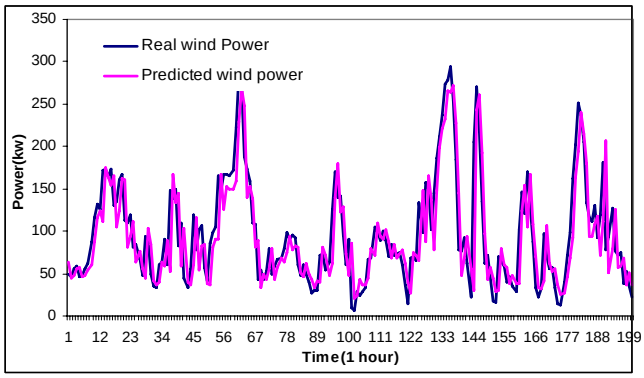

Figure.8 one hour wind power prediction

Table.2. Total error of one-hour power prediction system

TEST No	Perceptron			Kohonen		
	MAD (%)	MSE	MAE	MAD (%)	MSE	MAE
1	9.95	1.02	0.71	14.68	2.07	1.06
2	9.97	1.04	0.72	14.71	2.09	1.09
3	11.22	1.23	0.86	16.05	2.78	1.28
4	10.92	1.25	0.86	19.17	3.43	1.51
5	9.58	2.8	1.19	15.38	5.3	1.9
6	8.1	2.11	1.11	18.23	5.22	1.80
7	8.3	0.78	0.6	10.93	1.01	0.77
8	11.19	1.21	0.83	16.00	2.75	1.24

7. Conclusion

In this paper, a new model for prediction of hourly wind power was introduced. The construction of model based on two different neural network models was introduced and performance of each system was evaluated. Each models had some benefits and some problems. According to kind of use, hardware complexity and system costs, we can select one of these two models. Perceptron gave us better outputs than Kohonen but the complexity of Kohonen is much lower than Perceptron and it needs simple hardware systems.

Using neural networks in sub2 instead of power curve is a new method witch was used with a wind prediction system in a cascade structure. Experimental results in table.2 were shown that neural network has better accuracy instead power curve using.

8. References

[1] Corinna Moehrlen, "On the Benefits of and Approaches to wind Energy forecasting", University College Cork, Ireland, 2002

[2] Mukund R.Patel, "Wind and Solar Power Systems", CRC Press, 1999

[3] Soteris A. Kalogirou, "Artificial neural networks in renewable energy systems applications: a review", Renewable and Sustainable Energy Reviews 5 (2001) 373–401

[4] Mituharu Hayashi, Bahman Kermanshahi, "Application of Artificial Neural Network for Wind Speed Prediction and Determination of Wind Power Generation Output", Tokyo University, 2001

[5] P. Flores, A. Tapia, G. Tapia, "Application of a control algorithm for wind speed prediction and active power generation", Renewable Energy 30 (2005) 523–536

[6] J.Hojstrup, M.S.Courtney, C.J.Christensen, P.Sanderhoff,"Full Scale Measurement in wind turbine arrays", Norrekear Eng2.CEC/jole Department of Meteorology and wind Energy, 1995

[7] Shuhui Li, Donald C. Wunsch, Edgar A. O'Hair, and Michael G. Giesselmann, "Using Neural Networks to Estimate Wind TurbinePower Generation", IEEE Transactions on Energy Conversion, Vol. 16, NO.3, September 2001

[8] H. Madsen, G. Kariniotakis, H.Aa. Nielsen, T.S. Nielsen1, P. Pinson, "A Protocol for Standardizing the Performance Evaluation of Short-Term Wind Power Prediction Models", 2003

Experimental Study on the Thermal Performance of an Evacuated Tube Coated with Ballastic Black as Selective Coating Material

[1]T.Gyanaprakash, [2]G.C.L Andy, and [3]D.Mutharasu*
School of Mechanical Engineering
University of Science Malaysia,
Engineering Campus,
14300 Nibong Tebal, Penang, Malaysia.
[1]gp_gyana79@yahoo.com, [2]chialiang.andy@gmail.com, [3]mutharasu_2000@yahoo.com

Keywords: Ballastic black, Evacuated concentric tube, Selective material, solar absorber, Wet coating.

Abstract

A study has been carried out on the possibility of coating Ballastic Black (a special paint species) deposited on evacuated tubes as a selective coating material to study the efficiency and thermal performance of the system. The coated surface should ideally absorb all the heat either directly from sun light or scattered from surrounding. The study shows that temperature output is proportionally increased with solar flux, and the optimum angle at 15^o of inclination is found for 100 ml/min flow rate. Due to this minimum flow rate; it is not to encourage using inclination other than 15^o, because of insufficient pressure to force the water to flow through the evacuated concentric tubes. In order to obtain a higher temperature output (hot water), it has been suggested to use optimum inclination angle, diameter, concentration of coating materials etc., the thermal performance and the efficiency of the system has been studied and compared with the uncoated evacuated concentric glass tubes.

1. Introduction

The solar world market has expanded significantly since last decade. Therefore, a large scale of development in new technology and improved quality products and even lower manufacturing cost has been achieved by McVeigh [1]. Solar evacuated tube has better performance compare to flat plate collector, where solar evacuated tube can operates in high temperature. The water flow inside evacuated tube is directly contact with absorber surface where it coated with Ballastic Black.

In order to estimate the absorption of the tubes, it is necessary to know the reflectance and the transmittance of the tubes. Mustapha Merzouk [2] has derived the total directional ray transmittance for a tube solar collector cover glass. The numerical integration has been made for both beam and diffuse radiation. His research was conducted on flat plate collector and upon the derivation it can be used to estimate the average transmittance of a tubular cover glass using the mean beam transmittance expressions. Solar transmittance in evacuate tubular had been conducted by P.H. Theunissen and W.A. Beackman [3]. In this paper, they have introduced the partition matrix between light source and light sinks to evaluate the transmittance properties of optically asymmetric collectors constructed with evacuated tubes. They have used a ray-tracing model to compute the elements and the effects of polarization have been discussed. In this paper also has been discussed the beam and diffuse transmittance of a tubular.

The efficiency of evacuated tube is significantly dependent on the absorption and the emittance of the surface where the incoming solar radiation is converted to thermal energy. The absorbed radiation by the surface is converted into heat whereas the rest radiation, which is not absorbed, is reflected. The absorbing surface of the evacuated tube is usually black in color to maximize the absorption of the solar spectrum. In recent years, much research has been conducted on the absorptivity of the evacuated tube with the changes of the surface area with some chemical deposition, which has seen significant improvements in the efficiency of evacuated tube solar collector. T.Bostrom [4] have investigated on doing the solution chemistry method in fabricating a spectral selective solar absorber coating which consist of nickel nano-particle embedded in a dielectric matrix of alumina. There are some other techniques which researchers have utilized to produce absorber coatings such as electroplating, sputtering, anodization, chemical vapor deposition and evaporation processes. S. Suzer [5] has used Al_2O_3-Ni as selective absorbers for solar collectors and Yin Zhiqiang et al. [6] used Al-N/Al for all glass evacuated tubular collectors.

2. Experimental

A bench had been setup for holding the evacuated tubes in order to carry out the experiment. Together with this piping, six numbers of flow meters are installed accordingly for respective tubes. These flow meters are use to control the flow rate at any measurements from 10 ml/ min until 100 ml/ min.

A storage tank shown in Fig 1 is used to maintain the water pressure. In this experiment, water pressure plays a very important role in the sense of supplying enough fluid to pass through the evacuated tube. If water pressure is not maintain in a certain level, the flow rate's fluctuation will be very high and properly it will bring to uneven heat transfer to the flowing fluid. An insulated hose was used to connect the evacuated tubes to the storage tank.

Figure 1: Storage tank

As the direction of face of the evacuated tubes plays an important role it is placed directed to north and south as shown in Fig 2. So that solar flux trajectory will be always within the evacuated tubes through out the experiment.

Figure 2: A Cursor Show the Direction of the North and Tubes Direction Should be facing to North.

2.1 Experiment Procedures

This experiment is carried out everyday (from 5th of March 2006 until 14th of March 2006) every morning 8:30 am until evening 4:30 pm. The experiment is conducted on the different angle if incline and different flow rate. Data has been collected according to the different combinations of setting.

Experiment procedures:

An overhead water storage tank was used as the water source in the experiment which was filled by the residential water supply line. Insulated hose was used to connect between the storage tank and the experimental table. The location of the experiment was chosen appropriately so that a huge amount of direct sunlight would strike on the tubes without any obstruction such as shades. Each tube was connected with valves and flow meters to control the water flowing in the tubes. Tubes were filled with water and the presence of the bubbles should be eliminated so that it would not be affecting the readings. Through all the experiment day, solar flux is measured using a pyranometer (CM3), inlet and outlet temperature and the ambient temperature are measured at every half an hour interval using a data logger device (SR630). The experiments for the uncoated and coated tubes with different solutions were recorded for every half an hour started from 8.30 am to 4.30 pm. Experiments were repeated for various angles and flow rates.

Figures 3-6 shows the setup and layout of experiment

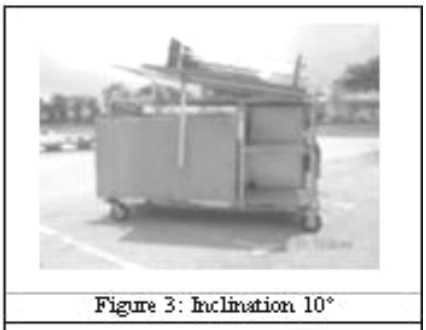

Figure 3: Inclination 10°

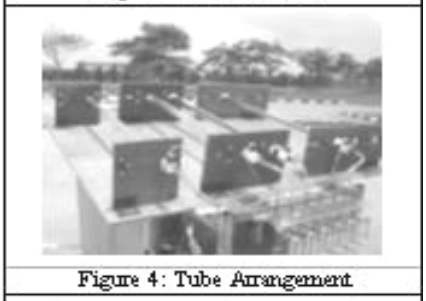

Figure 4: Tube Arrangement

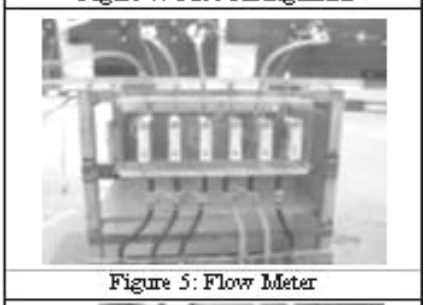

Figure 5: Flow Meter

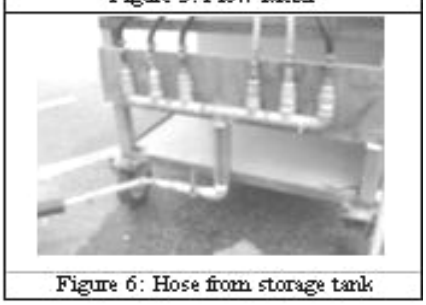

Figure 6: Hose from storage tank

3. Results and Discussions

The selective material for this experiment is known as Ballastic Black, which is a commercially available black paint from Jotun. This paint is mixed with thinner in different proportions and compared. The coated layer is used as an absorber to absorb maximum heat as a black body absorbs all the radiation that falling on the tubes. Heat transfer from the coated layer will be transferred to the fluid that flows through the evacuated tube.

3.1. Comparison between Coated and Uncoated Evacuated Tube for Tube's Incline 10° and Flow Rate 100 ml/ min

Figure 7 showed the temperature output distribution of 1.0 cm tube coated with 75% Solution and Figure 8 shows the temperature output distribution of 1.5 cm tube coated with 85% Solution. Coated tubes gave higher temperatures compared to the uncoated tubes throughout the experiment.

Both the tubes gave an apparent temperature increment, and from the experimental result it is seen that 1.5 cm inner diameter tube gives a better performance. This is because of useful energy output Q_u of a collector is proportional to the surface area at the evacuated tube as the below formula:

$$Q_u = A_c\left[I_s - U_L\left(T_{pm} - T_a\right)\right]$$

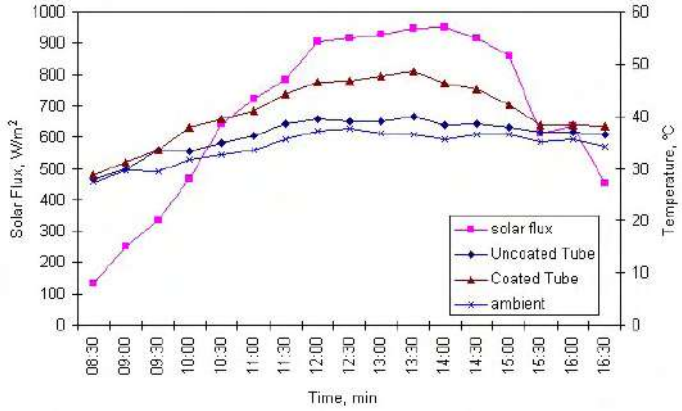

Figure 7: 1.0 cm tube; Temperature for Coated (75% Solution) and Uncoated for inclination 10° with the flow rate 100 ml/ min versus Time

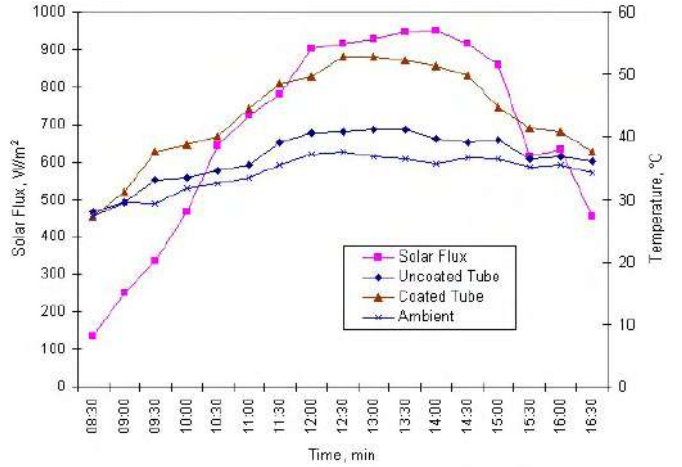

Figure 8: 1.5 cm tubes; temperature for Coated (85% solution) and Uncoated for inclination 10° with the flow rate 100 ml/ min versus Time

3.2 Comparison between Coated and Uncoated Evacuated Tube for Tube's Incline 15° and Flow Rate 100 ml/ min

Figure 9 shows the temperature distribution of 1.0 cm tube coated with 75% Solution and Figure 10 shows the temperature distribution of 1.5 cm tube coated with 85% Solution. Output temperatures are very much influenced by the solar flux. It can be observed from the Figures 9 and 10. When the solar flux drop from 769 W/ m^2 to 269 W/ m^2, the tubes temperature drops for coated as well as uncoated tube. Comparing both 1.5 cm tube shows a sharp temperature drop. The reason of this phenomenon is nothing but heat transfer occurred inside the evacuated tube. The formula below explains this effect where flow rate mean area is multiplied with velocity and with the roughness factor.

$$\dot{V} = A_b \times \dot{\upsilon} \times fr$$

$$\text{where } fr = \frac{Ar}{Ag}$$

Water flow rate was fixed at the beginning of this experiment. Therefore, every single tube will received a regular flow rate at 100 ml/ min. Assuming that 75% solution and 85% solution have a same value of roughness factor. Subsequently,

$$A_b \alpha \frac{1}{\dot{\upsilon}}$$

From this it is obvious that, 1.5 cm inner diameter evacuated tube has a bigger exposed area (A_b) compare to 1.0 cm inner diameter evacuated tube. In the other word, water velocity for 1.5 cm tube is lower than 1.0 cm tube. Therefore, heat transfer tends to occur more in 1.5 cm tube. So, when solar flux dropped, energy stored (heat energy) inside the black body layer tends to loose more in 1.5 cm tube due to larger exposed area to water and lower water velocity. When the solar flux continuously decrease, means no energy will be added to black body layer, but on the same time, black body layer still losing its energy to water due to heat transfer if water is flowing and Figure 10 indicates this phenomenon.

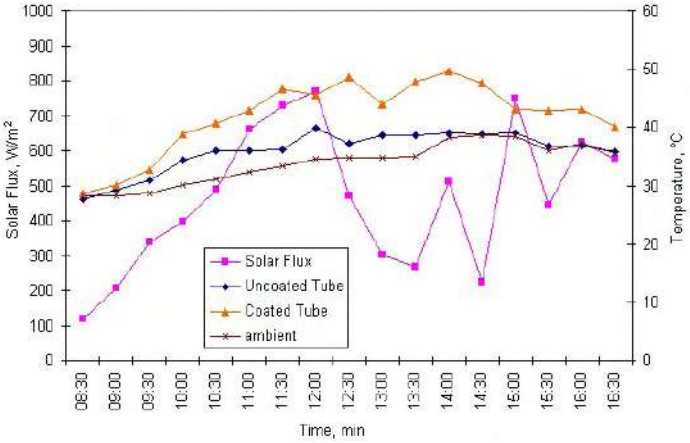

Figure 9: 1.0 cm tubes; temperature for Coated (75% solution) and Uncoated for inclination 15° with the flow rate 100 ml/ min versus Time

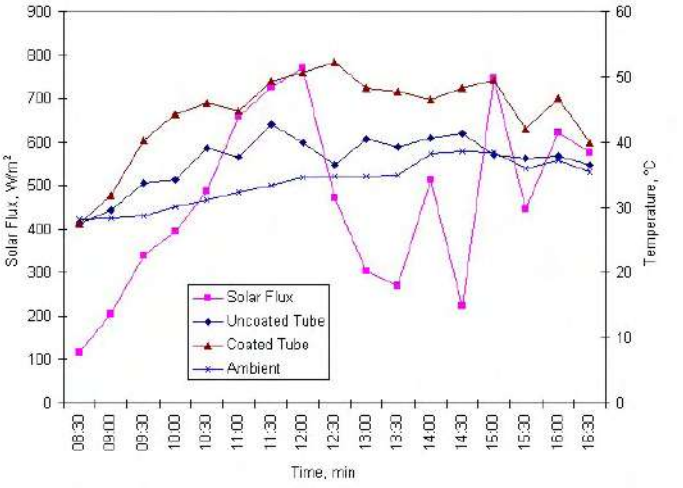

Figure 10: 1.5 cm tubes; temperature for Coated (85% solution) and Uncoated for inclination 15° with the flow rate 100 ml/ min versus Time

3.3 Comparison on the Different Inner Diameter for Coated Evacuated Tube at Flow Rate 100 ml/ min

Figures 11 and 12 show the temperatures output distribution according to solar flux from range 0 to 1300 W/ m^2 for 1.0 and 1.5 cm tubes respectively. At 100ml/min flow rate, both data clearly shown that temperatures output gradually increases when solar flux increase. Temperature output is

proportional to the increase in solar flux irrespective of angle of placement of the tubes. As a comparison between both graphs, 1.5 cm inner diameter tubes gave a higher temperature output compare to 1.0 cm inner diameter tubes. At the maximum point of solar flux, it can reach from 45 ^{o}C to 49 ^{o}C for 1.0 cm tubes. On the other hand, temperature output can reached 48^{o}C to 55 ^{o}C for 1.5 cm tubes considering a radial heat transfer, only along the pipe. At the steady state condition,

$$Q = -kA\frac{dT}{dx} \quad \text{(Fourier Equation)}$$

where A = 2πrL

From Fourier Equation, the bigger area is concern, the higher amount of heat transfer by conduction from the inner black coated layer to flowing fluid. Therefore, it just happen that higher temperature increment for 1.5 cm tubes compare to 1.0 cm tubes.

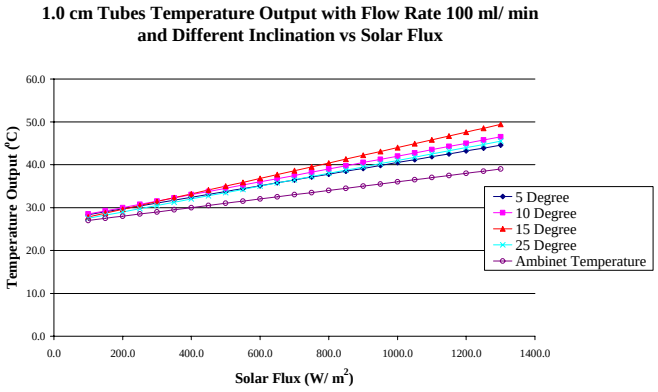

Figure 11: 1.0 cm Tubes Temperature Output with Flow Rate 100 ml/ min and Different Inclination versus Solar Flux

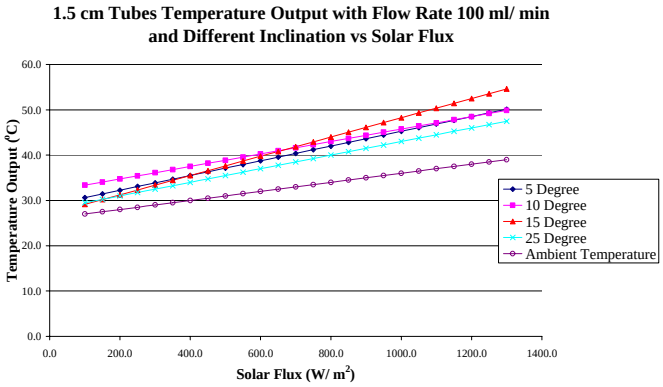

Figure 12: 1.5 cm Tubes Temperature Output with Flow Rate 100 ml/ min and Different Inclination versus Solar Flux

3.4 Effect of the Inclination Angle of Tubes

Geographical coordinates of Malaysia is:

Latitude of Malaysia: 2º30´ North of the Equator
Longitude of Malaysia: 112º30´ East of Greenwich

Whereas, Penang's geographical coordinates is located as:

Latitude of Penang: 5º25´ North of the Equator
Longitude of Penang: 100º19´ East of Greenwich

Therefore, it is believed that, at the specific location, it will give the best efficiency of solar evacuated tube with certain incline of angle.

3.5 Comparison on the Different Inclination Angle for Coated Evacuated Tube at Flow Rate 50ml/ min and 100 ml/ min

From Figures 11 and 12, shows the highest temperatures output are at the angle of 15^{o}. It followed by 10^{o}. Compared to Figure 13 and 14, shows the maximum temperature output at 10^{o} and followed by 5^{o}. So, it can be said that at 100 ml/ min flow rate, the optimum inclination is 15^{o}, whereas, the optimum inclination for 50 ml/ min flow rate is at 10^{o}. Therefore, flow rate did influent the inclination angle. As the smaller flow rate allowed to flow through the tubes, a higher inclination angle will cause the difficulty for fluid to flow from bottom inlet to higher elevation outlet on the other side. While the fluid could not flow smoothly from one side to another side, bubbling will happen and the consequently surface contact between coated layers with water will be lesser. Actually, this happened because of insufficient pressure at the lower flow rate to push enough water or and fluid to the other side of the tube.

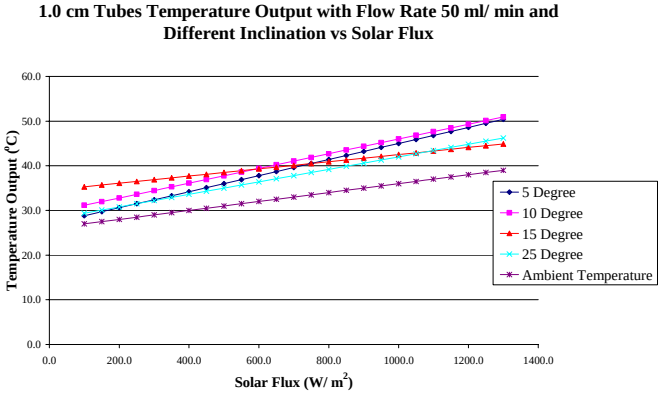

Figure 13: 1.0 cm Tubes Temperature Output with Flow Rate 50 ml/ min and Different Inclination versus Solar Flux

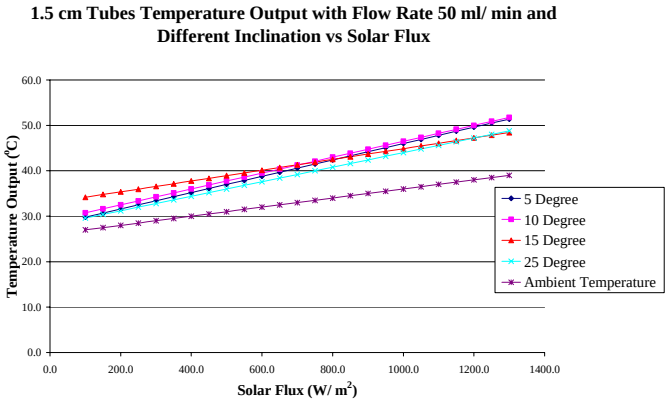

Figure 14: 1.5 cm Tubes Temperature Output with Flow Rate 50 ml/ min and Different Inclination versus Solar Flux

4. Conclusions

The performance of the evacuated tubes was observed to be better when it was coated. Under fixed flow rate and inclination angle conditions, temperature output of evacuated concentric tubes is proportional to solar flux. From this study it was observed that larger tube diameter can provide higher temperature output in the range studied where 1.5 cm inner

diameter tube showed the highest temperature output compare to 1.0 cm inner diameter tube. The optimised profile has a combination with 100 ml/ min as flow rate and inclination of 15^o. The results show that it is not recommended to use more than 15^o of inclination for flow rate less than 100 ml/ min. and it can be concluding that; higher inclination always comes with higher flow rate.

Nomenclature			
A	Cross section area [m^2]	T_a	Ambient temperature [K]
A_b	Absorber area exposed moving fluid [m^2]	T_m	Average manifold temperature [K]
A_c	Collector area [m^2]	T_{pm}	Mean absorber plate temperature [K]
A_r	Real surface (interface) area [m^2]	U_L	Overall heat loss coefficient [W/ m^2. K]
A_g	Geometric surface (interface) area [m^2]	$\dot{V}$	Water or fluid flow rate [ml/ min]
fr	Roughness factor (rugosity) (of a surface)	$\dot{\upsilon}$	Water or fluid velocity [m/ s]
G	Solar flux [W/ m^2]	Q	Heat flux [kJ]
h	Heat transfer coefficient [w/ m^2. K]	Q_u	Useful energy output [W]
I_s	Solar radiation reach the absorber layer [W/ m^2]	k	Thermal conductivity [W/ mC. ^oC]
L	Length of tube [m]	r	Inner tube radius [m]
T	Temperature [K]		

Greek symbols	
π	Phi [3.142]
σ	Stefan-Boltzman constant [W/ m^2. K^4]

5. References

1. J. C. McVeigh, S*un Power, An Introduction to the Applications of Solar Energy*", First Edition, Pergamon International Library, New York, (1977).

2. Mustapha Merzouk, Poubady Ramany Bala, Michel Feidt and Boumediene Benyoucef. (2003). Derivation of a tube solar collector transmittance for beam and diffuse radiation. International Journals of Thermal Sciences. 42: 317-322.

3. Theunissan P.H. and Beckman W.A. (1985). Solar transmittance characteristics of evacuated tubular collectors with diffuse back reflectors. Solar Energy. 35(4): 311-320.

4. Bostrom T., Wackelgard E. and Westin G. (2003). Solution chemical derived nickel-alumina coatings for the thermal solar absorber. Solar Energy. 74: 497-503.

5. Suzer S., Kadirgan F., Sohmen H.M., Wetherilt A.J. and Ture I.E. (1998). Spectroscopic characterization of Al_2O_3-Ni selective absorbers for solar collectors. Solar Energy Materials and Solar Cells. 52: 55-60.

6. Yin Zhiqiang, Xue Zuqing, Zhang Jian and Shen changzhi. (1999). Gradded Al-N/Al absorbing surface for all glass evacuated tubular collectors. Renewable Energy. 16: 624-627.

Geometry Alteration Effect on the Performance of a Solar-Wind Power System

H. H. Al-Kayiem*, Q. A. Al-Nakeeb **

*Associate Prof.; BSC, MSC, PHD Mech. Eng.
Academic Consultant of Y A/F & A/D
Email: hussain_faten@yahoo.com

**MSC in Mech. Eng.
Al- Nahrain Univ. /Iraq

(**Keywords**: Renewable energy, Computational modeling, Solar chimney, Energy technology,).

Abstract

The solar-wind power system consists of a solar collector part to collect and transfer solar energy to the working fluid and a chimney part to provide stack causing the fluid to flow continuously. The effects of geometries variation of the collector cover (canopy) and the chimney on the performance of the system are studied. The velocity, density, temperature and pressure distribution in the system are predicted in both, the collector and the chimney. The investigation was carried out by using numerical analysis based on the "Finite – Difference Technique" to solve iteratively the continuity, momentum, energy, and the stat equations under tow – dimensional flow assumption. Suitable assumptions have been used as an input to solve the governing equations under various solar intensities, ambient temperatures and wind speed, for four seasons in Baghdad city, to estimate the system performance during the year. Due to the nature of non parallel stream lines in the convergence or divergence passages, "Grid Generation and Axis Transformation Technique" was adopted to transfer the computational model from the physical to a computational plane.

The results showed that change of the canopy orientation in the solar collector have considerable effects on the performance of the system. The efficiency is increased in the diverging canopy case compared with the parallel case. The best flow characteristic is obtained with converging chimney, where, the flow accelerates towards the outlet of the chimney. This demonstrates the ability to shorten the chimney height, compared with the straight chimney case.

1. Introduction

Solar chimney is one of the systems that can be used to covert solar energy into direct usable form of energy, namely thermal. Air is heated by convection near a surface, which is heated by solar radiation under a low circular roof open at the periphery. In the middle of the roof is a vertical chimney with large air inlets at its base, as hot air is lighter than cold air it rises up in the chimney. The solar chimney consists of three essential elements: glass roof collector, chimney, and wind turbine. The sketch of a typical solar chimney is shown in Fig (1) which illustrates the principle of operation.

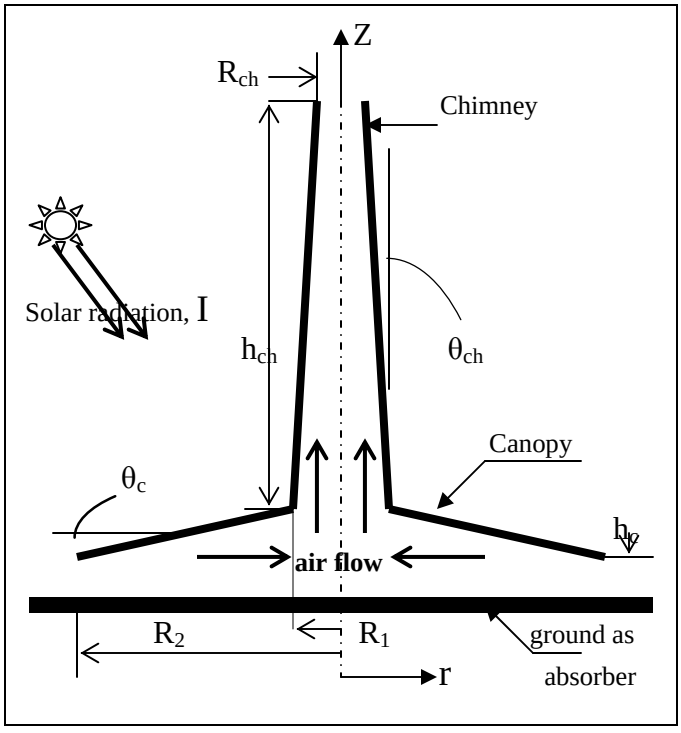

Figure 1: Operation principles of the solar chimney

The fundamentals of solar chimney power plant were investigated by Haff, et al., [1]. The planning of a pilot power

plant has been carried out and its construction started at Manzanares/ Spain. The site tests and results of that pilot was reported in details by Schlich [2]. Louis and Thomas, [3] studied the optimizing of collector efficiency for the solar chimney by using a model of calculation. Fluid dynamics for the solar chimneys was studied by Padki and Sherif [4]. A set of equations was developed to describe the fluid dynamic of such a chimney. Effects of various configuration parameters, such as the envelope shape, height of entrance to exit area ratio, the available power and chimney efficiency was considered. Among these, the last factor was found to have the most significant influence on the chimney performance. Theoretical analysis of solar chimney was presented by Sabah [5]. The results of theoretical work were compared with these of Manzanares plant experimental test under the same operation condition. The result had shown that the chimney height and the collector radius are the two main plant dimensions that govern the plant performance. Walter and Sergio [6] described the design, construction and testing the variation in the geometry of the chimney for solar dryer system, the results indicated that a slight geometry modification of the chimney (convert cone keeping height constant) will increase air velocity by a factor of 2- 3 with respect to a chimney of cylindrical shape. Al-Kayiem [7], studied the effect of ground type on the performance of solar collector for solar chimney power plant system. Five type of surface absorptivity have been tested as collection medium. He found that the asphalt was recommended type since its emissivity and absorptivity properties encountered in the best conversion of solar energy to thermal energy.
The present work is an addition in the field of natural air flow generators. It considers the effect of geometry variation in the canopy and chimney configuration on the system performance.

2. The Flow Governing Equations

The flow in the system is represented mathematically by application of the equations of motion and the state equation to solve for four unknowns in each point in the system, namely, the velocity, density, pressure and temperature. The analysis was carried out in the collector part and in the chimney part by solving the governing equations with suitable assumption in each part as in the following.

2.1 Analysis of the collector flow

To make the general formulation suitable to the collector heat transfer and air flow mechanism, the following were assume

- The system is steady

i.e. ; $\partial / \partial t = 0$

- There is no velocity component in θ – direction, and the flow in the collector passage has complete symmetry with the θ – direction, so
i.e. ; $\partial / \partial \theta = 0$

- The variation of temperatures is small, so the air thermal conductivity and viscosity are constants.

- Constant ground and floor temperature at time of analysis.

- The change in density to density ratio is greater than 0.05, then the compressibility effect must be considered.

Accordingly, the set of the general equations becomes:

The continuity

$$\rho.\frac{\partial Vr}{\partial r} + Vr.\frac{\partial \rho}{\partial r} + \frac{\rho.Vr}{r} = 0 \quad . \qquad (1)$$

The momentum

$$\rho Vr\frac{\partial Vr}{\partial r} + \frac{\partial P}{\partial r} - \mu\left[\left(\frac{4}{3}\right)\left(\frac{\partial^2 Vr}{\partial r^2} + \frac{1}{r}\frac{\partial Vr}{\partial r} - \frac{Vr}{r^2}\right) + \frac{\partial Vr^2}{\partial z^2}\right] = 0 \qquad (2)$$

The energy

$$K\left[\frac{\partial^2 T}{\partial r^2} + \frac{1}{r}\frac{\partial T}{\partial r} + \frac{\partial^2 T}{\partial z^2}\right] + 2\mu\left[\left(\frac{\partial Vr}{\partial r}\right)^2 + \left(\frac{Vr}{r}\right)^2 + \frac{1}{2}\left(\frac{\partial Vr}{\partial z}\right)^2 - \frac{1}{3}\left(\frac{\partial Vr}{\partial r} + \frac{Vr}{r}\right)^2\right]$$
$$-Cp\left(p.Vr\frac{\partial T}{\partial r}\right) + Vr\frac{\partial P}{\partial r} = 0 \qquad (3)$$

Where: V_r is the radial velocity component.
T and P are the temperature and pressure respectively at any point in the flow field.
ρ Is the air density at any point in the flow field

The transport coefficient μ and k must be considered for laminar flow and for turbulent flows. If the flow of air is laminar, so the values of k and μ are physical properties of the fluid. If the flow is turbulent, then the values of transport momentum and energy μ and k are function of temperatures and flow of the air. The turbulent transport gives rise to effective values of viscosity and thermal conductivity defined

as eddy viscosity (ε) and eddy thermal conductivity (k) respectively.

The values of viscosity and thermal conductivity in turbulent flow consist of (μ + ε) and (k + κ) where [8].

$$\varepsilon = \rho l^2 \left| \frac{\partial Vr}{\partial y} \right| \quad . \qquad (4)$$

And

$$k = \varepsilon . Cp \qquad (5)$$

Where ι is called the mixing length could evaluated for flow between two plates separated by 2h according to [8], (h is the distance from the wall to the mid distance between the plates) as

$$\frac{\iota}{h} = \left[0.14 - 0.08\left(\frac{y}{h}\right)^2 - 0.06\left(\frac{y}{h}\right)^4 \right] \qquad (6)$$

The collector performance η_c can be investigated for a specific geometry and weather (radiation condition) as the ration of gained heat to the working fluid to the total input solar energy:

$$\eta_c = \frac{C_p m \Delta T}{\pi\left(RC2^2 - RC1^2\right) I} \qquad (7)$$

2.2 Analysis of the Chimney flow

By adopting similar assumptions as in the collector part, then

- The system is steady

i.e. ; $\partial / \partial t = 0$

- There is no velocity component in θ – direction, and the flow in the chimney has complete symmetry with the θ – direction, so that

$$\partial / \partial \theta = 0$$

- The variation of temperatures is small, so the air thermal conductivity and viscosity are constants.
- The flow is subjected to heat transfer from the wall of the chimney.
- $\Delta\rho / \rho > 0.05$, then the compressibility effect is under consideration.

Accordingly, the set of the general equations becomes:

The continuity

$$\rho \frac{\partial Vz}{\partial z} + \frac{\partial \rho}{\partial z} Vz = 0 \qquad (8)$$

The momentum

$$\rho . Vz \frac{\partial Vz}{\partial Z} - \rho . g . \beta (T - Ta) + \frac{\partial P}{\partial z} - \mu \left[\frac{4}{3} \frac{\partial^2 Vz}{\partial z^2} + \frac{\partial^2 Vz}{\partial r^2} + \frac{1}{r} \frac{\partial Vz}{\partial r} \right] = 0 \qquad (9)$$

The energy

$$k\left[\frac{\partial^2 T}{\partial r^2} + \frac{1}{r}\frac{\partial T}{\partial r} + \frac{\partial^2 T}{\partial z^2}\right] + 2\mu\left[\frac{2}{3}\left(\frac{\partial Vz}{\partial z}\right)^2 + \frac{1}{2}\left(\frac{\partial Vz}{\partial r}\right)^2\right] - Cp\left(p . Vz \frac{\partial T}{\partial z}\right) + Vz \frac{\partial P}{\partial z} = 0 \qquad (10)$$

Where: V_z is the upward velocity component in the chimney. The turbulent analysis of the flow field through the chimney is similar to that of the collector flow inserting R instead of h and r instead of y to get:

$$\frac{\iota}{R} = \left[0.14 - 0.08\left(\frac{r}{R}\right)^2 - 0.06\left(\frac{r}{R}\right)^4 \right] \qquad (11)$$

The temperature of the chimney wall could be calculated by applying the equation:

$$T_w = T_a + \alpha I / h_w \quad . \qquad (12)$$

The temperature of the wall, $T_{w,}$ is the ambient temperature increased by an amount to account for the solar radiation. [9].

The hydrothermal efficiency of converting thermal energy to flow available power in the chimney (η_{th}) is:

$$\eta_{ht} = \frac{\frac{1}{2}\rho A V^3}{C_\rho m^\circ \Delta T} \quad . \qquad (13)$$

3. Computational Manipulation

Firstly, the mathematical model of the system represented by the set of the governing differential equations is transferred from the physical (r - z) plane to the computational (ζ - η) plane. The matrices of transformation are computed numerically according to ref. [10]

A completely general two- dimensional transformation function for a fixed grid is:

$$\zeta = \zeta (r, z) \qquad (14)$$

$$\eta = \eta (r, z) \qquad (15)$$

Secondly, these equations were transformed from their differential forms to the finite- difference form and substituting each node of the mesh. Thirdly, a system of non- linear simultaneous algebraic equations will be generated. To determine the variables in the system, the number of the algebraic equations must be equal to the number of the mesh nodes. Lastly, this system of equations is solved by Newton-Raphson iteration method as suggested by ref [10].

4. Discussion of Results

In fact, the main aim of the present paper is to investigate theoretically the air generation performance at

1. Different canopy orientations.
2. Different Chimney orientation.

4.1 The collector analysis

The reference of the canopy setting is the normal parallel orientation; i.e., ($\theta = 0^o$). The results were obtained at four different canopy setting with slope angles of $\theta = 0^o$, -0.5^o, -1^o and $+0.5^o$. The negative angles are referring to diverging passage, the positive angle is refer to convergence passage while the zero angle refers to parallel setting as stated in figure 2 bellow

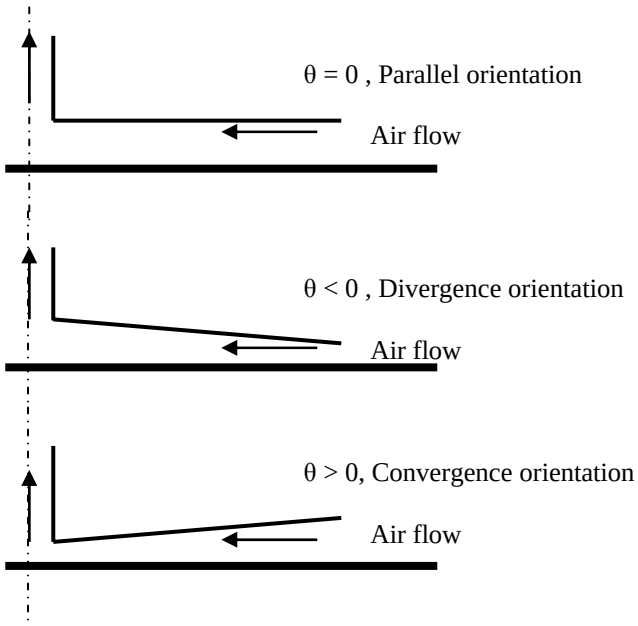

Figure 2: The tested canopy orientations

The results of the effect of the canopy slope changes on the collector performance are shown in fig (3).

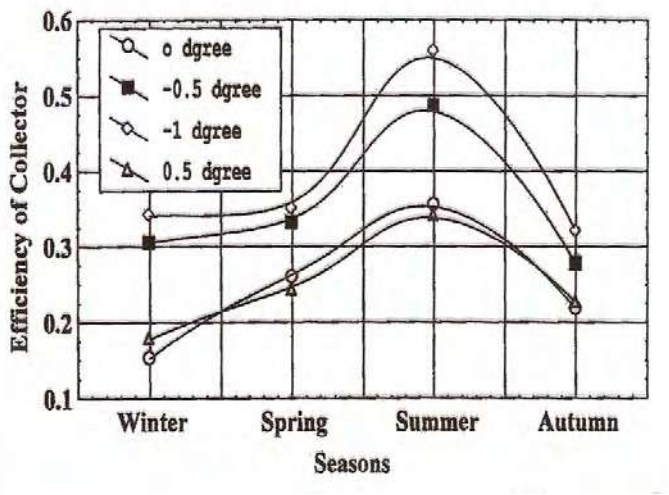

Figure 3: Effect of canopy orientation on the efficiency of the collector

The analysis of this part has shown that the canopy slope has considerable effect on the collector performance. Referring to Fig (3), it could be noticed that the collector efficiency is increased in the case of the divergence flow passage. In the case of setting the canopy at -0.5^o, the collector efficiency is enhanced by about 10% (as mean for the four seasons). Larger inclination of the canopy up to 1^o produces more enhancements in the collector performance up to further 4% in the collector efficiency. Going towards larger inclination is not practical where constructional problem will associated. If the inlet of the canopy is kept at its normal height (h_c) and the inner part is raised up, the construction requires stronger and more expensive structure. If the canopy is kept to its normal height (h_c) at the inner radius and lowered at the inlet, it's either hit the ground or the inlet area becomes small leading to possibility of blockage. When the canopy is set at convergence configuration with 0.5^o slope, a 2% reduction in the collector efficiency is occurred.

Generally speaking, the variation of the collector efficiency due to alteration of the canopy slopes may summarize as in table 1.

The canopy Slope	the resulted efficiency	percent of change
0.5	21.4%	- 2
0	26.7%	
- 0.5	29.4%	+ 10
-1	30.6	+ 14

Table 1: Collector efficiency at different canopy settings

The chimney performance was analyzed under three proposed design configurations. Firstly at the normal design, $\theta_{ch} = 0^o$, i.e., chimney as a pipe. Secondly as convergence (nozzle) setting, $\theta_{ch} < 0^o$, and thirdly as divergence (diffuser), $\theta_{ch} > 0^o$ which are clarified in figure 4 bellow.

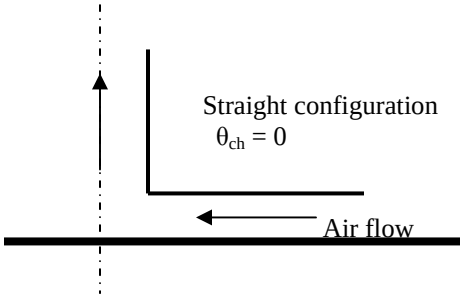

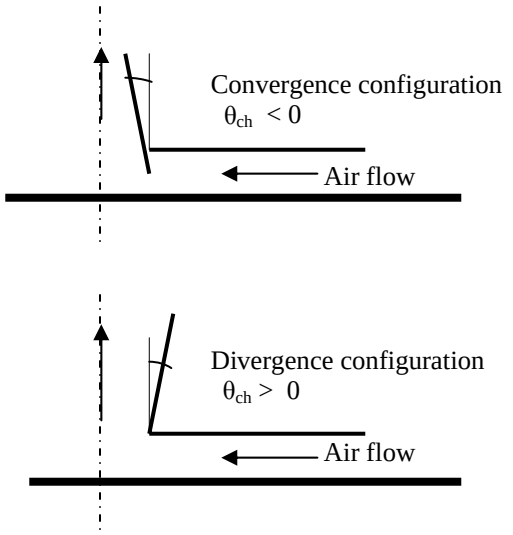

Figure 4: The tested chimney configurations

The results obtained are shown in fig (5). Setting the chimney at -0.5^o convergence is caused the hydro thermal efficiency to increase by about 0.4% due to the increase in the flow acceleration leading to better stack effect. Setting the chimney at a diffuser configuration with 0.5^o wall slope shows small reduction in the hydro thermal efficiency of the system. These results are demonstrating the founding of ref. [6] in experimental investigation of a solar dryer.

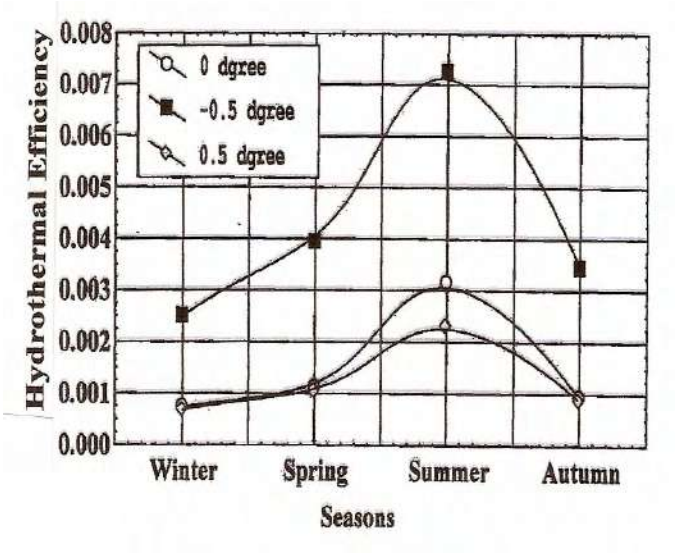

Figure 5: effect of chimney wall slope on the hydrothermal efficiency

5. Conclusion

The solar chimney as natural wind generator was modeled mathematically. The set of governing equations was solved numerically. The effect of varying the canopy orientation and the chimney configuration was the main objective of the present paper. The results demonstrated that setting the canopy at small angle to allow divergence air flow passage will enhance the collector performance considerably. The chimney results show small enhancement in the hydro thermal efficiency of the chimney when it sets in a nozzle configuration.

Acknowledgment

The authors would like to present their thanks to the Directorate of Scientific Affairs in the Presidential Divan in Iraq for supporting this project as part of the wind – solar research program. Also thanks are due to the University of Saddam (Al-Nahreyin University Recently) for the assist presented by the college of engineering during the research works of this project.

References

[1] Haff, W., Mayr, G. Schlaich, J., "Solar chimney", *Report, Germany, F. R.*, August 1981.

[2] Schlaich, J., "The solar chimney", *Axel Menges, Stuttgart*, 1995.

[3] Louis, Thomas, "Optimization collector efficiency of a solar chimney power plant", *IEEE, New York, NY, USA*, PP. 219-222.1985.

[4] Padki, M. M. and Sherif, S. A., "Fluid dynamics of solar chimneys", *ASME, Fluid Engineering Division, VOL. 70*, PP. 43-46, 1988.

[5] Sabah, K. M., "'*Performance Analysis of Solar Chimneys*", MSc. Thesis, College of Engineering, Saddam University, Baghdad, 1998.

[6] Walter Z., Sergio A., "Design, Construction and testing of a Chimney that Reduces Dangerous Temperature in a radiative Convective Solar Dryer", *Solar Energy, VOL. 32, NO. 5*, 1984.

[7] Al- Kayiem H. H., "Effect of ground type on electrical power production by solar chimney"; Journal *of Engineering and Development", Al- Mustanisrya University, Baghdad*, 2000.

[8] H. Schlighting, *Boundary- Layer Theory*, 7th Edition, McGraw-Hill Company, New York, 1979.

[9] F. W. Stoecker, J. W. Jones, *Refrigeration and Air Conditioning*, McGraw- hill Book Company, 1982.

[10] Anderson and D. A. Tannehill and C. John and P. H. Richard, *Computational Fluid Mechanics and Heat Transfer*, Hemisphere Publishing Corporation, New York. (1984).

Down-draft Gasification of Biomass/Coal Blends

Lukeman Yusoff* and Farid Nasir Ani

*Universiti Kuala Lumpur
Malaysia France Institute
Section 14, Jalan Teras Jernang
43650 Bandar Baru Bangi
Selangor Darul Ehsan, Malaysia
lukeman@mfi.edu.my

Faculty of Mechanical Engineering
Universiti Teknologi Malaysia
81310 UTM Skudai
Johor, Darul Ta'zim, Malaysia
farid@fkm.utm.my

Keywords: Oil palm shell, Mukah-Balingian coal, Downdraft gasifier, Gasification.

Abstract

Over 80% of the world energy generated presently is by fossil fuels where petroleum oil contributes 41%. By the end of this century with the present rate of extraction, the petroleum resources will be depleted. Depletion of global fossil resources as well as increasing of fossil fuel prices with deteriorating of the environmental quality from energy generation become major global problems. Alternative energy should be found and developed through research and development of new energy resources to replace the non-renewable fossil fuels. A potential renewable energy, which could replace the fossil fuels, is biomass energy such as wood, agricultural residues, municipal solid waste and forest residues. The largest biomass source that is easily available in Malaysia is the oil palm *(Elaeis guineensis)* solid wastes.

In this research, oil palm shell and Sarawak coal have been used as raw feeding materials in a downdraft gasifier. Pressurized primary air was supplied to the gasifier to assist the gasification process. An air ejector and gas burner was attached at the outlet of the gasifier. The producer gas produced in the gasifier was induced out by a secondary compressed air, through an air ejector. The air-producer gas mixtures were re-burnt at a gas burner. An orifice cylinder with vane was coupled inside of the gas burner to enhance the mixing process of air-producer gas mixtures. Oil palm shell, Mukah-Balingian coal, and their blends were investigated as feedstocks in this work. Emissions produced at the outlet of gas burner with different orifice cylinders diameter were investigated. Suitable orifice cylinder was attached with a 40^o swirler to investigate the effect of emissions and combustion efficiency. Temperatures of various zones in gasifier and emissions produce at the outlet of the gas burner with the variation of sizes of orifice cylinders and fuel ratio were given and discussed at constant induced pressure condition.

1 Introduction

Gasification is one of the thermochemical processes, which can convert the biomass solid residues and coal to the valuable form of gaseous fuel known as producer gas. The producer gas contains carbon monoxide (CO), carbon dioxide (CO_2), hydrogen (H_2) and methane (CH_4). Mixed with air, the producer gas can be used in gasoline and diesel engines with little modifications. In a downdraft gasifier, the air is introduced in downward flow through packed bed of solid fuels and gas is drawn off at the bottom. Downdraft gasifier is suitable to run internal combustion engines and other thermal energy applications.

Gasification process generally uses reactants such as oxygen or steam to increase gas yields while consuming char. In the gasifier where solid fuels are gasified in the presence of sub-stoichiometric air, several chemical reactions occur. The downdraft gasification reactions and temperature zone are shown in Figure 1.

In the reduction zone, there is a surplus of solid fuel, carbon dioxide and water vapor from the combustible zone can be passed through the glowing layer of charcoal and are reduced to carbon monoxide (CO) and hydrogen (H_2) in the region known as the reduction zone. In the combustion zone, the reactions which are exothermic are:

$$C + O_2 \rightarrow CO_2 \quad (1)$$

$$2H_2 + O_2 \rightarrow 2H_2O \quad (2)$$

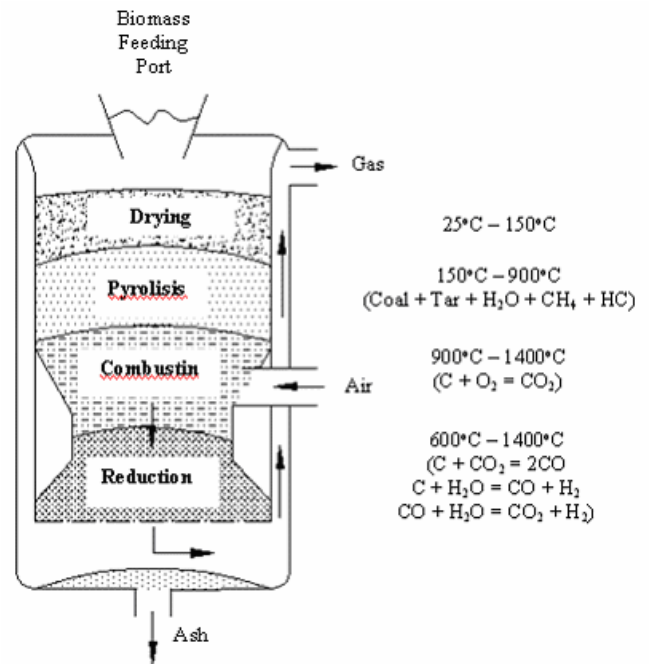

Figure 1: Downdraft gasification reactions and temperature zone

The reaction in the reduction zone which are endothermic, will decrease the temperature during the reduction process are :

$$C + CO_2 \rightarrow 2CO \quad (3)$$

$$C + H_2 0 \rightarrow CO + H_2 \quad (4)$$

$$C + 2H_2 \rightarrow CH_4 \quad (5)$$

$$CO + 3H_2O \rightarrow CH_4 + H_2O$$

$$C + 2H_2O \rightarrow CO_2 + H_2$$

$$CO + H_2O \rightarrow CO_2 + H_2 \quad (6)$$

Producer gas is therefore a mixture of the gaseous such as hydrogen (H_2), carbon monoxide (CO), carbon dioxide (CO_2), nitrogen (N_2), methane (CH_4), and small amount of other hydrocarbons. The combustible components of the gas are CO, H_2, CH_4 and C_xH_x, the percentages of which should be made as high as possible. The quantity of CO in the gas depends on the temperature in the reduction zone. To achieve complete reduction, the temperature in the reduction zone must be at least 1100 °C [1].

If water vapor is present, reaction (4) play an important role to enrich the gas with H_2 and thus enhance its heating value. However, if too much water is present, CO may react with H_2O to form CO_2 and H_2, as indicated by reaction (6) and the quantity of CO may be reduced.

In the present research, a downdraft gasifier has been used. Pressurized primary air was supplied to the gasifier to assist the gasification process. An air ejector and a gas burner were attached with the gasifier. Producer gas produced in the gasifier was induced out by the secondary compressed air at 2 bar, through the air ejector. The air-producer gas mixtures were re-burnt at the gas burner. Orifice cylinder and vane was coupled inside of the gas burner to enhance the mixing of air-producer gas mixtures.

Oil palm shell, Mukah-Balingian coal and the blend of both them were used as feedstocks in this work. Emissions produced from the combustion process at the gas burner with different orifice cylinders were investigated. Orifice cylinder produce the lowest emissions was attached with a 40^o swirler to investigate the effect of emissions and combustion efficiency.

2 Experimental Set-up

2.1 Downdraft Gasifier, Air Ejecetor and Gas Burner

Downdraft gasifier as shown in Figure 2 was designed and fabricated on 1988 by Salim in Universiti Teknologi Malaysia, Skudai, Johor, Malaysia [2]. Capacity of the gasifier is 43,000 cm^3, but only half of it can be used to get the best possible gasification process. A layer of refractory material was covered around the bottom of the gasifier for high temperature insulation around 1000^oC. There is also having a component called throat at combustion zone. The throat is function to increase the temperature concentration at combustion zone.

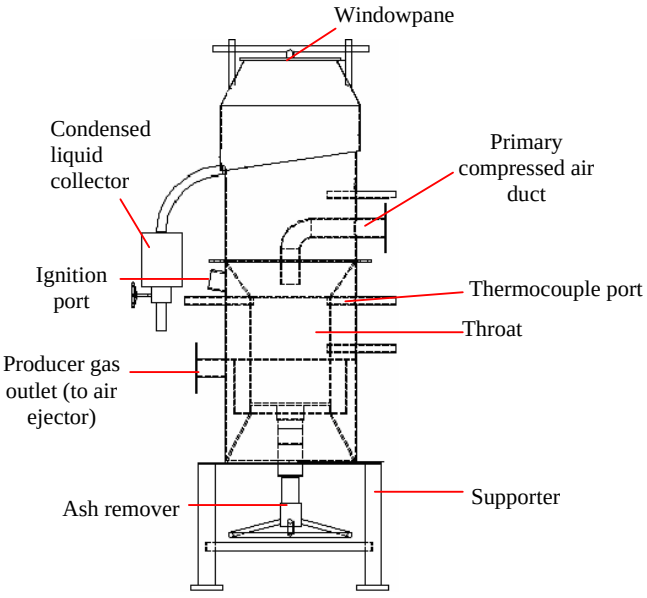

Figure 2: Downdraft gasifier

An air ejector as shown in Figure 3 is designed to supply secondary air to gas burner. The ejector also acts to induce producer gas from gasifier to the gas burner before its being burnt. An orifice cylinder was installed inside of gas burner to increase the air-producer gas mixing. The diameters of orifice cylinders are 80, 100 and 120 mm with same 30 mm length.

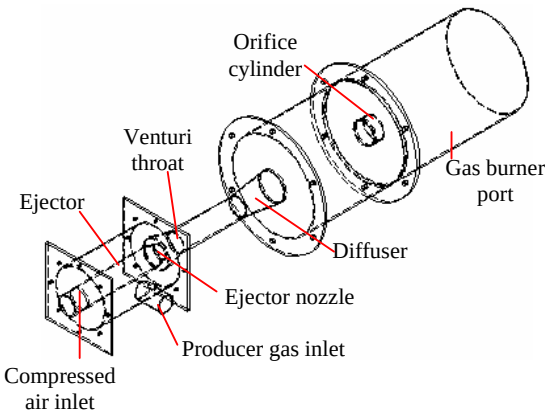

Figure 3: Gas burner and ejector

Gas burner without orifice cylinder is known as "GB", gas burner with 80 mm orifice cylinder is known as "GB80", gas burner with 100 mm orifice cylinder is known as "GB100", gas burner with 120 mm orifice cylinder is known as "GB120", and gas burner with orifice cylinder that produced the lowest emission and installed with 40^o vane is known as "GB80V".

2.2 Experimental Procedures

Oil palm shell is obtained from Federal Land Development Authority (FELDA) Palm Oil Mills, Kulai, Johor, Malaysia while Mukah-Balingian coal is obtained from Genesis Forces Sdn. Bhd., Sarawak. Oil palm shell solid density and apparent density is 1.53 g/cm^3 and 1.47g/cm^3, respectively [3]. The proximate, ultimate analysis and calorific values oil palm shell [4] and Mukah-Balingian Coal [5] [6] are shown in Table 1.

Analysis	**Oil palm Shell**	**Mukah-Balingian Coal**
Proximate analysis (wt. %)		
Ash	2.50	2.13
Volatiles matter	77.20	35.81
Fixed carbon	20.30	50.60
Moisture (wt. % air dry)	8.40	11.46
Ultimate analysis (wt. %)		
Carbon	55.35	51.31
Hydrogen	6.27	5.60
Oxygen	38.01	43.09
Nitrogen	0.37	0.00
Calorific Value (MJ/kg)	19.56	23.50

Table 1: Proximate and ultimate analysis of oil palm shell

Air ejector, gas burner (without orifice cylinder), air compressor, thermocouples, gas analyzer, pressure regulator, and gas-torch were placed to the gasifier. 4 kg oil palm shell was put in gasifier and was ignited. Primary air at 0.75-1.25 bar was supplied to gasifier. When thick white smoke appeared, another 1 kg oil palm shells were added to the gasifier. When the smoke became thicker, 2 bar secondary air were supplied to gas burner through air ejector. The air-producer gas was ignited and flame appeared at gas burner.

The emissions, combustion efficiency and flame temperatures were determined by using gas analyzer. Then, the oil palm shell feed was replaced with Mukah-Balingian coal, followed by the blend of oil palm shell and Mukah-Balingian coal. An 80 mm orifice cylinder was installed to gas burner and same tests were done, followed by 100 mm and 120 mm orifice cylinders. Orifice cylinder produced the lowest emission was coupled with 40^o vane to see the different in emission produced.

3 Results and Discussions

Three results have been investigated which are temperature variation inside of gasifier, emissions produced at gas burner and the flame colour and shapes.

3.1 Temperature Variation

By using oil palm shell as feed, the temperatures produced inside of gasifier are in the range of 351-1342 K, where 351 K is at drying zone, 573 K is at pyrolisis zone, 1342 K is at combustion zone and 1120 K is at reduction zone. When Mukah-Balingian coal is used, the temperature changed to 329 K at drying zone, 436 K at pyrolisis zone, 1183 K at combustion zone and 981 K at reduction zone. The values are lower than temperatures based on oil palm shell as feed as shown in Figure 4. By using the blend of

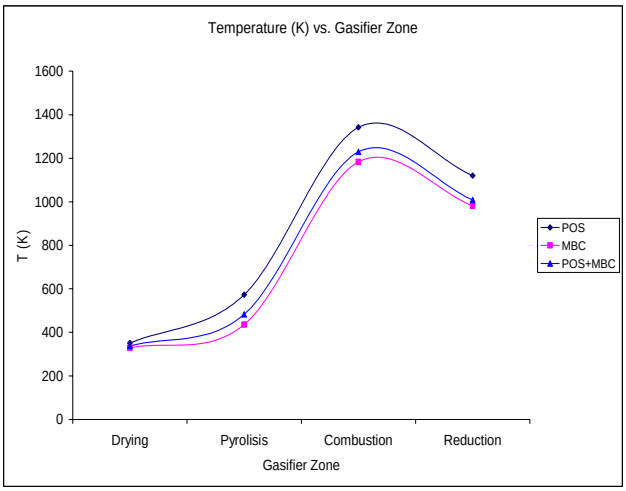

Figure 4: Temperature comparison for oil palm shell (POS), Mukah-Balingian coal (MBC) and the mixture of them (POS+MBC) as feed

oil palm shell and Mukah-Balingian coal as feed, the average temperatures inside of gasifier are 338 K at drying zone, 483 K at pyrolisis zone, 1230 K at combustion zone and 1008 K at reduction zone.

3.2 Emissions

Emission data contains NO_x (ppm), CO (ppm), percentage of CO_2, O_2 and excess air, flame temperature (K), and combustion efficiency (%). The NO_x value is high base on oil palm shell as feed. When Mukah-Balingian is used the NO_x was reduced. The blend of both fuel produced NO_x value in between of them. GB80V produced the lowest NO_x value for all fuel used, followed by GB80, GB100, GB120 and GB. The lowest NO_x value is 52 ppm, while the highest is 139 ppm as shown in Figure 5. CO produced is almost same with the NO_x profile as shown in Figure 6. The value is high based on oil palm shell feed, followed by the blend of oil palm shell and Mukah-Balingian coal, and the lowest is Mukah-Balingian coal. GB80V is also produced the lowest CO for all feed used, followed by GB80, GB100, GB120 and GB, while the highest and the lowest value is 258 ppm and 152 ppm.

CO_2 is increased when oil palm shell is changed to Mukah-Balingian coal feed, while GB80V produced the highest, followed by GB80, GB100, GB120 and GB as shown in Figure 7. The highest and the lowest value are 14.9 % and 12.2 % respectively. O_2 produced is contrasted with CO_2 profile as shown in Figure 8. Oil palm shell produced the highest with 8.7 % at GB, followed by the blend of oil palm shell and Mukah-Balingian coal. The lowest is Mukah-Balingian coal with 4.9 % at GB80V. Equivalent to O_2, percentage of excess air is also high base on oil palm shell fuel, and then decrease when the feed is changed to Mukah-Balingian coal. The value is high at GB for all feed base, with 19.5 % is the maximum. Minimum excess air is at occurred at GB80V, with 17.1 %, 15.5 % and 14.6 % base on oil palm shell, the blend of oil palm shell and Mukah-Balingian coal, and Mukah-Balingian coal, respectively, as shown in Figure 9.

Combustion efficiency is low base on oil palm shell as feed with 69 % for GB, 75.4 % for GB80, 72 % for GB100, 71.7 % for GB120, and 78.1 % for GB80V. This value is increase to 88.1 % for GB, 92.1 % for GB80, 91.7 % for GB100, 90.2 % for GB120, and 94.2 % for GB80V when the oil palm shell is changed to Mukah-Balingian coal. For the blend of them, the combustion efficiency is in between of them as shown in Figure 10. Flame temperature is almost equivalent to the combustion efficiency profile. Mukah-Balingian coal produced the highest temperature, followed by the blend of oil palm shell and Mukah-Balingian coal. Oil palm shell feed used produced the lowest. GB80V produced the highest flame temperature with 870 K as shown in Figure 11, followed by GB80, GB100, GB120 and GB with 863 K, 858 K, 838 K, and 828 K, respectively.

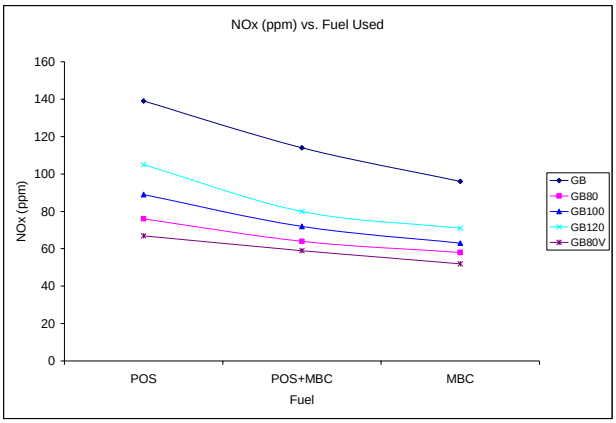

Figure 5: NO_x vs. type of fuel used

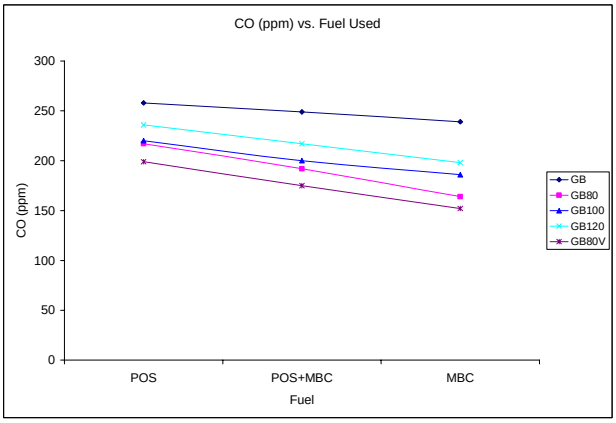

Figure 6: CO vs. type of fuel used

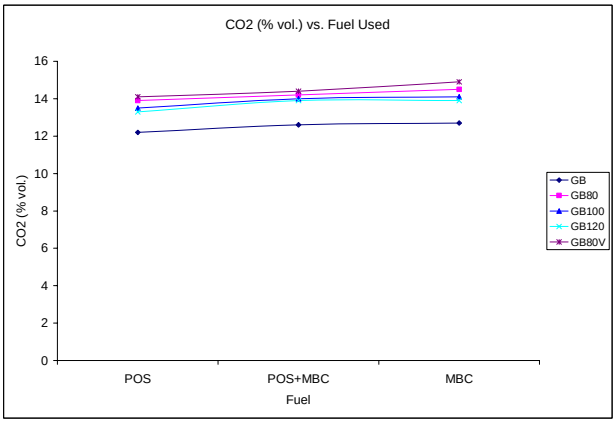

Figure 7: CO_2 vs. type of fuel used

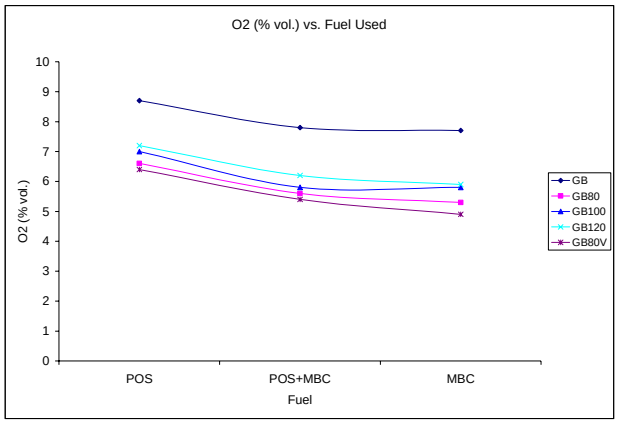

Figure 8: O_2 vs. type of fuel used

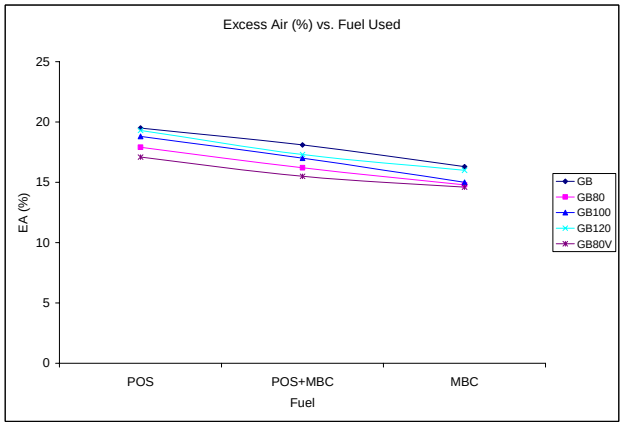

Figure 9: Excess air vs. type of fuel used

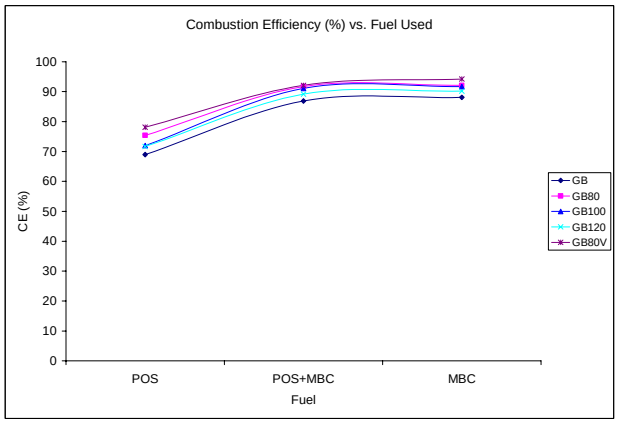

Figure 10: Combustion efficiency vs. type of fuel used

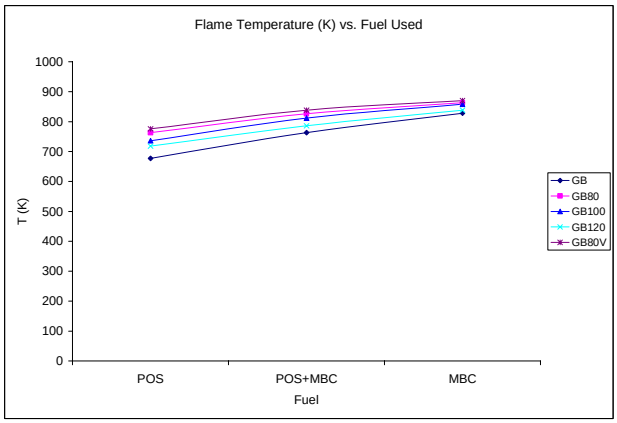

Figure 11: Flame temperature chart vs. type of fuel used

3.3 Flame Colour and Shapes

Blue and shorter flames were obtained at the burner port as the amount of coal increases in the feed mixtures. Coal gasification produces intense flames compared with biomass flames which produces disperse flames as seen in Figures 12, Figure 13 and Figure 14. The effect of using 40^o swirler inserted in the orifice port also gives control flames shape as compared without using swirler with the premixed gaseous fuel and air.

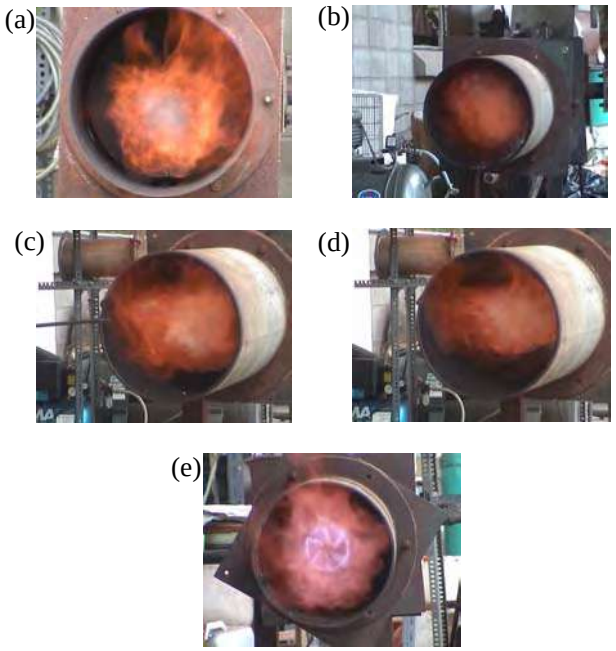

Figure 12: Flame emitted at (a) gas burner without orifice cylinder, (b) gas burner with 120mm orifice cylinder, (c) gas burner with 100mm orifice cylinder, (d) gas burner with 80mm orifice cylinder and (e) gas burner with 80mm orifice cylinder and 40^o swirler based on palm oil shell as feed.

Figure 13: Flame emitted at gas burner with 80mm orifice cylinder and 40^o swirler based on the blend of palm oil shell and Mukah-Balingian coal as feed.

Figure 14: Flame emitted at gas burner with 80mm orifice cylinder and 40^o vane based on Mukah-Balingian coal as feed.

4 Conclusions

The temperature profiles inside the gasifier for both coal and biomass were obtained, oil palm shell feed contribute a higher temperature profile inside of the gasifier, while Mukah-Balingian coal feed is the lower profile. Gas burner with 80 mm diameter of orifice cylinder produced the lowest emission compared to 100 and 120 mm, thus was installed with 40^o swirler. NO_x, CO, O_2 and excess air value is reduced when the oil palm shell fuel is changed to Mukah-Balingian coal. The decreasing values are 22.4 %, 23.6 %, 23.4 % and 14.6 %, respectively for gas all types of gas burner. GB80V produced the lowest, followed by GB80, GB100, GB120 and the highest is gas burner GB. For CO_2, combustion efficiency and flame temperature, the value is increased when the Mukah-Balingian coal is replaced the oil palm shell. The increasing is about 5.7 %, 12.1 % and 20.6 %, respectively. GB produced the lowest, and GB80V produced the highest with 17.3 %, 5 % and 6.9 % increasing, respectively. Blue and shorter flames were obtained as the amount of coal increases in the feed mixtures and when using the swirl burner.

References

[1] K. B. Henry, *Energy the Biomass Option*, John Wiley and Son Inc, New York, USA. (1981)

[2] S. M. Salim, *Penggasan Biomas (Ujikaji Keatas Enjin Petrol)*, B.Eng Thesis, Universiti Teknologi Malaysia, Kuala Lumpur, Malaysia (1988).

[3] J. Guo, and A.C. Lua, *Kinetic Study on Pyrolitic Process of Oil-Palm Solid Waste Using Two-Step Consecutive Reaction Model*, Biomass and Bioenergy, (2001), 223-233.

[4] R. B. Zailani, *Fluidized Bed Pyrolysis of Organic Solid Waste*, M.Eng Thesis, Faculty of Mechanical Engineering, Universiti Teknologi Malaysia, Johor, Malaysia (1995).

[5] Y. Lukeman, *The Effect of Pressurized Induced Flow on Downdraft GasifierPerformance with Low Emission Burner*, M.Eng. Thesis, Universiti Teknologi Malaysia, Johor, Malaysia (2004).

[6] S. S. Mohd, *Ciri-ciri Termodinamik Biojisim di Malaysia*, B.Eng Thesis, Universiti Teknologi Malaysia, Kuala Lumpur, Malaysia (1988).

[7] J.H. Tay, *Complete Reclamation of Oil Palm Wastes.* Resources, Conservation and Recycling, 5. 92-383 (1991).

Prospects for Ocean Energy in Malaysia

Omar Yaakob, Tengku Mohd Ariff Bin Tengku Ab Rashid, Mohamad Afifi Abdul Mukti
Department of Marine Technology
Faculty of Mechanical Engineering
Universiti Teknologi Malaysia
81310 UTM Skudai
MALAYSIA

Email: omar@fkm.utm.my

Keywords: alternative, renewable energy

Abstract

The ocean one of the most perpetual sources of energy and has already been exploited on a small scale. Some technologies are being developed to exploit the large potential of this energy source. This paper will focus on ocean energy as an alternative source in Malaysia. The current development of various devices to extract the ocean energy will be reviewed. Although technologies are currently being developed in the areas of tidal power, wave power, thermal energy gradient, current energy, winds and salinity gradient, not all of these are suitable for Malaysian sea areas. This paper surveys the available Malaysian oceanographic data and identifies the potential sources of energy.

1. Introduction

The world energy consumption is always on the rise. Our continuing dependence on non-renewable/fossil sources will only aggravate the situation. Several studies have predicted that if we continue consuming at the current rate, some of these energy sources will be exhausted within a century or if not a few decades.

In addition, environmental decays from release of pollutants are generating concern. Therefore, alternative sources of energy must be sought from sources that are not only renewable but also environmental friendly.

The ocean which covers more than 70% of our planet is a huge reservoir of renewable energy. If properly exploited, this environmental friendly resources can contribute towards meeting the increasing global energy demand.

2. Sources of Ocean Energy

The potential of the ocean as a source of alternative energy is great. To underline this potential, a number of initiatives are being pursued by various governments, such as New Zealand [1], United Kingdom [2], Australia [3], European Union [4], the United States [5], [6] and Japan [7].

The energy can be extracted in the form of:

- Thermal Difference
- Tides
- Waves
- Ocean Current
- Salinity gradient

The concept being developed for each category will be briefly explained in the following sections.

2.1 Ocean Thermal Energy

Ocean thermal energy is based on the principle of thermodynamics, that is useful work can be generated when a fluid can be kept at two different temperatures. In this case, temperature difference between the surface waters and colder waters found at ocean depths may reach 20 degrees Celcius; large enough to generate work through a turbine. Good descriptions of the system, called Ocean Thermal Energy Conversion (OTEC), are given in [8], [9] and [10]. Figure 1 shows a schematic view of the concept.

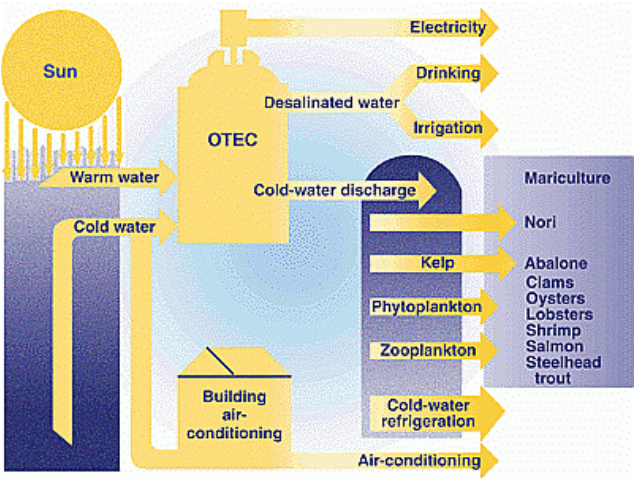

Figure 1: Ocean Thermal Energy Conversion Concept [8]

There are three types of electricity conversion systems: *closed-cycle*, *open-cycle*, and *hybrid*. *closed-cycle* systems use the ocean's warm surface water to vaporize a *working fluid*, which has a low-boiling point, such as ammonia. The vapor expands and turns a turbine. The turbine then rotates a generator to produce electricity. Open-cycle systems operating at low pressures actually boil the seawater. This produces steam that passes through a turbine/generator. A hybrid system combines both closed-cycle and open-cycle systems. The system is most promising for areas with deep water not too far out from shore, such as small island states of the Pacific [9], [10].

2.2 Tidal Power

Tidal energy exploits the natural rise and fall of ocean surface caused principally by the interaction of the gravitational fields of the Sun and the Moon. Some coastlines, particularly estuaries accentuate this effect creating tidal ranges of up to 11 m.

Tidal energy potential has been investigated by a number of countries, notably France where a 240 MW demonstration plant was built on the Rance estuary during the 1960's and has now completed 30 years of successful operation. The semi-permeable barrage was built across an estuary, allowing rising tide of seawater to fill a basin via a series of sluices. At high water the sluice gates are closed, creating a head of water on the ebb tide. Electricity is generated by releasing the water through a series of conventional bulb turbines. The Russians have built a small 400kW device near Murmansk that was later followed by a 17.4MW experimental device, built by the Canadians at Annapolis on a small inlet off the Bay of Fundy [11]. Australia is also developing tidal power technologies [3]

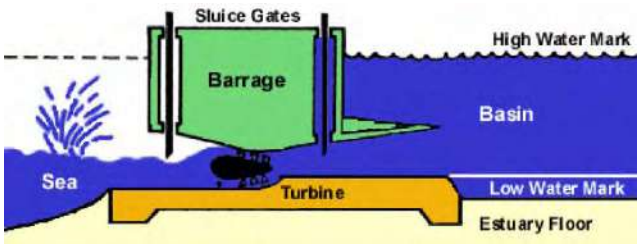

Figure 2: Tidal Barrage System [11]

Another concept being explored is the tidal fence. These are vertical axis turbines mounted within a fence structure, and operate like a revolving door as shown in figure 2.

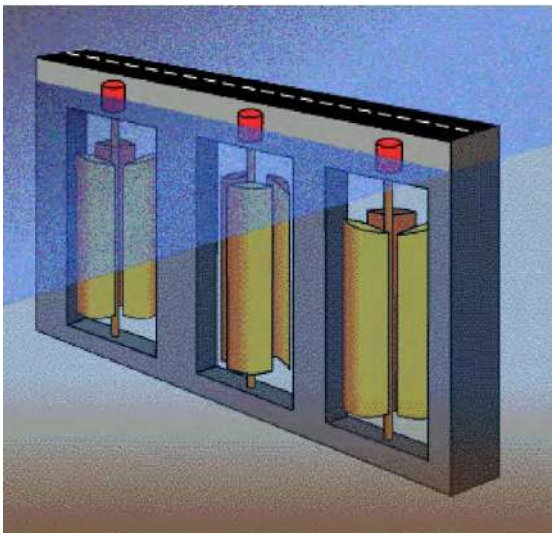

Figure 3: Tidal Fence System [3]

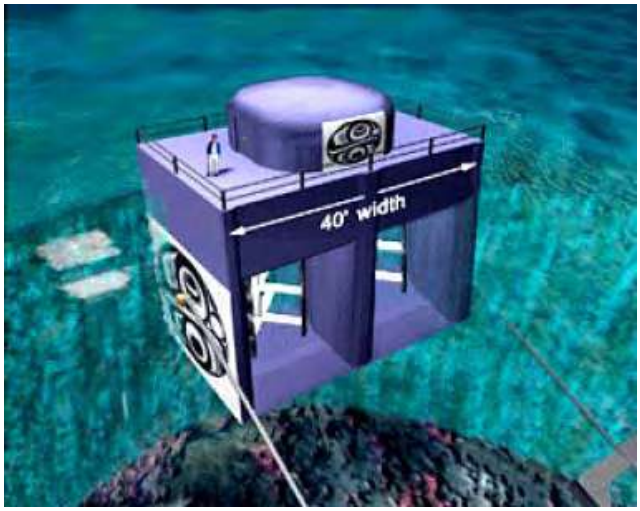

Figure 4: Tidal Barrage System [11]

2.3 Wave Power

Wave power devices extract energy directly from surface waves or from pressure fluctuations below the surface. Wave energy can be converted into electricity through conversion of the movement of water surface or changes in water pressure as waves propagate.

Most devices use the undulating motion of the water waves to mechanically power a pump or turbine that creates electricity. Other devices use hoses connected to floats that ride the waves. The rise and fall of the float stretches and relaxes the hose, which pressurizes the water, and in turn, rotates a turbine.

The oscillating water column wave energy device consists of a partially submerged concrete or steel structure that has an opening to the sea below the waterline. It encloses a column of air above a column of water. As waves enter the air column, they cause the water column to rise and fall. This alternately compresses and expands the air column. As the wave retreats, the air is drawn back through the turbine as a result of the reduced air pressure on the ocean side of the turbine. A number of OWC devices have been installed worldwide, with several of them being built into a breakwater to lower overall construction costs. One recent development is given in ref [12].

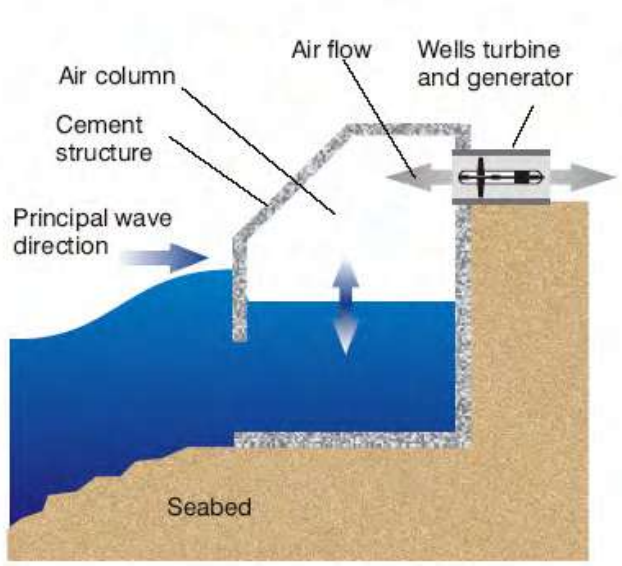

Figure 5: Oscillating Water Collumn Concept [4]

The Japan Marine Technology Center has developed a prototype wave power vessel that carries three air turbine generator units. Commissioned as the Mighty Whale, the vessel was designed to be anchored to the seabed but can be remotely controlled from shore. Beyond producing electricity, Japanese researchers have found that the calm seas created astern of the Mighty Whale can be used for fish farming or water sports [7].

The tapchan, or tapered channel system, is a wave-energy power generation device that has its roots in traditional hydroelectric power plant technology. The system consists of a tapered channel, which feeds into a reservoir constructed on cliffs above sea level. The narrowing of the channel causes the waves to increase in height as they move toward the cliff face. The waves spill over the walls of the channel into the reservoir and the stored water is then fed through a turbine. The requirements of low tidal range and suitable shoreline limit the worldwide replicability of this device. Recent development in this area is reported in ref [13].

Other devices such as the McCabe Wave Pump [4] and the Pelamis (sea snake) [4], [14] use the attenuator concept. In this case, the differing heights of waves along the length of the device causes flexing where the segments connect, and the energy is transferred to hydraulic pumps or other converters

2.4 Ocean Current Energy

Comprehensive reviews of the development of technology and resources on ocean current energy devices are given in ref. [1], [6] and [15].

The circulation of wind above surface water together with the uneven heating of the seawaters from the sun creates the ocean currents throughout the world**.**

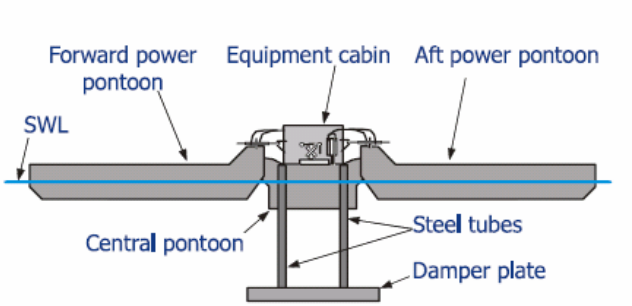

Figure 6: McCabe Wave Pump [4]

Areas that typically experience high marine current flows are in narrow straits, between islands and around headlands. Entrances to lochs, bays and large harbours often also have high marine current flows.

Several studies have been carried out on the energy potential of marine currents, but there have been few on the engineering requirements for utilization of the resource. Countries where theoretical studies and experimental projects have been performed include the UK, Italy, Canada, Japan, Russia, Norway, Australia and China.

Marine current energy is at an early stage of development, and a small number of prototypes and demonstration units having been tested. Most concepts involves turbines rotating either in the vertical or horizontal axes:

i. **Horizontal axis turbines** (axial flow turbine).

This is similar in concept to the widespread horizontal axis wind turbine. Prototype turbines of up to 10 kW have been built and tested using this concept. There are currently plans to install a demonstration machine of 300 kW off the south coast of the United Kingdom. This concept has also been tested on a small scale in a number of countries, including Norway. [6]

i. **Vertical axis turbines** (cross flow turbine).

Both drag and lift turbines have been investigated, although the lift devices offer more potential. The best-known example is the Darrieus turbine with three or four thin blades of aerofoil cross-section. Some stand-alone prototypes have been tested, including a 5 kW Darrieus turbine in the Kurushima Straits, Japan. The concept of installing a number of vertical axis turbines in a tidal fence

is being pursued in Canada, with plans to install a 30 MW demonstration system in the Philippines. [6]

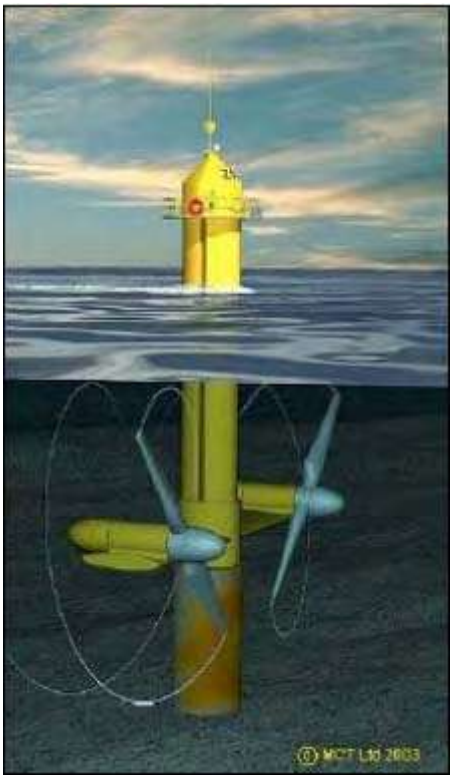

Figure 7: Horizontal Axis Current Turbine [15]

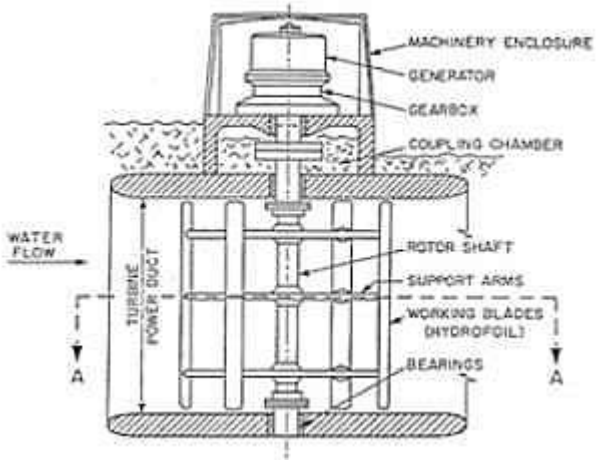

Figure 8: Example of Vertical Axis Ocean Current Turbine [1]

3. Malaysian Ocean Characteristics

In this section, a survey of relevant Malaysian oceanographic data will be presented. This will be compared to the limitations presented for each device**.**

3.1 Malaysian Ocean Thermal Energy

The ocean thermal energy devices require a large difference in sea surface and bottom temperatures. A temperature difference of 20°C or more between surface waters and water at depths of up to 1000 m is required. According to ref. [17], ocean depth within Peninsular Malaysian waters range from 50 to 90 meters at distances around 100km to 200 km from the shoreline. Waters off Sarawak show slightly greater depth of up to 150m. The most promising is Sabah whose waters have depth plunging to 3000m. However, the deep-water region is located around 200km from the coastline, on the outer fringes of the Exclusive Economic Zone (EEZ).

There is no available data on bottom temperature. However Malaysian Meteorological Services [18] recorded surface water temperature range from 26°C to 31°C in the South China Sea. To get a 20°C temperature difference, the bottom temperature should range from 6°C to 11°C.

3.2 Malaysia Ocean Tides

Tidal energy device such as tidal barrage requires a dam to collect the water in the basin. So, for this purpose, it needs to have a large tidal difference between low and high tides. The well-developed technology of this device is in tidal different range above five meter in height.

The tidal data at several places in Peninsular Malaysia Ocean is shown as in Table 1. It can be observed that the tidal range in Malaysia Ocean is too small and not suitable for this device development.

Table 1: Tide height above mean water level [19]

Location	High Tide (m)	Low Tide (m)	Maximum Difference (m)
Kedah Pier, Pulau Pinang	1.8 to 2.7	-0.1 to 0.8	2.8
Port Klang, Selangor	4.0 to 5.9	0.6 to 1.9	5.3
Pasir Gudang, Johor	3.0 to 3.6	0.3 to 1.4	2.7
Tanjung Gelang, Pahang	2.1 to 3.3	0.3 to 1.1	3.0

From Table 1 above, the average differences between low and high tide is between 2.5 to 3.0 meters. Although the maximum difference is 5.3 meters at Port Klang, from the tide table prediction, it only occurs once in a month and a few times in a year. It is not suitable to build a dam or tidal barrage. However, other types of tidal devices such as tidal fence and tidal turbine can still be explored.

3.3 Malaysian Ocean Waves

The wave devices were divided into two categories, shoreline and offshore devices. Physics show that wave energy is proportional to the square of the wave heights.

The compiled significant wave heights from two data sources viz. satellite altimetry and Malaysian Meteorological Services between 1999 and 2001 are shown in Figure 9 [18], [20]. The data shows that the average significant wave heights mainly lie in the 0.5m to 1.5m range.

Although the wave height in Malaysia is average, several of the wave devices incorporating some modifications can still be developed to extract the energy. There is a conflict in the design requirement that need to be resolved. On one hand, in order to be efficient, the device must be situated in the area with the highest wave heights. On the other, high wave heights means tougher design requirements for the structure required to house the system.

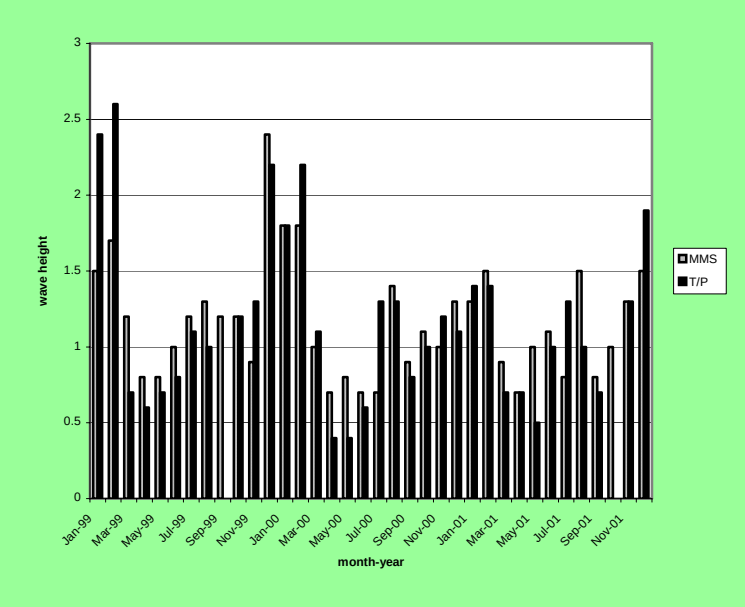

Figure 9: Comparison of average of significant wave height between MMS and TOPEX/Poseidon for 1999- 2001 [19]

3.4 Malaysian Ocean Currents

The criteria of the marine current turbine (for cost-effective power generation from the current flow tidal streams) were speed and depth of the water. The basic requirements for cost-effective power generation from tidal streams using one of the horizontal axis turbine technology are a mean spring peak velocity exceeding about 2.25 m/s to 2.5m/s (4.5 knots to 5 knots) with a depth of water of 20m to 30m. This is suitable condition to develop a marine current turbine with turbine blades of around eight to 12 meters from hub to tip. [15]

A summary of current speeds and direction at four locations in Peninsular Malaysia is given in Table 2.

Table 2: Current Speeds at Various Locations

LOCATION	Maximum speed (knots)	Typical speed (Knots)
One Fathom Bank [19]	2.3 t	0.8 to 1.5
Off Raleigh School [19]	2.2	0.9 to 1.5
Tg Segenting [19]	2.0	0.8 to 1.3
Pulau Tioman (Kampung Teluk Salang) [21]	1.14	0.1 to 0.58

From Table 2, the maximum speed is only 2.3 knots at One Fathom Bank, i.e. half of the requirement of the device. Any development in this area must take into account the slow speed and turbine design must be modified accordingly. If horizontal axis technology is adopted, this could mean larger diameter turbines with the associated problem of water depth limitation. On the other hand, other types of turbine such as vertical axis turbine may be more suitable in this case.

4. Potential Ocean Energy Devices

In developing of the energy devices, the suitability of the devices with the ocean characteristic in Malaysia must be considered. Tidal energy barrage requires at least 5-meter difference between low and high tides. In Malaysia, the average of the differences is only around 2.5 to 3.0 meters. So, this source of energy device is not appropriate to be developed. However, other types of tidal turbines can be considered as potential candidates.

For ocean thermal energy source, the requirement of its device is at least 20°C in difference between warm water at sea surface and cold water at seabed. The average depth of Malaysia Ocean is only around 50 to 200 meters measured 100 km to 200 km from shoreline. The depth of more than 1000 meters can be found around 200 to 300 km from shoreline of East of Sabah. This is too far from the shoreline and the development of it calls for high capital cost especially cost of under water cable. So, this source of energy is also not very suitable for Malaysia. On the other hand, this energy source can still be explored for small isolated islands around Malaysia.

The average wave heights in Malaysian ocean are between 0.5 to 1.5 meters. In this kind of wave, the energy that can be produced is only 15 kW per meter of wave front. This energy is too small to meet the high demand of energy. However, special devices may be developed which can make use of the relatively smaller wave heights.

The marine current device requires a current speed of 5 knots and above, with 10 to 15 meters turbine blades to make it cost effective. In Malaysian ocean, the current speed is only around 1.5 knots with maximum speed between 2.0knots to 2.3 knots. With a little modification with the turbines blades, this device can be developed. For

medium speed ocean current, the blades must be longer than 15 meters for horizontal axis turbines. However, vertical axis turbines using Voith-Schneider propeller concept is expected to be more suitable in shallow water application. Knowledge-base from vertical axis wind-turbine development work such as ref. [22] could be utilised towards this end.

The above discussions point to three potential energy resources that can be developed in Malaysia; tides, wave and marine current. Although the physical data indicate a less favourable magnitude compared to the present development in other places, modifications and new design development can be initiated.

Table 3 shows the comparison on a number of renewable and non-renewable energy sources such as fossil, nuclear, wind, solar, hydro, wave, marine current, tidal and ocean thermal [15]. The comparison covers the nature of resources, capital cost, running cost, environmental impact, predictions and visual impact of the energy. This could form a guideline

Table 3: Comparison of world energy resource [15]

	Renewable Source	**Low Capital Cost**	**Low Running Cost**	**Minimal environmental impact**	**Predictable**	**Minimal Visual impact**
Fossil	✗	✓	✗	✗	✓	✗
Nuclear	✗	✓	✗	✗	✓	✗
Wind	✓	✗	✓	✓	✗	✗
Solar	✓	✗	✓	✓	✗	✗
Hydro	✓	✓	✓	✗	✓	✗
Wave	✓	✗	✓	✓	✗	✓
Marine current	✓	✗	✓	✓	✓	✓
Tidal	✓	✗	✓	✓	✗	✗
Ocean Thermal	✓	✗	✗	✗	✗	✗

Among all of the energy sources compared, the marine current energy shows the greatest potential. Although its capital cost is expected to be high, its merit lie in low running cost, minimal environmental impact, minimal visual impact and predictable.

4.5 Concluding Remarks

Depletion of fossil fuel is a mathematical certainty although the rate is still debatable. As such, efforts to look for cleaner and renewable fuel are being pursued all over the world. Malaysia should not be left behind. Research groups in Universiti Teknologi Malaysia and Universiti Tenaga Nasional are carrying out pioneering efforts in this regards. The direction and area for development is still open although the initial studies presented in this paper have given some pointers.

References

[1] Zealand Energy Efficiency And Conservation authority, *Marine Energy: Summary Of Current Developments And Outlook For New Zealand*, May 2006

[2] UK Department Of Trade And Industry, *Wave And Marine Current Energy: Status And Research And Development Priorities*, DTI Report Number Fes-R-132, 2003

[3] Sustainable Energy Development Office, *Study Of Tidal Energy Technologies For Derby Government Of Western Australia*, Report No.: Wa – 107384 - Cr-01, December 2001

[4] Centre For Renewable Energy Sources (CRES), Wave Energy Utilization In Europe, *Current Status And Perspectives*, European Commission Directorate-General For Research, 2002

[5] U.S. Department of the Interior, *Technology White Paper on Wave Energy Potential on the U.S. Outer Continental Shelf*, Minerals Management Service Renewable Energy and Alternate Use Program, Washington May 2006

[6] U.S. Department of the Interior, *Technology White Paper On Ocean Current Energy Potential on the U.S. Outer Continental Shelf, Minerals Management Service Renewable Energy and Alternate Use Program*, Washington May 2006

[7] Japan Marine Science and Technology Centre, *Research and Development Technology on Wave Energy Utilization*, JAMSTEC, 2004.

[8] National Renewable Energy Laboratory (NREL): Ocean Thermal Energy Conversion Homepage, http://www.nrel.gov/otec/, 12 July 2006, 1.30pm.

[9] L. A. Vega, Ocean Thermal Energy Conversion (OTEC), http://www.otecnews.org/ articles/vega/ 00_vega_otec_ovverview.html, 12 July 2006, 1.45pm.

[10] South Pacific Applied Geoscience Commission, *Ocean Thermal Energy Conversions and the Pacific Islands*, SOPAC Report No 417, March2001.

[11] Tidal Power (Index of Resources), http:// freeenergynews.com/ Directory/Tidal/index.html, 16 July 2006, 10.00 am

[12] Energetech 2006, Media Release: Port Kembla Trial Deployment Results, Nov. 2005. Available at www.energetech.com.au, 12 July 2006, 1.30pm.

[13] S. Petroncini, R.W. Yemm, Introducing Wave Energy into the Renewable Energy Marketplace, www.oceanpd.com/PDFS/SimonaPetrocini-Paper.pdf, 12 July 2006, 1.35pm.

[14] Ocean Power Delivery Ltd., "Media Release: Leading Wave Energy Company secures £13m Investment". June 2006. Available at http://www.oceanpd.com/docs/ OPD%20Press%20 Release% 20June%2006.pdf, 13 July 2006, 11.00am.

[15] Marine Current Energy, "www.worldenergy. org/wec-geis/publications/ reports/ser/marine/marine. asp",14 July 2006, 10.00 am.

[16] MCT Home, www.marineturbines.com/ home.htm, 13 July 2006, 12.00pm

[17] National Geographic, *Atlas of The World*, Seventh Edition, page 100.

[18] Malaysia Meteorological Service, *Monthly Summary of Marine Meteorological Observation*, 2000, Kuala Lumpur

[19] Hydrographic Department, *Malaysia Tides Table*, Royal Malaysian Navy, Kuala Lumpur, 2002.

[20] Omar Yaakob, Norazimar Zainuddin, Ramli Shariff, Developing Malaysian Ocean Wave Database Using Satellite Altimetry, 5th Regional Conference on Marine Technology, Johor Bahru, September 2004.

[21] Ridham Upe, Pencerapan Data Hidraulik dan Persampelan Tanah Di Pesisiran Pantai Kg Salang, Pulau Tioman, Phan, Final Year Project Dissertation, Universiti Teknologi Malaysia, 2000.

[22] Paul Cooper and Oliver Kennedy, Development and Analysis of a Novel Vertical Axis Wind Turbine, 42nd Annual Conference of the Australian and New Zealand Solar Energy Society, 1 - 3 December 2004, Perth.

BUILDING UP RENEWABLE ENERGY: CLEAN DEVELOPMENT MECHANISM AN OPTIONS

R.D.R. Ahmad, F. P. Koh and K. Mariyappan
Pusat Tenaga Malaysia
Level 8, SAPURA@MINES,
No. 7, Jalan Tasik,
The MINES Resort City,
43300 Seri Kembangan,
Selangor

ABSTRACT

The objective of UNFCCC in the stabilisation of greenhouse gas (GHG) calls for a linking between energy and environment policies with the economic development. The future energy and emission intensities from the developing countries shall be invariably decided by their development patterns. Developing countries can leapfrog the conventional development path through the policy decisions on projects like renewable energy and energy efficiency. To date, there are more than 100 renewable energy projects registered with CDM EB internationally and million tonnes of CERs were issued by CDM EB. The CDM offers the possibility to increase the economic viability of energy projects, increase IRR and expand technology transfer opportunities. CDM also provides a new business platform in renewable energy sector.

Key words: Greenhouse Gas, CDM, Environment, Renewable Energy, Sustainable Development

INTRODUCTION

Energy is a key development component in Malaysia's economy, as the development and utilisation of energy resources have contributed and will continue to contribute to the industrialisation of the economy, the socio-economic welfare of the people, as well as exports earnings. This, in part, is a direct result of the rich energy resource base. Malaysia is well endowed with conventional energy resources such as oil, gas and coal, as well as renewable energy resources such as hydro, biomass and solar energy.

Malaysia is building up the renewable energy and energy efficiency in the country to address both global environmental protection and local development needs. The crucial opportunity to develop sustainable development for energy sector is through implementing Clean Development Mechanism (CDM). CDM was established under the Kyoto Protocol to provide a cost-effective emission reduction mechanism for developed countries with GHG targets commitment. In the same time, this mechanism strives to contribute to the sustainable development of developing countries.

As a developing country, Malaysia is not subject to any commitments towards reducing greenhouse gases emission under the Kyoto Protocol. However, through participation in the CDM, Malaysia could benefit from the foreign investments financially and technologically and the overall improvement of the environment from the GHG emission reduction projects in the country.

It is clearly mentioned in the 9th Malaysia Plan that CDM will be utilised to provide support for the implementation of SREP projects. This is clearly stated that CDM is supporting Government policies in achieving sustainable goals of the energy sector. Today, there are 5 energy projects from Malaysia registered as CDM projects internationally.

The CDM Potential for Renewable Energy in Malaysia

Malaysia signed the Kyoto Protocol on 12th March 1999 and ratified it on 4th September 2002 with the Ministry of Natural Resources and Environment as the national focal point for CDM. On 31st May 2002, the National Steering Committee on Climate Change (NSCCC) agreed National Committee on CDM (NCDDM) and two technical committees to implement CDM in Malaysia.

In Malaysia, the energy projects have been placed as top priority for CDM implementation. With the focus of RE and EE efforts in the Eighth and Ninth Malaysia Plans, CDM projects also conform to national developmental plans.

The NCCDM approved the **National CDM Criteria** for CDM projects in the year 2003 and revised the criteria in the year 2006good. The revised criteria are as follows:

(i) The project must support the sustainable development policies of Malaysia and bring direct benefits towards achieving sustainable development

(ii) Implementation of CDM projects must involve participation of Annex I Party/Parties;

(iii) Project must provide technology transfer benefits and/or improvement in technology;

(iv) Project must fulfill all conditions underlined by the CDM Executive Board as follows:

i. Voluntary participation
ii. Real, measurable and long-term benefits related to mitigation of climate change; and
iii. Reductions in emissions that are additional to any that would occur in the absence of the certified project activity.

(iv) Project proponent should justify the ability to implement the proposed CDM project activity

Local project developers are in the great position to incorporate CDM in their renewable projects particularly to boost the biomass related industry as the biomass resources are abundant in Malaysia. Further more, CDM actually can support the implementation of SREP projects in the country as the maximum capacity of SREP projects is 10MW and apply to all types of renewable sources of energy.

There are international modalities and procedures developed for interested parties to be involved in this mechanism. Procedures and standardise baselines for small scale projects have been developed and approved by CDM Executive Board (consist of 10 international governmental panel members of Kyoto Protocol to the UNFCCC). The streamlined procedures and standardised baselines have been defined as below:-

1. Renewable energy projects with and installed capacity under 15MW;

2. Energy efficiency projects that reduce energy consumption by up to 15 GWh per year; and

3. Activities that emit less than 15,000 tonnes of CO_2-equivalent per year.

Today, Malaysia received 53 project applications mainly on renewable energy from the oil palm sector for CDM. The Figure 1 shows the potential estimated emission reductions that will be achieved by each different sector[1] among the applications. The total

[1] The estimated emission reductions are calculated based on the data given by project developers in PIN or PDD. However, the calculations exclude projects that are "rejected", "withdrawn" and "application accepted, but no action".

estimated emission reductions can reach as high as 5 million tonnes CO_2-equivalent/ year. With the most conservative price of USD$5.00 offered for each tonnes of CO2-equivalent, the revenue can be generated from these projects has great potential to increase the economically viability of renewable energy projects.

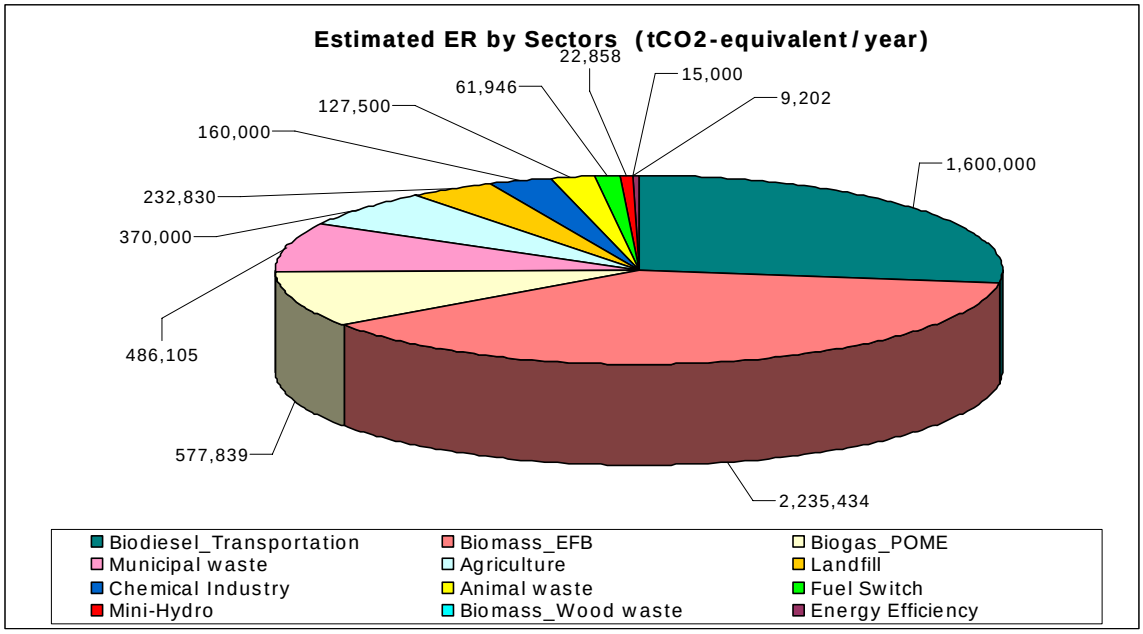

Figure 1: The Estimated Emission Reduction by Sectors

All the energy projects will result in a total production of 169 MW of new renewable electricity. Of this, 96.37 MW comes from biomass and biogas project, 15.3 MW from landfill projects, 48.35 from MSW projects and 9 MW from a mini hydro.

For fuel switching project which replace the fossil-fuel, the emission reduction is 62,011 tCO_2/yr while the energy efficiency project which introduce improvement on the equipments, the emission reduction is 16,130 tCO_2/yr.

Today there are 9 projects received Host Country Letter of Approval from DNA Malaysia. These projects are estimated to generate 1,150,232 tonnes CO_2-equivalent per annum. Among these 9 projects, there are 3 projects registered with CDM Executive Board and 5 projects are submitted for registration. Two (2) of the registered CDM projects are biomass with a potential of ER amounted 148,477 tCO_{2e} annually. By the end of June 2006, more projects are expected to be registered with CDM Executive Board.

Potential of CDM to assist SREP projects

The CDM can give a financial contribution to projects reducing the emission of greenhouse gasses (GHG). This is often true for renewable energy projects since they are accounted as having zero emissions of CO_2. That is also the case for biomass projects as the CO_2 emitted from burning the biomass is equal to the uptake of CO_2 by the plants.

With the well structured national CDM approval system and implemented CDM projects in Malaysia, the situation is an advantage to the effort of promoting Small Renewable Energy Projects (SREP) in Malaysia. A study was carried out showing the potential of SREP could generate 17. 8 million tonnes of CO2-equivalent per year and contribute to 350 MW electricity generation based on renewable energy sources. Based on this study, the potential projects include the landfill, biogas and biomass. A renewable energy project could be financially attractive with CDM. The IRR increase with CDM can be up to 17%.

The results of the study analysing the impact of CDM to promoting RE in Malaysia indicate that the impact is different for different types of projects. Table 1 presents a summary of the results of the study.

Table 1: Results of the impact of CDM per type of project

Impact of CDM on project implementation	*CDM is a major incentive*	*CDM can be a supporting measure*	*CDM has only marginal impact*
Types of projects	**Landfill gas** **Biogas from POME or other sources** **Biomass replacing coal in industry or power sector** **Reduction of gas flaring**	**CHP based on EFB** **Mini hydro**	**PV** **Domestic and commercial sector EE** **Transport**

The saving of GHG emission stems from the fact that fossil fuels are replaced. For off-grid projects diesel for engines is often the replaced fuel. For grid-connected electricity producing projects the avoided emissions from the power stations connected can be calculated according to international standards. A preliminary calculation for Peninsular Malaysia gives savings of approximately 0.6 kg CO_2 per kWh.

For combined heat and power projects, GHG emissions may also be saved from the production of heat. For palm oil mills – where many SREP projects are located – biomass

would be used for heat production and thus no extra GHG savings accrue for the heat produced from biomass combustion.

Finally some project types involves collection of methane that would otherwise have escaped to the atmosphere can give a significant contribution to the GHG savings of a project. This is particularly true since methane is 21 times more potent GHG than CO_2. Table 2 gives a summary of the different possibilities for GHG emission reductions.

Table 2: Sources of GHG-emission reductions for different types of projects

	Replacing fuel directly	Replacing grid electricity	Replacing fuel for heat production	Capture of methane
Off-grid biomass CHP	X			
Grid connected biomass CHP		X	(X)[2]	
Grid connected mini-hydro		X		
Landfill gas flaring				X
Land fill gas power		X		X
Biogas from POME		X		X

Table 3 below shows the expected potential for implementing CDM projects in Malaysia and the extent to which this could lead support for SREP-projects. It should be stressed that the results are still preliminary and also that the realisation of the potential for SREP project will depend upon the removal of other barriers for SREP-projects such as high costs for grid connection and difficult negotiations with TNB.

[2] If fossil fuel was used before

Table 3: Potential volume of CERs and MW for different types of SREP projects

Project type	CERs per year in 2010	MW electricity as SREP
Biogas POME + animal manure	5,900,000	190 MW
Landfill gas	3,700,000	45 MW
Reduction of gas flaring from oil production	4,600,000	N/A
Mini hydro	70,000	25 MW
Biomass CHP	380,000	90 MW
Other projects[3]	3,150,000	N/A
Total	**17,800,000**	**350 MW**

The study also explained the increment of the Financial IRR with and without CDM that landfill gas, biogas and biomass project is the project which can remove the barriers in implementing it.

There are both direct and indirect benefits of using CDM as an element in the energy policy. The direct benefits are linked to the income from the sale of Certified Emission Reductions (CERs). With the current price level of 6 USD/ton CER and the above calculated potential sale of 17.8 million ton CERs per year the annual income will be in the order of 300 million RM per year or a total of 1.5 billion RM before 2012.

CONCLUSION

CDM projects can lead to various benefits to Malaysia. The CDM promotes investment in projects that both reduce green house gas emissions and foster sustainable development in developing countries. Firstly, there will be a transfer of technology and know-how; secondly, this can help improve foreign exchange as well as enhance international competitiveness; thirdly, create employment by being the project-host country; fourthly, development of human capital skills through exchange of technology and know-how; and finally promote environmental preservation and awareness.

All these benefits clearly adhere to the basis of CDM wherein non-Annex 1 parties will benefit from project activities resulting in certified emission reductions and Annex 1 parties can use the certified emission reductions to comply to their emission limitation and reduction commitments.

CDM has attracted greater attention and expectation than any other mechanism in the KP, because it is the main element of the treaty that bridges the divide between the developing and developed countries. Developed countries see CDM as a source of low cost emission credits, while developing countries hope it may attract additional investment to foster rapid and more sustainable development. CDM would help propel

[3] Including energy efficiency projects and biomass for industry and central power

developing countries onto cleaner development paths and achieve real reductions in GHG emission.

Therefore, it is important to have effective policies which will set our country on a new course, one characterized by cleaner energy sources, improved ecosystems, healthy societies, technological innovation, and economic opportunity.

REFERENCES

PTM-DANIDA (2005) Study on CDM Potential in SREP

CDM Project Lists 2006 *by* CDM Energy Secretariat, Pusat Tenaga Malaysia

N. Maya A.W.. Jasmin I. and R.Diana R.A., 2004. ***Renewable Energy Policy and the Clean Development Mechanism.***

K. S. Kannan, Wong H. K., N. M. A. N. Ibrahim, 2003. ***Potential of CDM in Renewable Energy Projects in Malaysia***. *Proceedings of the International Symposium on Renewable Energy: Environment Protection & Energy Solution for Sustainable Development, 14 - 17 September 2003, Kuala Lumpur, Malaysia.*

Review of current state of Energy Scavenging Technologies

Rezal Khairi Ahmad, Hanim Salleh, Fazrena Azlee Hamid

Universiti Tenaga Nasional, Km 7 Jalan Kajang-Puchong 43009 Kajang Selangor, rezalk@uniten.edu.my, hanim@uniten.edu.my, farzrena@uniten.edu.my

Keywords: Harvesting, Scavenging, Vibration, Solar, Thermoelectric

Abstract

This paper discussed the overview and recent trends for energy harvesting technology for both domestic and industrial applications. Harvesting energy refers to the extraction and conversion of energy from the surrounding environment into the usable form of electrical energy. The technologies include solar photovoltaic, thermoelectric and piezoelectric devices. The scale of which these devices are fabricated is the pre-determining factor on the application area; hand-held sizes for domestic and mobile usage, plus micro and nano-scales for scientific activities and industries. Energy scavenging gives the people the right to free electricity and to the industries, reduced costs and overheads hence increased efficiencies.

1 Introduction

Energy scavenging or energy harvesting technologies refer to those technologies that convert energy from the surrounding environment into a useable form of energy. The ambient energy source can be from solar power, thermal power, volume flow and vibrational power. There has been a significant increase in the research on energy harvesting for low power applications as well as increasing the output power of established energy harvesting concepts for domestic power applications in recent years. This is due to smaller electronics applications such as wireless and mobile electronics and the demand for better lifespan of batteries. The applications such as for wireless medical implants and embedded sensors in buildings and similar structures, and basic or typical home appliances such as lighting and fan are just a few of many examples. The trends are now to develop clean and efficient domestic and mobile power generators as well as micro power generators [1] or even nano power generator that can harvest energy [2]. The objective of this paper is to discuss the overview and trends of four main types of energy scavenging generations namely, vibration-based, solar cells, thermoelectric and hybrid design.

2 Vibration-based generation

There are several conversion mechanisms for vibration-based micro power generator which are piezoelectric, electromagnetic and electrostatic. In piezoelectric transduction, the vibration will cause the piezoelectric material experience strain and thus to convert it to electrical signal. In electromagnetic transduction, a magnet will vibrate and induces voltage in a coil. In electrostatic, an electret arragement with a permanent charge embedded in the mass induces a voltage on the plates of a capacitor as it moves.

On of the first piezoelectric transduction mechanism was patented in 1969 which produced 150 μW to power bioelectric implant. [3]. Roundy et al. [4] has demonstrated work on piezoelectric converters, by using PZT bimorph. A power density of 70 $\mu W/cm^3$ was obtained and with simulations, an optimized design would be capable of producing 250 $\mu W/cm^3$ from a vibration source with an amplitude of 2.5 m/s^2 at 120 Hz. William and Yates [5] analyzed the feasibility of using electromagnetic mechanism for micro generator by using a simple mass, spring, damper model. The predicted power generation was 1 μW at an excitation frequency of 70 Hz. Another work in this area has found that it is feasible to generate power on the order of 400 μW [6]. The test chip integrates an ultra-low power controller to regulate the generator voltage using delay feedback techniques, and a low power sub band filter DSP load circuit. Tests verify 500 kHz self-powered operation of the sub band filter, a level of performance suitable for sensor applications. The entire system, including the DSP load, consumes 18 μW of power. The electrostatic generator consists of a charged capacitor with moving plates. Unlike electromagnetic and piezoelectric, this type of generator needs to have an initial voltage before they can produce power. Although some researchers have developed larger electrostatic generators to scavenge low-frequency vibrations in wall or wearable applications, electrostatic generator is attractively been used as MEMS scale devices. They typically yield in the order of 10 μW [1].

A recent analysis indicated that we can expect up to 4 $\mu W/cm^3$ from vibrational micro generators that typical human motion (5 mm motion at 1 Hz) stimulates and up to 800 $\mu W/cm^3$ from machine-induced stimuli (2nm motion at 2.5 kHz) [7]. However, most vibration-based micro generators are designed to scavenge vibration for a specific frequency and thus limited power output. There is a need to design a generator which can scavenge vibration at a wide range of frequency for wide range of output. Thus, the aim of this work is to design of the vibration-based micro generator using the concept of passive optimum tuning of the ambient vibration [8]. The approach is to have a smart mechanism that can scavenge wide range of

ambient vibrations to be converted to electrical power for wider range applications. This approach can be applied to different conversion mechanisms and the performance can be compared. Important key parameters that affect the power output will also be simulated and verified with macro scale prototype. The prototype can further be developed into MEMS scale prototype for wireless applications.

2.1 Applications

In perspective of the Malaysia industry, one of the useful applications of this device is for condition monitoring using wireless devices. This device can be positioned on a gas turbine in power plant where at a critical vibration pattern it will generate power to activate a wireless sensor to caution for maintenance. Similarly, it can be placed on the railway track, where at certain critical vibration, the device will power a wireless sensoring system to alert for necessary maintenance to avoid any accident. In addition to that, the ever-vibrating shock absorbers in moving automobiles should provide enough power for in-car electronics and battery charging support system. The application can also be extended to biomedical field where low vibration from blood pulse or heart beat generates low power to activate a sensor to monitor human organ condition or to assist an organ implant. Another example is to place it anywhere at the human body which can produce movement and low vibrations which then generate power to activate small wireless gadgets such as torch light, personal safety alarm, hearing aids and mobile phone. In short, this technology has been a trend and very recent all over the world, and thus research in this area shown a potential for future market in Malaysia to be at pace with global technology.

3 Solar Cells

Solar power is the most known source of ambient energy. Photovoltaic cells have been around for quite some time with recent technological advance emphasising on extracting more power from the solar radiation input. High efficiency photovoltaic or solar cells offer the best solution for powering domestic or hand-held mobile appliances.

A solar cell is a semiconductor device that converts photons from the sun into electricity. Photovoltaic cells in turn are solar cells that include both solar and non-solar sources of light. The current best commercially available solar cells have 30% efficiency. There has been surge of activities in increasing the efficiency of the solar cells and exploring alternative conducting materials to fabricate solar cells.

Researchers in Berkeley Lab have made a recent discovery that a single system of semiconductor alloys incorporating indium, gallium and nitride having band-gaps of 0.7 eV to 3.4 eV, can convert virtually the full spectrum of sunlight to electrical current. Using multi-junction layers structure, more than 70% theoretical maximum efficiency can be attained [9] without the stacking problem faced by other semiconductor materials. Advantages include ruggedness - tremendous heat capacity and radiation-hard - and relatively inexpensive apart from being potentially the most efficient ever.

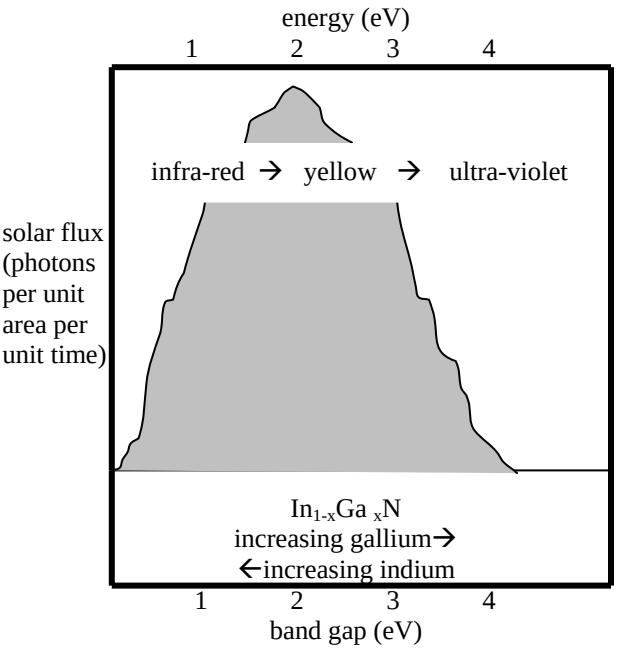

Figure 1: A simplified graph of solar flux versus band gaps of $In_{1-x}Ga_xN$ showing full spectrum coverage

Using the nanotechnology approach, Richard D. Schaller and Victor I. Klimov of Los Alamos (N.M.) National Laboratory aim to exploit the impact ionization phenomena in semiconductors to increase the efficiency of solar cells. Theoretical calculations indicate that nanocrystal-based solar cells could convert 60 percent of sunlight into electricity [10]. Photon energies carrying at least 3 times as much energy as required to knock an electron loose caused impact ionization to occur thus creating more electrons to join an electric current. Whereas, NanoHorizons' design utilizes a single nanoscale-engineered structure to perform both absorption and collection of solar radiation, which enables photovoltaics builders to use an optimally thick absorption layer while dramatically shortening collection distance by as much as 1000-fold (tens of nanometers vs. tens of microns in today's best two-layer cells) - eliminating the impact of absorption layer thickness on collection distance [11]. Efficiency is assumed to also have increased here, however the production cost must be reduced in order to make this a viable option for electricity generation or harvesting.

The highest efficiency cells usually are not the most economical. As an example, a 60% efficient nano-structured

solar cells produced in low volume might well cost one hundred times as much - or perhaps even more - as an 8% efficient amorphous silicon cell in mass production while only delivering just 7.5 times the electrical power. However, if the economies of scale are reached, reduction of cost would be inevitable.

Alvin M. Marks is currently working with Westinghouse Electric Corporation in developing solar cell prototypes made from materials he patented, Lepcon and Lumeloid, which could turn 70 to 80% of the energy from sunlight into electricity [12]. The electricity would cost USD 0.03 or 0.04 per kilowatt-hour, as against about USD 0.10 per kilowatt-hour for commercially generated electric power. Most photovoltaic cells produce energy for around USD 1.00 per kilowatt-hour.

Other recent initiatives include new technology developed by UC Berkeley, LBNL chemists of which they have found a way to make cheap plastic solar cells flexible enough to paint onto any surface and potentially able to provide electricity for wearable electronics or other low-power devices. The group's first crude solar cells have achieved efficiencies of 1.7 percent [13], still well below the 10% scalability mark for real applications. The solar cell they have created is actually a hybrid, comprised of tiny nanorods dispersed in an organic polymer or plastic [13]. The “h-alpha solar” project group consisting of researchers from France, Portugal and the Netherlands managed to develop solar cells using polymorphous silicon with thickness about 1μm with an efficiency of only about 7% [14]. However, these panels will be cheap, as they can be mass-produced in rolls that can be cut as required and wrapped around clothes for everyday wearable energy scavenging. The Akzo Nobel, a partner in the research is projecting a cost of 1Euro/Watt-peak [14].

Konarka Technologies is developing solar cells made from flexible plastic – 10 cm long 5 cm wide each - indistinguishable from photographic film [15]. They can also be built into all sorts of surfaces. Fabrication are done using a production line of coating machines and rollers thus making them more importantly cheap and easy to make. Christoph Brabec of Siemens managed to increase the power output of buckyball-plastic (polymer) photovoltaic cells by tweaking the nanomaterials inside and shifting to a more industrial-style coating method. A 10% efficiency was achieved in an experiment conducted in a clean room with the maximum module size of 15cm [15]. Further work needs to be done to replicate such achievement in the mass-production environment.

Nanosolar is working on to boost nano-solar cells’ power output and make them easier to deploy, eventually spraying them directly onto any surface. Prototypes developed achieved the 10% [15] threshold efficiency mark and this offers great potential for energy harvesting applications on structures or buildings, even perhaps feeding electricity to the grid system. Nanosolar is also planning to mass-produce 200 million solar cells per year which translates to a maximum output of 430 MW per year. The type of solar cells to be produced exploits the technology of thin film copper indium gallium diselenide (CIGS). 1 μm thickness of thin film CIGS can generate as much electricity as 200-300μm thick crystalline silicon wafer, and with an efficiency of 20%[16]. More importantly, they can be manufactured at relatively much lower cost and this is a promising sign of widespread use of solar cells in the near future.

The development of a photovoltaic-thermoelectric hybrid cells is also worth mentioning here. A temperature gradient existing between the optically active region of the cell and its surrounding gives rise to the thermoelectric effect. However, efficiency enhancement was found not to exceed 1%, even under strong concentration of sunlight [17]. A combination of solar cells element with thermoelectric element has been shown to increase the overall electrical efficiency, but only from the thermoelectricity point of view. The author suggests the application of nanotechnology to achieve secondary harvesting of the wasted extra energy from solar radiation. Such mechanism would push up the overall electrical efficiency of any solar cells, giving rise to the much-awaited 3rd generation solar cells.

3.1 Applications

Hand-held solar-powered or enabled devices are already in the market. The Nokia phone 6161 has a compatible solar cell phone battery manufactured by Sunpower. Another fine example is the Solarcharger, a product from iSun, which is a solar powered charger for phones and PDAs. In a larger scale, the promising high efficient solar-generated electricity can be fed into the electricity grid using inverters (grid-connected PV systems). Homes can use stand alone systems to power a 17-inch black and white TV, a radio or a fan [18], this is especially true for remote locations electrification thus eliminating the need to build expensive transmission lines or truck in fuel-based generators. A suitably designed solar-based lighting system can provide 10 hours of lighting each evening. Batteries can be used to store the electricity that is not needed immediately and when in used, they can provide up to 5 nights of energy for an 8-watt DC fluorescent light. The Mazda 929 car used solar cells to activate a fan to ventilate the car when the car is idle and parked during a sunny hot day [18] is just one of many fine examples of solar energy scavenging. Flexible and wearable solar panels promise to be convenient mobile energy harvesting tools for cars, phones, PDAs, game consoles and other mobile devices. Paint-able solar panels on the other hand are useful for building or infrastructure electrification and interestingly, electric and hybrid cars as the dependency on fossil fuel can be greatly reduced.

The working lifetime of solar panels is typically expected to be around 40 years. The cost recovery or energy payback time of a solar panel is anywhere between 1 to 30 years (usually under five) depending on the type and where it is used. This means solar cells can be net energy producers and can "reproduce" themselves (from just over once to more than 30 times) over their lifetime [19].

4. Thermoelectricity

Temperature difference creates electric current, and electric potential creates temperature difference – this is thermoelectricity. Thermoelectricity can only work when there is thermoelectric (TE) material, and an environment with a thermal gradient. As temperature difference is continuously available, thermoelectricity has tremendous potential for generating electricity from wasted heat.

The efficiency of thermoelectric material is characterized by the figure of merit, ZT:

$$Z = \frac{S^2 \sigma}{k} \qquad (1)$$

where S = Seebeck coefficient i.e. dV/dT (microvolts per Kelvin)

σ = electrical conductivity

k = thermal conductivity

The dimension of Z is T^{-1}, thus ZT is a dimensionless figure of merit. Among the most common TE material is bismuth telluride, lead telluride and silicon-germanium alloys. Bismuth telluride has ZT of about 1, and is widely used for refrigeration and portable power generators. Since 1960s up until a few years back, thermoelectric materials are limited with unity ZT and efficiency of about 5 – 7%.

Breakthrough in the ZT for TE material started after the mid - 1990s, when nanostructures with ZT of 2 – 4 are being reported. This is because in low-dimensional TE material, electrical conductivity increases, but thermal conductivity decreases. The previous bottleneck in macrostructures causing ZT to hover around 1 is due to the proportional increase in thermal conductivity when electrical conductivity increases. For example the thin-film supperlattice thermoelectric technology [19] is expected to contribute to the advancement in solid-state cooling and power generation for various applications. The most recent progress shows that a new design principle developed for nanostructured thermoelectric materials that could achieve a ZT value of around 10 at room temperature[19] and surely, higher ZT values can be attained at higher temperatures.

With this recent progress in TE material development, various applications for thermoelectricity become possible. The most important would be thermoelectricity generation from various waste heat sources.

4.1 Thermoelectric generation

The basis for TE power generation is thermocouple, which is n and p materials that are electrically connected in series, and thermally in parallel. One side of the couple absorbs heat, and the other side rejects heat. Current will flow in the configuration, which is proportional to the temperature gradient between the hot and cold junction.

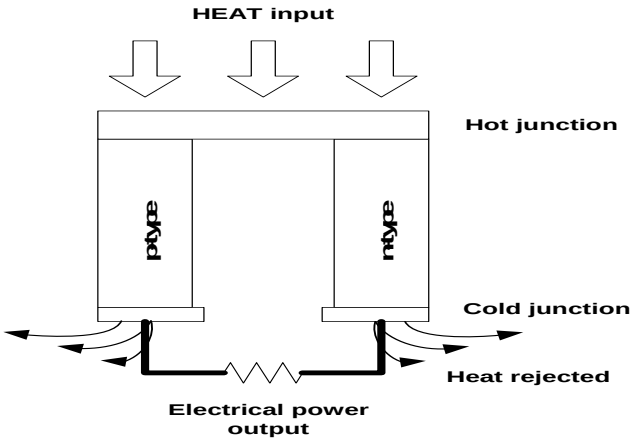

Figure 2: Thermoelectric generation illustrating the Seebeck effect.

4.2 Applications

As mentioned previously, temperature difference is readily available between ambient and any excess heat from appliances, even from human. For example, there exists wristwatch that operates using microwatts obtained from thermoelectric modules and small thermal gradient between body heat and ambient [20]. Minute wearable thermoelectric generator for powering low-drain biosensor is also available.

Domestic thermoelectricity is most often overlooked. Refrigerators offer a good constant source of waste heat, which could be scavenged for immediate electrification and energy storage in batteries.

At a larger scale, specifically in the automotive industry, it has been reported that 1 kW of power can be obtained from heat generated in the exhaust system and under-armor of an army vehicle [21]. Application of TE in transportation, amongst others, is mainly to use waste-heat energy to increase the efficiency of fuel consumption. Generated electricity is utilized to support electrical system of the vehicle. Also it is envisaged that sufficient power would be available to utilize electrical systems rather than mechanical in the vehicle, specifically the possibility to replace conventional heating and cooling systems thus eliminating refrigerants and emission problems.

Current research in heat-recovery for heavy-duty truck systems predicts savings of fuel consumption translating to travelled distance of up to 150 000 miles per year. Improvement of up to 6% of the cost of fuel per horsepower per hour (for which a 5% improvement would mean a saving of $4500 of 1500 gallon of fuel per vehicle) was reported. Increased fuel efficiency has also a direct impact on environment – reduction in harmful emissions.

The potential of generating electricity from industrial waste heat must also not be discounted. The tremendous amount of heat being systematically thrown away can be thermoelectrified to provide basic electrical needs such as lighting and fans in the factories. Other interesting utilization of thermoelectricity is exploiting the natural thermal difference between soil [22], from which a thermoelectric microgenerator can charge a battery cell.

5 Conclusion

The energy harvesting technology presented and discussed here are economically viable solutions to the current escalating energy prices. Each has it's own merit and areas of applicability. Vibration-based energy is most suited to instrumentation and conditioning monitoring, with very limited applications in day-to-day civilian activities. This due to the single fact that areas or structure with strong vibrations are typically considered to be unsafe. The constant radiating energy from the sun makes photvoltaic cells the optimal solution to power almost every scale electrical necessities and would make immediate positive economic and environment impact to any society in general. Thermoelectricity on the other hand requires fairly extreme temperatures to generate enough electricity to be making any substantial socio-economic impact. With recent discoveries of new thermoelectric materials, this method of energy scavenging could be the thing of the future together with the up and coming cheap and high efficiency solar cells.

The determining factors for successful implementation of the above mentioned technologies are cost, manufacturability of the harvesting devices, level of energy conversion efficiency, environmental-friendliness, awareness of the available technologies, governmental incentives and regulations pertaining to the energy or power industry.

Thermoelectric generation offers several advantages as they are made from environmentally friendly material, robust and can last for a very long time compared to batteries. Although research activities are spearheaded by USA, Japan and Europe, the area of waste heat recovery is still new and have potential in application in Malaysia.

Malaysia being a sunshine-rich country has yet to take full advantage of the solar cells technology. Recent initiatives by Pusat Tenaga Malaysia on the Building Integrated Photovoltaic (BiPV) project is seen as a good start in the long road to create the necessary commercial awareness of photovoltaic technology in general and the viability of locally researched and manufactured solar panels to realise the long-term prospect of "free" electricity.

References:

[1] Paradiso, J. A. and Starner, T. "Energy Scavenging for mobile and wireless electronics .Pervasive Computing. IEE CS and IEEE ComSoc. Volume 4 , Issue 1:18-27 .January 2005.

[2] Wang, Z.L. and Jinhui Song, J. "Piezoelectric Nanogenerators Based on Zinc Oxide Nanowire Arrays" Science vol 312 no. 5771 : 242-246. April 2006

[3] Piezoelectric Energy converter for electronic implants. US Patent 3,456,134. 1969.

[4] Roundy, S, Wright, P.K. and Rabaey, J. "A study of low level vibrations as a power source for wireless sensor nodes". Computer Communications 26:1131-1144.2003

[5] Williams C.B and Yates R.B. "Analysis of a micro-electric generator for Microsystems ". Sensors and actuators A 52 8-11.1996

[6] Amirtharajah, R.; Chandrakasan, A.P. "Self-powered signal processing using vibration-based power generation " Solid-State Circuits, IEEE Journal Volume 33, Issue 5, :687 – 695 . 1998

[7] Mitcheson P.D. et al. "Architectures for Vibration-Driven Micropower Generators," J. Microelectromechanical Systems, vol. 13, no. 3, pp 429-440. 2004

[8] Salleh, H. and Brennan, M.J. "Design of a wideband vibration neutraliser to control flexural waves on an infinite beam". Proceedings of the Institute of Acoustics, Vol 26 Pt2, 555-556. 2004

[9] Bruess, P,. "An unexpected discovery could yield a full spectrum solar cell", Research News, Berkeley Lab, 2002

[10]Weiss, P., "Photon Double Whammy: Careening electrons may rev up solar cells", Science News, Vol. 165, No. 17, p. 259, 2004

[11] "NanoHorizons Patents Cost and Efficiency Breakthrough for Solar Cells and Organic LEDs", Nanotechnology, PhysOrg, 2005

[12] Bronstein, S. "New Plastic Solar Design Promises Efficient Power", ATHOL, Mass.

[13] Sanders, B. "Cheap, plastic solar cells may be on the horizon, thanks to new technology developed by UC Berkeley, LBNL chemists", University of California, Berkeley, Press Release, 2002

[14] "Wearable Cheap Solar Panel", Technology, PhysOrg, 2004

[15] Bailey, P. "Solar Cell Roll-Out", Technology Review, MIT, 2004

[16] Curtis, S. "Nanosolar to build world's largest solar cell factory", Business News, OpticsOrg, 2006
[17] Luque, A., and Mart, A. Phys. Rev. Lett. 78 (1997) 5014
[18] Lecture Notes, "Photovoltaic Cells", History, University of Rochester, 2006.
[19] Pearce, J. and Lau, A., "Net Energy Analysis for Sustainable Energy Production from Silicon Based Solar Cells", Proceedings of Solar 2002 Sunrise on the Reliable Energy Economy June 15-20, Reno, Nevada, 2002
[20] "New Nano Design Principle Could Dramatically Increase Efficiency of Thermoelectric Material", Energy, Technology, Issues and Policies for Sustainable Mobility, Green Car Congress, 2005
[21] Venkatasubramanian R et al, Thin-film Thermoelectric Devices with High Room-temperature Figures of Merit. Nature, 413:597-602, October 2001.]
[22] Bass J.C. et al, "Development of an Underarmor 1- kW Thermoelectric Generator Waste Heat Recovery System for Military Vehicles", Diesel Engine Emissions Reduction (DEER) Conference, 2004
[23] Lawrence E, "A Study of Heat Sink Performance in Air and Soil for Use in a Thermoelectric Energy Harvesting Device", Proceeding in IEEE International Conference on Thermoelectronics, 2002
[24] Schock, H, "Thermoelectric Conversion of Waste Heat to Electricity in an IC engine powered vehicle, Diesel Engine Emissions Reduction (DEER) Conference, 2005

Wind regime and wind power in the southern coastal islands of Bangladesh

Sanjoy Dey

Department of Electrical and Computer Engineering, Wichita State University, Wichita, Kansas, USA. Email: sxdey@wichita.edu

Keywords: Wind power, coastal islands, Bangladesh.

Abstract

An assessment of the wind resource available at any prospective area is essential to secure the maximum output power from a given type of wind electric generator. This paper presents wind and wind power characteristics in the southern coastal islands of Bangladesh which are surrounded by the Bay of Bengal. Mean flow pattern was studied in four coastal island: Hatia, Sandwip, Bhola and Kutubdia. Data collected from the Bangladesh Meteorological Department (BMD) are used to estimate the available meteorological wind power for these four sites. It is found that Hatia is an Island of high wind power potential. Some design parameters for the wind electric generators (WEG) to be setup in these islands are also analyzed in this paper. It is observed that small WEGs with cut-in speed ~1 m/s are best suitable for these islands.

1 Introduction

Wind energy has become a prominent source in the present global energy picture. For wind power generation a good knowledge of wind related characteristics such as, site selection, energy output is necessary. In Bangladesh various windy regions have been identified, having potential for generating electricity [1]. Bangladesh has 724 km long coastal line and it has about 30 big islands in the costal areas. Strong south-westerly trade wind and sea-breeze blow in the summer season and there is gentle north-easterly trade wind and land breeze in winter months in these islands. So wind energy potential in the coastal areas is significant. All the coastal islands of Bangladesh are not connected with the national power grid line. Some of them have diesel driven power generating stations. But during the monsoon period when the sea is turbulent it becomes hard to carry diesel to the islands which are far away from the main land. So generation of electricity from the renewable energy sources like wind has become an important issue for these islands. In this paper wind power potential at four coastal islands of Bangladesh has been studied. The islands are Hatia, Sandwip, Kutubdia and Bhola. The approximate positions of these islands are shown in Fig. 1. Average monthly wind speeds at these islands are evaluated from the three hourly data recorded by Bangladesh Meteorological Department (BMD). Probability distribution of wind speed, probability of wind speed greater than a particular speed and some design speeds for the wind electric generators to be setup in these islands are calculated.

2 Data

The data used in the present paper were collected from Bangladesh Meteorological Department (BMD). BMD has four stations in four coastal islands-Kutubdia, Sandwip, Hatia, and Bhola which are in the southern coastal region of Bangladesh. They record data every three hours using three-cup type anemometer kept at standard height of 10 meter. For this study data from 1981 to 2002 is used for Sandwip and Bhola, data from 1982-2002 is used for Hatia and data from 1985-2002 is used for Kutubdia.

3 Short Description of the islands

(a)Sandwip: The location of Sandwip is $22^0 29^/$ N and $91^0 26^/$ E. This island is located in the Bay of Bengal, adjacent to Chittagong and is about 15 km from the mainland. Its population is around 330,000 on an area of 240 sqkm. The entire island is a mudflat created from the Ganges delta. A short electricity grid connects the main commercial areas on the island. The electricity demand is met up by two diesel generators each of 200 KW which run for a few hours in the late afternoon/early evening. There are some households which have batteries and some diesel generators are used for powering rice threshers.

(b)Bhola: The location of Bhola is $22^0 41^/$ N, $90^0 39^/$ E. This Island is located in the mouth of the Bay of Bengal and has a population of 1.6 million. The total area of this island is 3403.48 sqkm. The main occupations are agriculture related 67% and fishing 5%. The demand of electricity in Bhola is about 6 MW. At present the existing diesel generator has a capacity to produce 4 MW of electricity.

(c)Kutubdia: The location of this island is $21^0 49^/$ N, $91^0 51^/$ E. This island is also located in the Bay of Bengal, which is around 20 km far from the mainland and approximately 50 km south of Chittagong port. The area of the island is 9.82 sqkm with a thriving population of 4000. The main occupations are agriculture related 32.13% and fishing related 4.67%. There is a 250 KW diesel power station in this island.

(d)Hatia: The location of this island is 22^0 $26^/$ N, 91^0 $6^/$ E. The island group of Hatia is located on the western end of Chittagong State. Hatia Island consists of about 25 single islands. The island group is about 40 miles from north to south and up to 15 miles wide.

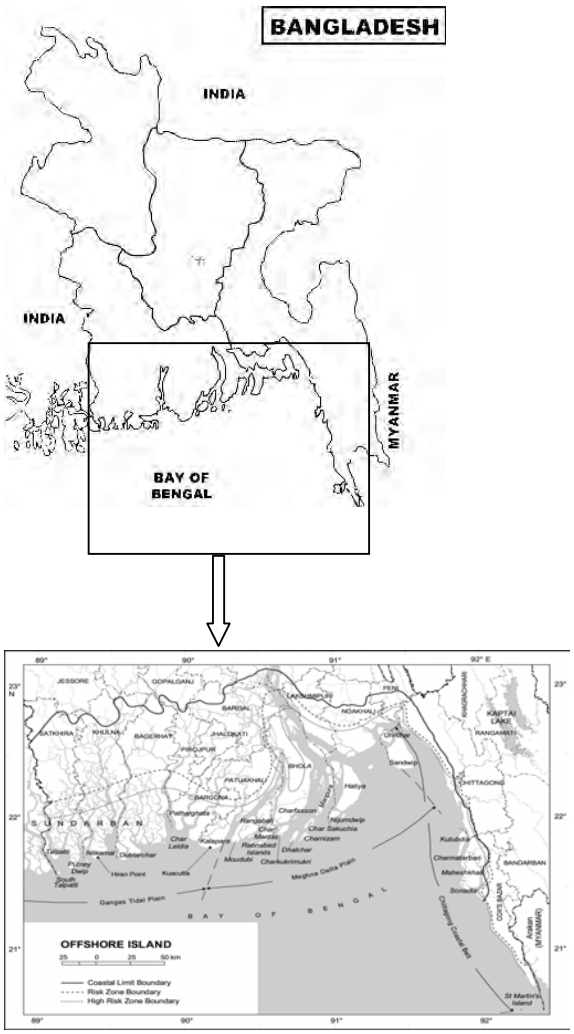

Fig. 1: Approximate study points in the map of Bangladesh.

4 Meteorological data analysis

4.1. The monthly mean wind speed

The annual energy from wind depends on the available wind potential. Hence, the annual energy production can be fairly estimated on the basis of the local mean wind speed. The long term monthly averages of wind speed for the four meteorological stations of the coastal islands are plotted in Fig. 2. It is observed that all of the stations experience their respective lowest wind speed through post monsoon (October-November) to winter (December-January). From the pre-monsoon (February-May) the speed starts to rise and attains their maximum by May-June and then it gradually decreases till to October.

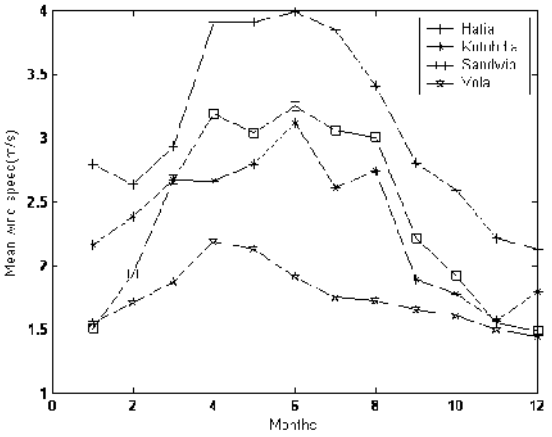

Fig. 2: Average monthly wind speeds of the four stations.

4.2 The yearly wind Weibull distribution

For detailed energy production calculations, the complete wind speed time-series data for every wind turbine at hub-height is required. Thus the expected annual energy production is based on the well-known Weibull parameters long-term values. In other words the estimation of Weibull parameters is related with the expected wind energy generation. The weibull distribution which is frequently used to describe wind data series can be expressed as [2, 3],

$$f(v) = \frac{k}{c}\left(\frac{v}{c}\right)^{k-1} \exp\left[-\left(\frac{v}{c}\right)^{k}\right] \quad (k>0, v>0, c>1) \tag{1}$$

Here v is the wind speed at a turbine height of 30m, k is the shape parameter and c is the scale parameter. The shape parameter k measures the shape of the probability distribution curve and is a climatic characteristic of each site and also may change with seasons in a given site. The performance of a wind turbine can be significantly affected by this parameter involving the unit cost of generation. The values of k and c are expressed as,

$$k = \left(\frac{\sigma}{\bar{v}}\right)^{-1.086} \quad (1 \le k \le 10) \tag{2}$$

$$c = \frac{\bar{v}}{\Gamma(1+\frac{1}{k})} \tag{3}$$

Here $\bar{v}$ stands for the mean speed of wind and it is found as,

$$\bar{v} = \frac{1}{n}\sum_{i=1}^{n} v_i \tag{4}$$

The gamma function, $\Gamma()$ used in equation (3) is normally computed from a sufficient number of terms of an infinite series. The value of $\Gamma(1+\frac{1}{k})$ is found as [4],

$$\Gamma(1+\frac{1}{k}) \quad = \quad 0.825 + 0.0135k + \exp\left[-\left(2+3(k-1)\right)\right] \tag{5}$$

Normally for wind power generation estimation the wind data at a hub height of 30m are used for analysis. Because most of the small-scale wind turbines which are suitable for the islands studied here are situated at a height of 30m.It needs a simple conversion formula to convert the 10m data to that applicable for 30m and it is expressed as,

$$v = v_0(\frac{h}{h_0})^{\alpha} \tag{6}$$

Here α is the ground surface friction co-efficient, h_0 is the reference height and h is the measured data height. The variance of wind speed σ^2 is expressed as,

$$\sigma^2 = \frac{1}{n-1}\sum_{i=1}^{n}(v_i - \bar{v})^2 \tag{7}$$

The probability distributions of wind speeds are plotted in Fig. 3. It indicates that Kutubdia, Sandwip, Bhola have wide variety of winds. On the other hand, Hatia has the widest variability that is Hatia has the highest probability of getting high wind speed. Here the modes of the distributions are 2.0, 2.0, 1.5, and 2.5 for Kutubdia, Sandwip, Bhola and Hatia respectively.

Table 1:Calculated results of wind data for the four sites

Site	Hatia	Sandwip	Kutubdia	Bhola
Mean wind speed, m/s	3.10	2.40	2.35	1.75
Parameter, k	1.97	1.96	2.01	1.99
Parameter, c	3.50	2.78	2.66	1.98
$\bar{\bar{P}}_w$, W/m^2 (At 30m)	16.92	7.94	7.20	3.03

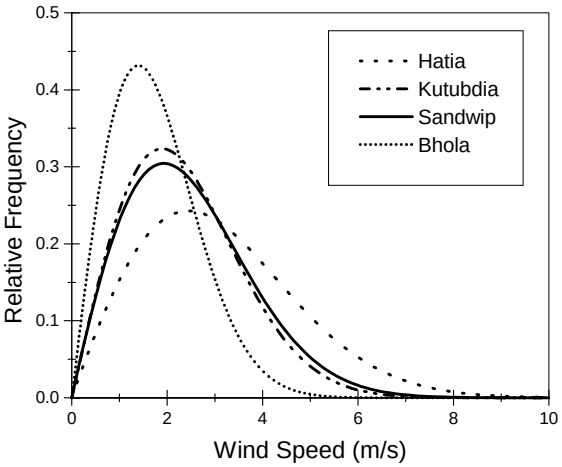

Fig. 3: Probability Distribution of wind speed.

4.3 Probability distribution of wind speed equal to or greater than a particular value

For the tower height of 30m the probability distribution of wind speed equal to or greater than a certain value is calculated by using the following form,

$$F(v) = \int_0^v f(v)dv = 1 - \exp\left[-\left(\frac{v}{c}\right)^k\right],$$

$$P(v \geq u) = \exp\left[-\left(\frac{u}{c}\right)^k\right] \tag{8}$$

Here $F(v)$ is the probability density function and u is a speed extreme value and $P(v \geq u)$ is the probability. The results are shown in Fig. 4 demonstrates that during the analyzed year, speeds higher than 3.0 m/s were observed in 47% of Hatia total cases, 31% of Sandwip cases, 29% of Kutubdia cases and 10% of Bhola cases. Speed higher than 5.0 m/s were observed 16% in Hatia, 6% in Sandwip, and 4% in Kutubdia and almost zero percent for Bhola. For most wind turbines, the range of cut-in speed is between 3.0 m/s and 4.5 m/s.

4.4 Yearly frequency distribution of wind directions

Table 2 represents the yearly frequency distribution, in percentage terms of wind directions. Then these values are plotted in Fig. 5. Taking the whole year, almost 46% winds are from the South and 28% are from the North for all four sites. The third largest wind direction is the South-East from which about 15% of winds blow.

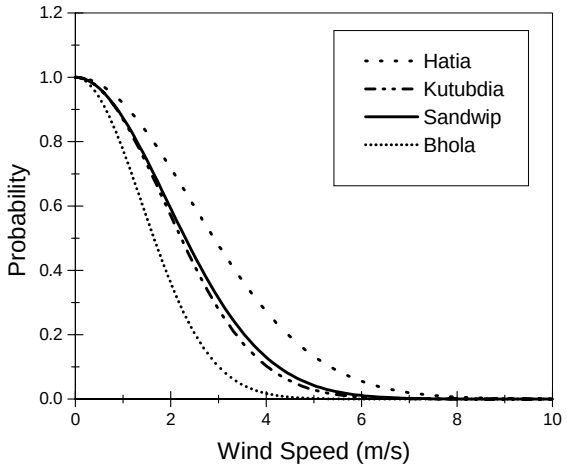

Fig. 4: Probability distribution of the wind speed equal to or greater than a certain value in four sites.

Table 2: Yearly Frequency Distribution of Wind Directions

Direction	Bhola	Sandwip	Kutubdia	Hatia
N	22.69	29.34	28.7	30.9
NE	3.07	1.16	1.85	5
E	1.54	0	0	0
SE	16.53	12.35	21.75	5.58
S	45	51.35	37.03	54.5
SW	4.23	0.39	1.38	0.42
W	2.3	0	0.46	1.28
NW	4.62	5.4	8.76	2.15

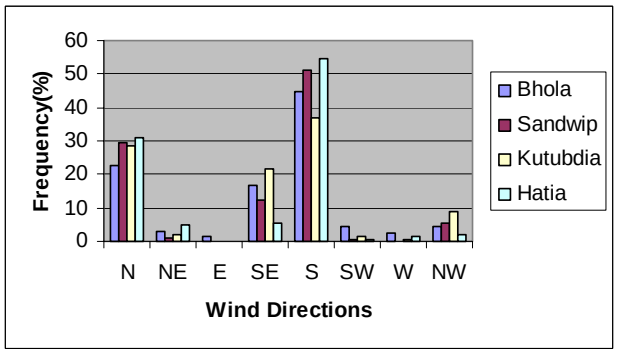

Fig. 5: Yearly frequency distribution of wind directions in four sites.

4.5 Design speeds for WEG to be used in these islands:

There are three design speeds for the WEG. These three speeds are, cut-in speed (V_c), rated speed (V_r) and furling speed (V_f) which can be expressed as,

$$V_c = 0.6 - 0.7V_m \quad (9)$$

$$V_r = 1.5 - 2.0V_m \quad (10)$$

$$V_f \geq 3V_m \quad (11)$$

Table 3.Design speeds for the four islands

	V_c	V_r	V_f
Kutubdia	1.41~1.65	3.53~4.7	7.05
Sandwip	1.44~1.68	3.6~4.8	7.21
Hatia	1.86~2.17	4.65~6.2	9.29
Bhola	1.05~1.23	2.63~3.5	5.25

These three speeds for the four stations are stated in Table 3.

4.6 Capacity factor for the four sites:

Capacity factor is the ratio of output energy to the nominal energy. Capacity factor can be expressed as [5],

$$CF = \frac{\exp\left\{-\left(v_c / c\right)^k\right\} - \exp\left\{-\left(v_r / c\right)^k\right\}}{\left(v_r / c\right)^k - \left(v_c / c\right)^k} - \exp\left\{-\left(v_f / c\right)^k\right\} \quad (12)$$

For greater efficiency the capacity is needed to be more than 20%. In this study the capacity factor for the four sites are calculated for different cut-in speeds and rated speeds and are shown in Table 4. For Bhola it is found that the capacity factor is higher for a rated speed of 2.5 m/s and for a cut-in speed of 1m/s. But as the rated speed is lower so this condition will not give more power. So it needs to trade off between the rated speed and capacity factor. So we can choose a rated speed of 3 m/s with a cut-in speed of 1m/s. By the same way a cut-in speed of 1m/s with a rated speed of 4m/s is found to be the best condition for Kutubdia, a cut-in speed of 1m/s with a rated speed of 5m/s is found to be the best condition for Hatia and a cut-in speed of 1m/s with a rated speed of 4m/s is found to be the best for Sandwip.

5 Conclusions

An analysis of wind speed across four of the most important and big coastal islands of Bangladesh show that Hatia has good wind potential which can be very helpful for a wind turbine industry in this island. The results show that the sites have a good exposure to the southern wind direction. The analysis also reveals that all the four demonstration sites should have a wind speed more than 3.0 m/s for about 30% time of the total year. Some calculations are also made to select the best design criteria for wind electric generators (WEG) to be installed in these sites. Results show that a WEG with a cut-in speed of 1.0 m/s and a rated speed of 5.0 m/s should be the best to extract more power with highest operating hours for operating in Hatia Island.

Table 4. Capacity Factor for the four sites for different cut-in and rated speed.

Bhola:

V_c=1 m/s			V_c=1.25 m/s			V_c=1.5 m/s		
V_r= 2.5 m/s	V_r= 3 m/s	V_r= 3.5 m/s	V_r= 2.5 m/s	V_r= 3 m/s	V_r= 3.5 m/s	V_r= 2.5 m/s	V_r= 3 m/s	V_r= 3.5 m/s
0.4262	**0.3301**	0.2548	0.3908	0.3005	0.2301	0.3523	0.2684	0.2036

Kutubdia:

V_c=1 m/s			V_c=1.5 m/s			V_c=2 m/s		
V_r= 3 m/s	V_r= 4 m/s	V_r= 5 m/s	V_r= 3 m/s	V_r= 4 m/s	V_r= 5 m/s	V_r= 3 m/s	V_r= 4 m/s	V_r= 5 m/s
0.5193	**0.3588**	0.2453	0.4683	0.3193	0.2154	0.4067	0.2721	0.1798

Hatia:

V_c=1 m/s			V_c=1.5 m/s			V_c=2 m/s		
V_r= 4m/s	V_r= 5 m/s	V_r= 6 m/s	V_r= 4 m/s	V_r= 5 m/s	V_r= 6 m/s	V_r= 4 m/s	V_r= 5 m/s	V_r= 6 m/s
0.5305	**0.4053**	0.3065	0.4987	0.3788	0.2848	0.4584	0.3455	0.2576

Sandwip:

V_c=1 m/s			V_c=1.5 m/s			V_c=2 m/s		
V_r=3 m/s	V_r= 4 m/s	V_r= 5 m/s	V_r= 3 m/s	V_r= 4 m/s	V_r= 5 m/s	V_r= 3 m/s	V_r= 4 m/s	V_r= 5 m/s
0.5449	**0.3888**	0.2733	0.4956	0.3498	0.2429	0.4363	0.3032	0.2070

References

[1] M. U. Mahfuz, "Wind Energy Status in Bangladesh", *Wind Engineering*, Vol 25, No. 3, 2001, Pp 179-190.

[2] Lu Lin and Yang Hongxing, "Wind Data Analysis and a Case Study of Wind Power Generation in Hong Kong", *Wind Engineering*, Vol 25, No. 2, 2001, Pp 116-123.

[3] C. Palese, L. J. Lassig, G. M. Cogliati, A. M. Bastanski, "Wind Regime and Wind Power in North Patagonia,Argentina", *Wind Engineering*, Vol 24, No. 5, 2000, Pp 361-377.

[4] S. Biswas, B. N. Sraedhar, Y. P. Singh, "A Simplified Statistical Technique for Wind Turbine Energy Output Estimation", *Wind Engineering*, Vol 19, No. 3, Pp 147-155.

[5] M.Hasanuzzaman, J.K. Shaha, M. Morshed and R.C.Roy," Determination of Design Wind Speeds for Optimum Use of Wind Electric Generators at St.Martin's Island", *Proc. Of the International Conference on Renewable Energy for Rural Development*, Jan 2002, Pp 139-143.

Design Considerations for Upgrading Diesel Powered System to a Hybrid Energy System in Rural Sarawak

Than Soe, Nabil Afifi and Balakrishna Singam

School of Engineering and Science
Curtin University of Technology, Sarawak campus
CDT 250, Miri, Sarawak, Malaysia 98009
Tel, +60 85 443 939,Fax, +60 85 443 837
Email: than.soe@curtin.edu.my; nabil.afifi@curtin.edu.my; balakrishna@curtin.edu.my
Web: http://www.curtin.edu.my

Keywords: Hybrid energy system, system sizing, rural, Sarawak

Abstract

In this paper, the design of a hybrid energy system for rural areas not connected to the national grid in Sarawak is presented. The design aims to reduce the dependency on diesel by upgrading a diesel generator system with a PV array. However, the high capital cost of such hybrid energy systems is the main obstacle to proliferate their use. Under-sizing the system to reduce the cost reduces the system reliability and performance, over sizing the system increases the cost drastically. As such, an optimum design that balances the performance and cost is needed. The design presented here aims to provide a reliable self-sufficient hybrid power system, by proper sizing of the components in the system while minimizing the capital cost. To make the design realistic, the design is based on a real life data captured at a long house, Rumah (RH) Kudang (Bakas Sibuti) in Sarawak. To proliferate the use of hybrid energy systems, long term cost analysis is also presented to show the cost advantages of using hybrid energy systems.

1 Introduction

In rural Sarawak, areas not connected to the national grid are powered by stand-alone power systems (SAPS). These small power systems are solely powered by diesel generators. With the current increase in oil prices and the decreasing subsidy of the government to diesel, pressure is mounting on rural people who rely heavily in their power requirements on diesel. To help release this burden and improve the quality of lives of rural people, stand-alone power systems based on hybrid energy system backed up by diesel generator need to be proliferated. Renewable energy sources offer a viable alternative to the provision of power in rural areas. The distance from the centralised electric network increases the costs of the energy dramatically that most of the remote users are disconnected from the main grid. Currently, the electrification of these users is left to diesel generators sets for single house or small community power needs. The main problem related to the use of diesel generators sets is the operation and maintenance (O&M) of these gensets. Photo Voltaic (PV) hybrid system backed-up by an engine-generator set – are low maintenance systems and has greater reliability for electricity production, and often represents a better solution for electrifying remote areas [1]. In these systems, the engine generator supports proper operation of the PV system and reduces the PV size, while the PV system decreases the operating time of the generator, reducing its fuel consumption and O&M [2].

2 Background

In rural Sarawak, people often live in long houses. The equivalence of a long house in a city, is a terrace house. The structure of a modern long house has a long corridor that runs along the length of the house. The corridor provides a social gathering and also access to the flats, often referred to as "doors". Long houses come in different sizes; some are long as over 30 doors and some are small as 10 doors and less. The house considered in this paper is Rumah (RH) Kudang located 80Km from Miri on the road to Bintulu. The long house is a double storey; reinforced concrete as shown in figure 1. The long house has been constructed 2 years ago and has 27 doors (27 families). In this long house the diesel generator is used to supply electricity from 6:30 pm to 10:30 pm everyday. There is also no electricity for one to two days in every month due to shortage of diesel.

Figure 1: RH Kudang, a long house in Sarawak

Long houses in Sarawak similar to this one often rely on a diesel generator only for the supply of electricity. The major problem is the cost of the diesel. People have to travel for along period of time to acquire diesel sometimes via roads or rivers. This process is an added cost to the actual cost of diesel in the nearest city. As such our objective is to upgrade an existing diesel generator set with a renewable energy sources to help reduce the dependency on diesel and extend the operating hours of such energy system.

3 Renewable Energy Resources

The daily average insolation in Sarawak is 4.85 kWh/m2/day as shown in figure 2 [7]. The minimum insolation is 4.32 kWh/m2/day in December and the maximum is 5.342 kWh/m2/day in April. The figure also shows that there is little variation of the insolation over the year. This indicates that the electrical power output from Photovoltaic array is stable throughout the whole year when compared to locations with four seasons e.g. California.

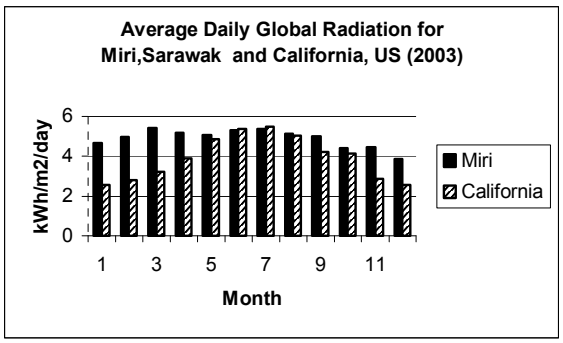

Figure 2: Average Daily Solar Radiation for Miri and California, 2003[8]

Figure 3 shows that Malaysia is located in the moderately feasible belts for solar application. As such solar energy is the preferable choice when compared to other sources of energy such as wind and ocean energy. Therefore, photovoltaic array is considered as the renewable component in our design.

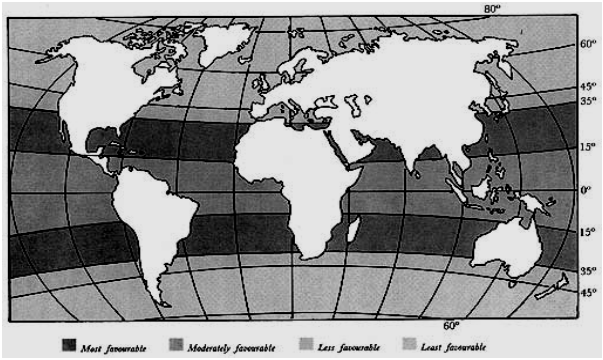

Figure 3: Worldwide distribution of solar radiation into belts indicating feasibility of solar application [11]

4 Hybrid Energy System Design

The considered system is presented in figure 4. In this design a PV array is used to charge a battery bank during the daytime. The deep cycle battery bank is used for electricity storage (charging) at daytime and supply DC current to inverter (discharging) at nighttime. The lead acid sealed type deep cycle batteries are suitable for renewable energy power system because the charging and discharging processes can be performed continuously for several hours. Inverter (Converter) is used for the purpose of rectifying AC to DC and inverting DC to AC. The diesel generator is used for supplying power to the load when the storage capacity of the battery bank is insufficient. The generated excess electricity of generator will be useful to charge the battery bank.

In this paper we provide three designs. The first design refereed to as system I, considers satisfying the existing load and uses 50% of the required power from the PV array, while the second, system II considers the long term performance by increasing the load profile used in system I, while the last design, system III, examines a cost effective solution by using 80% power from the PV array and can support future expected higher load and longer hours. We then compare these designs with the existing diesel generator set only.

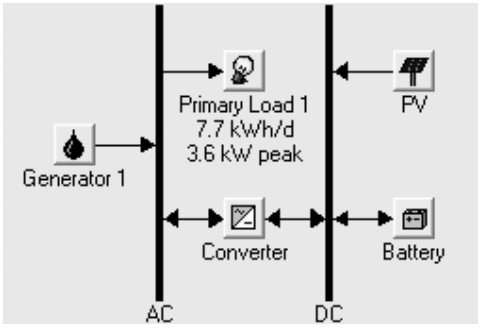

Figure 4: a PV/ battery/ diesel hybrid energy system [8]

5 Sizing Methodology for system I

In this section we provide detailed sizing procedure for system I. The sizing for system II and III follow similar procedures.

5.1 Load Profile

The captured load profile for the long house is shown in figure 5 and figure 8. The load profile was captured at the three-phase output of the diesel generator between 06:30 and 10:30pm. The load profile shows that the average power consumption throughout the operation period is almost fixed and averages about 2kW. There are no noticed peaks in this load. In this long house the electricity is mainly used to turn lights on in the main corridor, outside the long house and inside each door. Power is also used to power small house appliances such as TV, DVD player etc. From this, the average daily power consumption is 7.7kWh and the Cost of Electricity (COE) is 3.46 RM/ kWh, which is at least 10 times the cost of power from the grid.

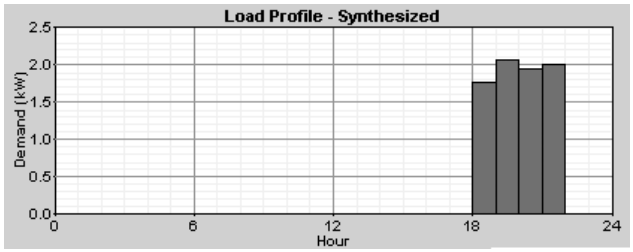

Figure 5: Daily load profile

5.2 PV array sizing

The PV power production $P(t)$ is computed as the product of the PV efficiency, the hourly irradiation $I(t)$ and the PV module area [3]. Using Miri daily average solar radiation (4.84 kWh/m2/day) and solar panels from British Petroleum (BP 380 U) with a panel surface area of 1209mmx 537mm and efficiency of 10%. The power production is then calculated as $1209x537x10^{-6} \times 4.84 \times 0.1 = 0.314$kWh/day. In the first design the PV supplies 50% power to the system, 7700 Wh/2 = 3850 Wh. Using this, the number of PV panels is 3850/314=12.26. However, the design uses a 24V DC system; as such the PV array must be multiple of 2 resulting in 14 PV panels. The 'peak Watt' (or 'Wp') price is used as a fixed economic parameter [4]. In [4] the peak watt was found to be $US 5.8 /Wp (5 ECU/Wp), when using the prices of the French producer PHOTOWATT. In our design the peak watt is 15RM/Wp when using the BP solar prices.

5.3 Battery Bank Sizing

The battery bank plays an important role in any off-grid power system. It's a major cost factor as well as the insurance for uninterrupted supply throughout shortages of irradiation. The sizing of the battery bank considers two important criteria, first, the number of days of autonomy and the state of charge of the battery. Both determine the life of the battery bank. The data sheet for the battery obtained from the manufacturer is shown in figure 6. The figure shows that, the smaller the discharging current, the higher the capacity to be used.

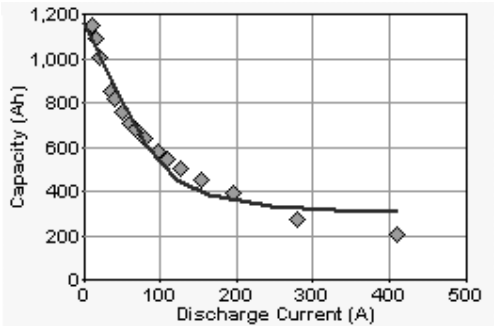

Figure 6: Capacity vs discharge current curve for a Surrette6CS25P battery [9]

To optimize the design, a 24 V DC battery bank system is used. The average power consumption is 2100 W= 7700/4/0.9 where the inverter efficiency is 0.9 and each battery is rated at 6V. Therefore, the discharge current is 88 A = 2100 / 24. In accordance with figure 4, the estimated capacity of the battery at 88A discharge current is 600 Ah. For a 24 V system, the number of batteries is a multiple of 4 since each battery is rated at 6V. With each battery capacity at 600 Ah, the total battery capacity is 14400Wh = $600 \times 4 \times 6$. The actual power capacity is less because of the inverter and the battery efficiency, which are 90% and 80 % respectively. As such the actual power capacity of the battery bank is 10368Wh = $14400 \times 0.9 \times 0.8$. With this design, there are 2 days of autonomy and the total number of batteries is 8 pcs.

The battery bank typically accounts for about 40% of the total system cost [5]. The cost of the battery is quite significant, because the initial investment is high and the battery has to be replaced several times during the PV system lifetime.

The cycle life of sealed lead-acid is directly related to the depth of discharge. The typical number of discharge/charge cycles at 25°C (77°F) with respect to the depth of discharge is: 150 - 200 cycles with 100% depth of discharge (full discharge), 400 - 500 cycles with 50% depth of discharge (partial discharge), 1000 and more cycles with 30% depth of discharge (shallow discharge) [10]. In this design, the estimated life of the battery is 9645kWh.

5.4 Diesel generator lifetime

Table 1 shows the life expectancy of various diesel generators. In this design, the diesel generator is set to 6000 hours lifetime and the rating of the generator is sized to 3.5 kW to get average load ratio 55% of demand.

References	Operating hours
Calloway (1986)	5000
Beyer *et al*. (1995a)	30 000
Energie Relais (1995)	1200
Sandia National Laboratories (1990)	6000
Energelec (1995)	3000 -8000
Energelec (1995)	1500 -12 000

Table 1: Back-up generator lifetime in hours (literature)[2]

6 Simulations & Results

The three designs are simulated using "Homer", a simulation tool from the National Renewable Energy Laboratory [8]. The purpose of the simulations is to evaluate and compare the three systems in terms of capital cost, COE and the state of charge of the batteries. Table 2 shows the obtained results.

From table 2 the following observations are made:

- For the existing diesel system, we have noticed that the long house is consuming less electricity than the actual capacity of the generator set. The main reason is that people at the long house try to reduce their diesel consumption by reducing their load. Engine-driven generators are inherently

inefficient when operated at light loads (below 40-50% of their rated capacity), which can also shorten their operating life and result in high maintenance costs [6]. The outcome is, the diesel genset is not operating at a high efficiency and the cost of electricity in this case is high. This is the dilemma that rural people face when using a diesel generator. Surprisingly, if the load is increased, the cost of electricity will be lower however; people still have to pay more for the extra diesel. For example, the cost of electricity (COE) can be reduced from 3.752 RM/kWh to 1.962 RM/kWh by increasing the average daily load from 7.7kWh to 16.6kWh. Briefly, doubling the load reduces the COE by half. This is further compounded by the usual one or two days of electricity shortage in every month.

Parameter	Hybrid System-I	Hybrid System-I	Hybrid System-II	Diesel only
Total energy demand (Wh/day)	7700	11600	11600	7700
Energy covered by PV	42%	27%	79%	
Energy covered by Diesel Generator	58%	73%	21%	100%
Demand at PV array (Wp)	1120	1120	3000	
Total number of Batteries	8	8	12	
Nominal capacity of battery	1156Ah	1156Ah	1156Ah	
Battery life time (kWh)	9645	9645	9645	
Estimated battery life time in cycles at 50% SOC	3170	3170	4220	
Generator life time (hrs)	6000	6000	6000	
Demand at Battery bank 600 Ah x 8pcsx 6V (Wh)	28,800	28,800	43,200	
Total number of PV 80W, 12V	14	14	38	
Annual fuel usage (litres)	863	1607	447	4834
Carbon emission (ton/yr)	0.623	1.16	0.323	3.49
Cost of electricity COE (RM/kWh)	2.915	3.343	2.871	3.46
Annual electricity shortage (Days)	0	0	0	24
Days of autonomy	2.69	1.78	2.68	0

Table 2: results outcome from optimization

- When the genset is upgraded and integrated in hybrid system I, the COE is reduced from 3.46 RM/kWh to 2.9 RM/kWh. Furthermore there is no interruption of power with 2 days of autonomy. The highest benefit comes from the lower consumption of diesel. In this case diesel consumption is reduced from 4834 liters to 863 liters, which is our main objective.
- If the load is increased from 7.7kWh/d to 11.6kWh/d over the next few years then, this is the case of system II, the genset will be operated for a longer time to compensate for the extra load. This is reflected by the increased percentage of genset from 58% to 73%. The COE in this case will increase to 3.34 RM while the diesel consumption is still reasonably low at 1600. However, because the system is hybrid, the supply of electricity is more reliable with increased load and offers 2.69 days of autonomy.
- If system III is used, the PV component supply of power is now almost 80%, and the COE is 2.87 RM/kWh, the lowest among these systems despite the high capital investment. The diesel consumption in this case is at the lowest at 447 liters/year. This is a significant improvement on the diesel genset solution only. The carbon emission is also at the lowest. This hybrid solution offers a good long-term solution by relieving rural people from the process of buying diesel.
- Diesel prices have almost doubled just over the past two years, causing the COE to almost double. This is because of the full dependence on diesel. By decreasing the dependency on diesel the COE of electricity is expected to increase slightly when diesel prices increase. For example in a diesel genset only, if the diesel prices double, the COE will double to 6.92 RM/kWh, however for system I the COE will be 4.6 RM/kWh. While system II that depends largely on diesel genset because of the increased load, the COE is 5.8 RM/kWh. System III on the other hand offers the best stability to diesel price changes and the COE in this case is 3.47 RM/kWh.
- Hybrid energy systems are also modular, and can be upgraded easily when the load demands increase beyond its capability.
- Figure 7, shows that some of the diesel operation is mainly to charge the batteries and maintains the SOC of the battery bank. In this figure, the generator output power reaches the maximum point to recharge the battery bank almost once every two weeks.

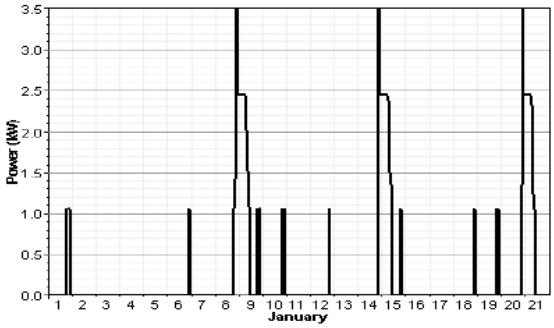

Figure 7: generator output curve

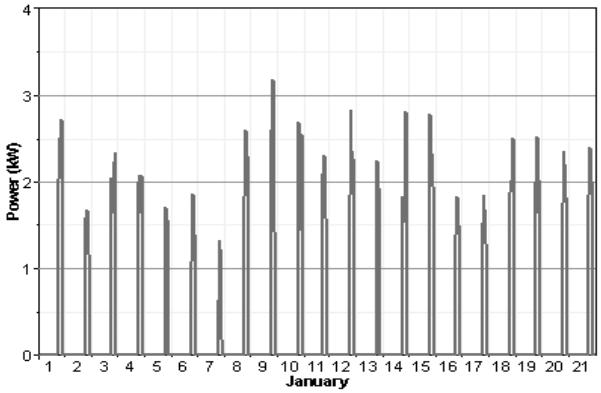

Figure 8: load profile

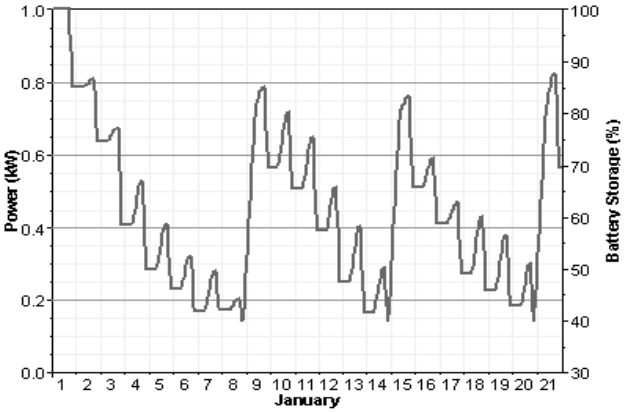

Figure 9: State of charge of battery bank

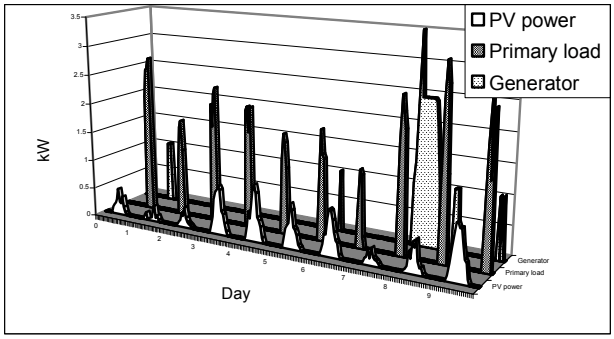

Figure 10: PV/ Generator power output and load consumption

7 Summary & Conclusion

In this paper, design considerations for upgrading a diesel genset supplying power to a rural long house in Sarawak are presented. As diesel prices have almost doubled over the past few years, our main objective is to reduce the dependency on diesel and reduce the dependency of the COE on diesel. In the existing genset solution, the diesel consumption is almost 4838 litres/year, and the COE is 3.46 RM/kWh. When the genset is integrated with a PV system, the COE is reduced to 2.915 RM/kWh and the diesel consumption is 863litres/year. This significant reduction in the consumption of diesel will maintain the COE as diesel prices raise in the future. Better results can also be achieved by increasing the component of the PV system. When the renewable energy component is increased to 80% the COE is at minimum and the dependency on diesel is also at minimum of 447litres/year. This design offers long-term stability of the COE despite the high capital cost. Hybrid energy systems are also low maintenance systems and insures that the supply of electricity without interruption. The modular nature of hybrid energy systems makes them advantageous for future upgrade.

The main point to be made here is that when supplying rural areas with electricity solutions, COE is a good indicator of hybrid systems rather than the simple capital investment.

Reducing the dependency on the ever-increasing diesel prices will ensure the stability of COE over a long period of time.

8 Acknowledgment:

We would like to thank Mr Robin from RH Kudang for inviting us to his long house and the wonderful hospitality extended to us by his family and all the people at the long house and in particular the Tuai Rumah for allowing us to have access to the diesel genset.

9 References

[1] V.A.P van Dijk, *Hybrid photovoltaic solar energy systems: design, operation and optimization of the Utrecht PBB system,* Ph.D. Thesis, University of Utrecht, 1996.

[2] M. Muselli, G. Notton and A. Louche, Design of Hybrid-Photovoltaic Power Generator, with optimisation of Energy Management, *Solar Energy*, vol. 65, no. 3, pp. 143-157, 1999.

[3] Iskander C. and Scerri E, "Performance and cost evaluation of a stand-alone photovoltaic system in Malta", *World Renewable Energy Congress* 8, 1–4, pp. 437–440, 1996.

[4] Keller L. and Afolter P, Optimizing the panel area of a PV system in relation to the static inverter–practical results, *Solar Energy,* vol. 55, 1–7. 1995.

[5] Notton G., Muselli M. and Louche A, Autonomous hybrid photovoltaic power plant using a back-up generator: a case study in a Mediterranean island, *Renewable Energy, vol.* 7, pp.371–391, 1996.

[6] M. Tomas, *Solar Electricity,* John Wiley and Sons, Inc., England, 1997, ch. 4-7.1.

[7] National Aeronautics and Space Administration http://eosweb.larc.nasa.gov

[8] National Renewable Energy Laboratory http://rredc.nrel.gov

[9] Rolls Battery Engineering *www.rollsbattery.com*

[10]Cadex Electronics Inc.,http://www.batteryuniversity.com

[11] UNICEF, Guidelines for Household Application in Developing Countries, *(http://almashriq.hiof.no/lebanon/600/610/614/solar-water/unesco/24-26.html)*

Computer Simulation of Solar Updraft Tower Systems to Describe the Variation of Velocity with Essential Parameters of the Systems

Sh. Khoshmanesh

"M.S of mechanical engineering, Sharif University of science and Technology, Tehran, Iran, email: sharif_khoshmanesh@yahoo.com"

Key words: Solar energy, solar chimney/tower, solar collector

Abstract

At this research the computer modeling of solar updraft tower systems would be consider to describe the variation of velocity with five parameters of the systems by the fluent software. The solar updraft tower systems consist of three essential element- glass roof collector, chimney/tower, and wind turbine. The output power of systems is depended on the input velocity to wind turbine. The turbine inlet velocity (V) is the function of five parameter of the solar updraft tower systems such as absorber diameter (D_p), roof glass angle (β), entrance height (h), tower's height (h_t), tower's diameter (D_t) .the finite volume modeling and analyzing of solar updraft tower systems to solve the momentum and energy equation have been carried out by fluent software. The results such as the velocity profile at the inlet to chimney, velocity contour, and dependency of turbine inlet velocity to D_p, β, h, h_t, D_t have been shown. The importance of knowing the velocity's variation with above five mentioned parameters, is to minimize the cost of plant by changing the parameters D_p, β, h, h_t, D_t to obtain the desire output power with the minimum cost.

1-Introduction

The solar chimney is a simple method of production the electricity from the sun. The solar chimney has three essential element-Solar air collector, chimney/tower and wind turbine-that combination of them produces the power. First time in 1931 combination of three above mentioned element for producing the power has been described by Günter (Günter, 1931). Solar chimney, Principal and construction of the pilot plant in Manzanares
was described by W. Haaf, K. friedrich, G. Mayr, and J. Schlaich,(1983, 1984) [6]. The test result and
a theoretical description of solar tower prototype in Manzanares has been take placed by Haaf (1983, 1984)[7]. Naim (1985, 1989) present a scheme of chimney like device for creating a vertical flow of air with the help of solar radiation [10].Kreetz (1997) introduce the concept of water-filled bags under the collector roof for thermal storage.Gannon and V.Backstrom present a thermodynamic cycle analysis of solar tower (2000), and also an analysis of turbine characteristics in 2003.Ruprecht (2003) give results for a 200 MW solar tower. For Australia, 200 MW solar tower project is currently being developed.

In this paper we describe the variation of velocity with five parameters of a system such as, entrance area, absorber area, roof glass angle, tower height, tower diameter, see fig1.The governing equation on the system has been written, and the simulation and numerically solution of problem in fluent to describe the variation of velocity with above mentioned parameter has been followed.

2-Research objective

The solar updraft systems bring three well-known robust principals together in unique way; the use of sun's radiation to heat a large body of air by the absorber plate and roof glass cover, rising of hot air through the chimney, using of the air moving as a energy source to drive large turbine to generate electricity. Fig1 shows the schematic view of solar updraft systems.

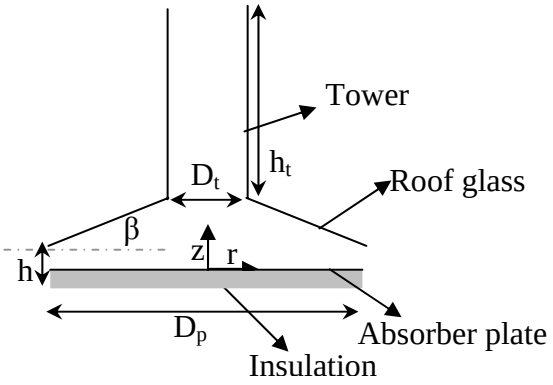

Fig1: schematic view of solar updraft systems

The input velocity trough the turbine is the main parameter that denotes the output power of systems, so we consider the velocity as a function of entrance area (h), tower height (h_t), tower diameter (D_t), absorber diameter (D_p), roof angle (β). This dependency was established by solving the governing equation numerically by finite volume method with fluent software.

3-Governing equation and computer simulation

to set up the governing equation on the systems, consider the solar updraft systems in the cylindrical coordinate see fig1, because the systems is symmetric relative to Z axis so we can with good approximation, consider the two dimensional flow

in r-z direction and write the continuity, momentum and energy equation respectively[2].

$$\frac{\partial v_r}{\partial r}+\frac{v_r}{r}+\frac{\partial v_z}{\partial z}=0 \quad (1)$$

$$\rho v_r\frac{\partial v_r}{\partial r}+\rho v_z\frac{\partial v_z}{\partial z}=-\frac{\partial p}{\partial r}+\mu\left(\frac{\partial^2 v_r}{\partial r^2}+\frac{\partial v_r}{r\partial r}-\frac{v_r}{r^2}+\frac{\partial^2 v_r}{\partial z^2}\right) \quad (2)$$

$$\rho v_r\frac{\partial v_z}{\partial z}+\rho v_z\frac{\partial v_z}{\partial z}=-\frac{\partial p}{\partial z}+\mu\left(\frac{\partial^2 v_z}{\partial r^2}+\frac{\partial v_z}{r\partial r}+\frac{\partial^2 v_z}{\partial z^2}\right)-\rho g \quad (3)$$

We use the Boussinesq approximation to relate the density to temperature in the momentum equation.

$$\rho g=\rho_0 g-g\beta(T-T_0) \quad (4)$$

$$\rho C_p\left(v_r\frac{\partial T}{\partial r}+v_z\frac{\partial T}{\partial z}\right)=k\left[\left(\frac{\partial(r\frac{\partial T}{\partial r})}{r\partial r}\right)+\frac{\partial^2 T}{\partial z^2}\right] \quad (5)$$

The above equations are subset of general transport equation,

$$div(\rho\phi\vec{U})=div(\eta grad\,\phi)+S_\phi \quad (6)$$

$$\vec{U}=v_r\vec{e_r}+v_z\vec{e_z} \quad (7)$$

If we replace φ by V_r, V_z and C_vT, and S_Φ by the appropriate source term the r-momentum, z-momentum and energy equation will obtain [3]. We use the divergence theory of Gauss and integrate the equation (6) on small control volume,

$$\int_A n.(\rho\phi u)dA=\int_A n.(\eta grad\phi)dA+\int_{cv} S_\varphi dV \quad (8)$$

n is the unit normal vector on control volume faces that is positive outward the faces.
The η is the diffusion coefficient, for the momentum equation is kinematics viscosity μ and for energy equation is conduction heat transfer coefficient k.
We can solve the above equations numerically by finite volume method that discrete the equation (8) on small control volume by second order upwind in staggered network by simple algorithm.

The finite volume method that mentioned above can be take place by fluent software that has been following here.

4-Solution and data verification

We model the updraft systems in fluent software, with natural convection model by activate the gravity at the operation condition, and use the Bossiness model for relating the density to temperature at material panel. To simulation the radiation we use the DO model radiation in radiation panel. To check the output result of the fluent, we reference the experimental result of K.Ghosh[8] that has been obtain for the solar chimney prototype with, h_t=91.4cm,β=0, D=150cm, D_p=38cm, and two inlet gap h=12.7cm and h=19.5cm that show in Fig3. For each inlet gap the data has been read two times for more accuracy.

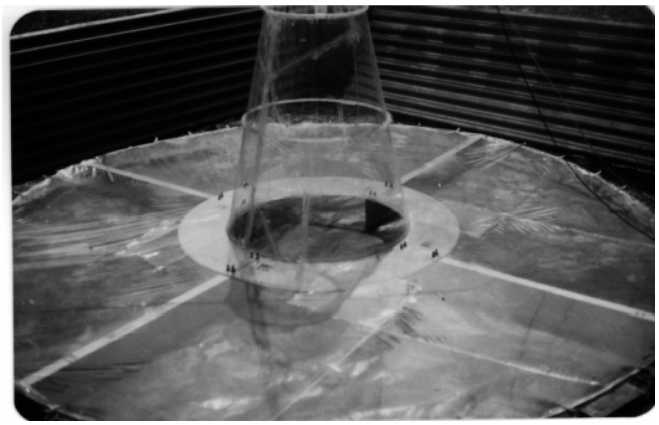

Fig2: photograph of solar chimney that was tested by Dr Gosh

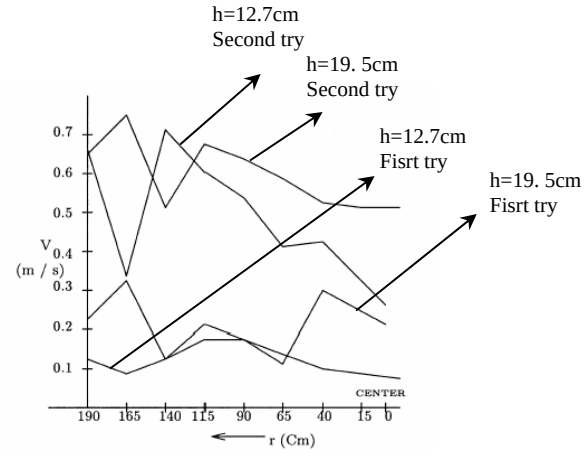

Fig3: velocity variation with inlet gap h=12.7cm and h=19.5cm at the inlet to chimney

We model the prototype above with the fluent software and compare the result with experimental data, the fluent result are for solar noon 11Am with the solar intensity of 950w/m^2 in Boushehr province in IRAN. The difference in the result is

due to different ambient condition of places, different solar intensity. Regardless of these differences the results of computer modeling data is in acceptance range.

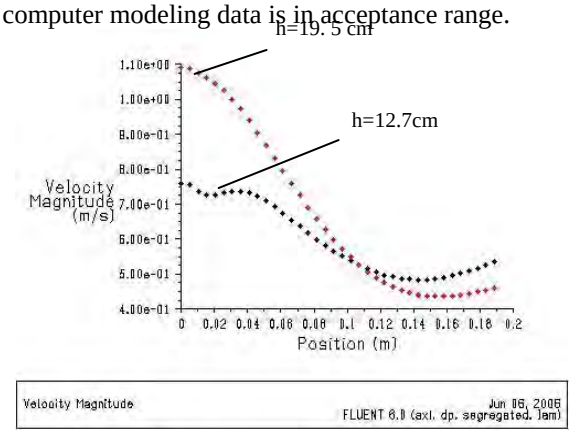

Fig4: velocity variation with inlet gap h=12.7cm, h=19.5cm at the inlet to chimney

We can see the contour of constant velocity across the solar updraft systems at Fig5, 6

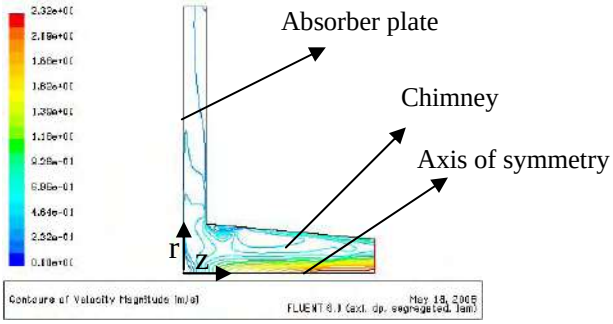

Fig5: countour of velocity for updraft systems (solar chimney) with the inlet gap h=0.127

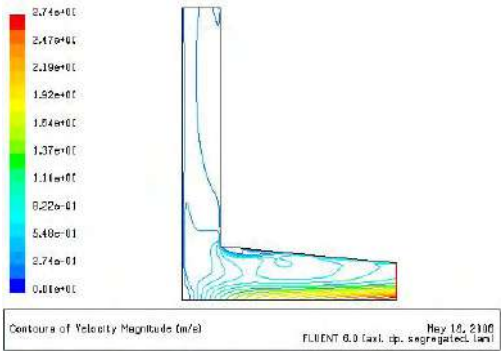

Fig6: contour of velocity for updraft systems (solar chimney) with the inlet gap h=0.195

We see that the result of fluent model is very close to experimental data, so we can confide to fluent model for calculation of the velocity's variation with h_t, h, β, D, D_p in forward steps.

5-Result

We reference the solar updraft systems with the dimensions of, h_t=91.4cm,β=0, D=150cm, D_p=27.5cm and inlet gap h=19.5cm.To demonstrate the variation of velocity with one of above parameters, we fixed the others parameters and change the desired parameter and calculated the input velocity at the section of entrance to tower. The velocity variation with the five parameters with referenced to above mentioned dimensions has been categorized at the following subsection

5-1-Velocit variation with inclined roof angle

To considering the result we reference the solar chimney with the dimension in fig3 (β=0) as the base and change the inclined roof angle to see the variation of velocity with this variable, the result of velocity for β=0, β=10°, 20°, 30° has been shown in fig7, as you see with increasing the inclined roof angle the velocity magnitude increase.

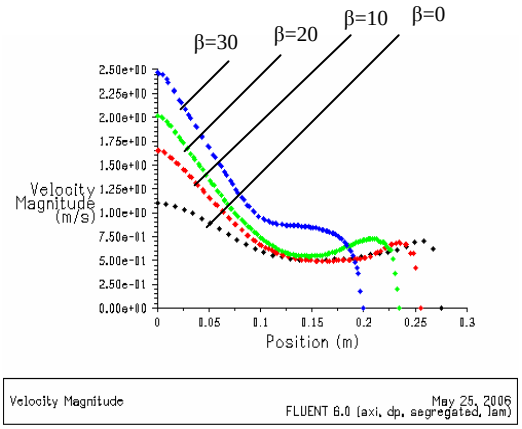

Fig7: Velocity variation with various roof angle; black line for β=0, Red line for β=10, Green line for β=20, Blue line for β=30

5-2 Velocity variation with tower(chimney)height

With increasing the tower height the bouyancy force will increase so we can anticipate increasing the velocity with increasing the tower height.
The aproximate formulation to calculate the velocity with incresing the height is (Unger, 1988),

$$V = \sqrt{2gh_t \Delta T / T_0} \qquad (9)$$

ΔT is the incresing the air temprature due to gain of heat from absorber plate (collector)and h_t is the tower height.
the variation of velocity with tower height has been shown on Fig8 that verify the increasing of velocity with tower height is in the range of equation (10).if we compare the Fig7 and Fig8 we conclude that the increasing the β causes the faster

increasing the velocity than the tower ,so during the construction of solar updraft systems the β angle shall be consider as a important parameter to increase the velocity.

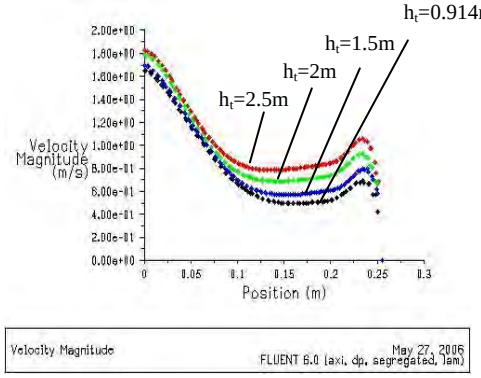

Fig8: Velocity variation with various tower height; black line for h_t=0.914m, Blue line for h_t=1.5m, Green line for h_t=2m, Red line forh_t=2.5m

5-3 Velocity variation with entrance height(inlet gap) to solar updraft systems

One paraeter that can effect the velocity is the inlet gap between the collector and glass roof (entrance area).We change the inlet gap and for each inlet gap the velocity profile at the inlet to tower has been calculated and shown in fig9.it shows that increasing the inlet gap causes to increase the velocity at the inlet to chimney

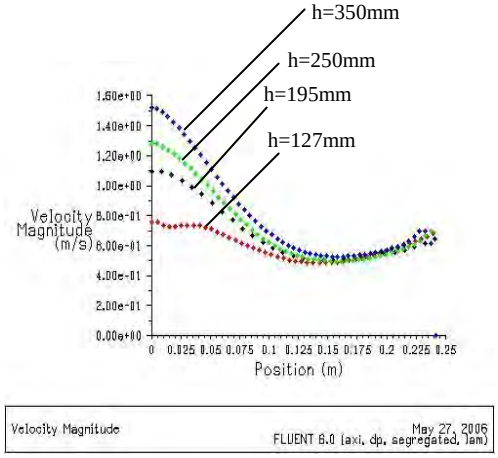

Fig9: Velocity variation with various Inlet gap; black line for h=195mm, Blue line for h=350mm, Green line for h=250mm, Red line forh=127mm

5-4 Velocity variation with diameter of tower (chimney)

Velocity with increasing and decreasing the chimney diameter decrease and increase respectivly, if the chimney diameter dos'nt decrease to critical value.if we decrease the dimeter less than the critical value the velocity also decrease at the inlet section to chimney,because of overcoming the friction and disturbuncy in flow field.at this research for this type the D_{cr} is 0.25m .

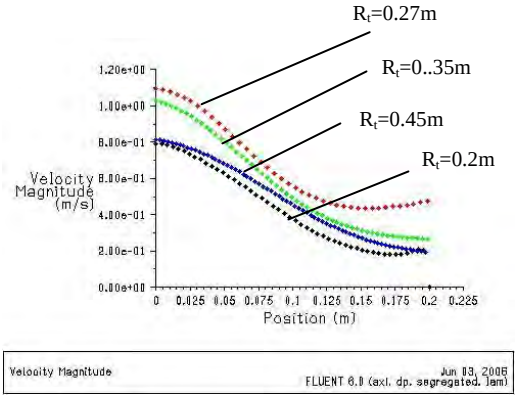

Fig10: Velocity variation with various tower radious; black line for R_t=0.2m, blue line for R_t=0.45m, green line for R_t=0.35m,red line for R_t=0.275m

5-5 Velocity variation with absorber plate radious

If we look on equation (10) ΔT is mainly related to absorber plate area, and increasing the area causes the increasing the ΔT so the velocity will be increse, but this incresing is limited becase the more area increasing causes to have more heat loss and no more increasing in ΔT . In fig10 we can see the velocity variation with incresing the radious of absorber plate.the most important result that we can extract from that figure is that the increasing the radious of absorber plate dosnt increase the maximum velocity but increase mean velocity. on the other hand increasing the absorber plate area causes to flatern the velocity profile,so we shall optimise the collector area to reach the desire profile.increase the collector area more than maximum area collector cause only the wasting the construction time and money so we define the dimeter ratio as

$$DR = \frac{D_p}{D_t} \qquad (10)$$

For this prototype the DR is nearly 20 an for the Manzanares prototype [6] that produce 50kw in Spain, DR is nearly 24.Velocity variation with various collector radious has been shown in fig11.

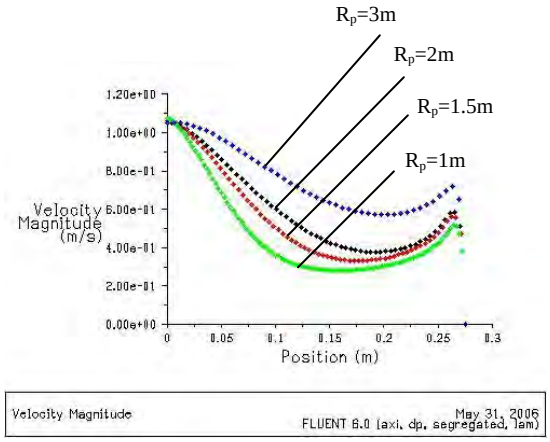

Fig11: Velocity variation with various collector radious; green line for R_p=1m, red line for R_p=1.5m, black line for R_p=2m,blue line for R_p=3m

6-Conclusion

At this research three important results that can be usfuel to maximise the output power at minimum plant cost are summerise as bellow

1)maximum collector area should be calculated for each prototype and with increasing the collector area more than the maximum value the velocity doesn't increase, because more area collector causes more heat loss radiation to glass and more air volume for heating.

2)minimum or critical tower radious for each prototype of solar chimney should be calculated, because if we decrease the tower radious more than minimum value it causes to decrease the velocity and reduce the power output of plant.

3)roof angle is the important parameter to increase the velocity, so the only parameter that constrain the roof angle is construction problem

Nomencluture

h	Inlet gap between collector plate and glass cover(m)
h_t	Tower height(m)
D_p	Collector's diameter(m)
D_t	Tower's diameter(m)
β	Roof angle(degree)
ν	Velocity(m/sec)
T	Temprature(k)
P	Pressure(Pa)
ρ	Density(kg/m^3)
β	Volume expansivity(1/k)
μ	Dynamics viscosity(kg/m.sec)
C_p	Pressure Specific heat(kj/kg.k)
K	Thermal conductivity(w/m.c^o)
S_Φ	Source term

Subscripts

t	tower
p	absorber plate(collector)
o	ambient
r	r-direction
z	z-direction

References

[1] J.A Duffie and W.A Beckman, Solar engineering of thermal processes, 2nd edition, Wiley and Sons Inc, New York, 1991
[2] J.A Jones, Convection heat transfer, 2nd edition, Wiley and Sons Inc, New York, 1995
[3] H.K.Versteeg and W Malalasekera, an introduction to computational fluid dynamics the finite volume method, Addison Wesley Longman Limited,1995
[4] M.A. Dos Santos Bernardes,G. Weinrebe, thermal and technical analyses of solar chimney, Solar Energy Volume 75,PP 511-524,1983
[5] J. Schlaich and W.Schiel, Solar chimney 3rd , Acadamic Press Lonon, 2001
[6] W. Haaf, K. friedrich, G. Mayr, and J. Schlaich, Solar chimney part I, Principal and construction of the pilot plant in Manzanares, Solar energy, Volume2, PP 3-20
[7] W.Haaf, Solar chimney, Part II, Preliminary test result from the pilot plant in Manzanares, Solar energy, Volume2, PP 141-161, 1983
[8] K. Ghosh, Measurement of wind velocity created by a solar chimney and hybridization of wind and solar thermal power, British wind energy association, Indian institute of technology, Kanpur 208016, India
[9] T.W. Van Backstrom and A.J Gannon, solar chimney turbine characteristics, Solar energy, Volume 76, PP 235-241, 2003
[10] NM.Naim,Wind energy from solar energy,8th Miami Confrence on alternative energy source, December, 14-16, Florida, USA